JPRS-JST-94-008
31 MARCH 1994

JPRS Report

Science & Technology

Japan

JAPAN SURFACE SCIENCE SOCIETY SEMINAR

JPRS-JST-94-008
31 MARCH 1994

SCIENCE & TECHNOLOGY
JAPAN

JAPAN SURFACE SCIENCE SOCIETY SEMINAR

936C1098 Tokyo JAPAN SURFACE SCIENCE SOCIETY in Japanese 25 Jun 93 pp 1-160

[Selected papers presented at the 13th (1993) Seminar of the Japan Surface Science Society: "Development of Nanotechnology With Scanning Probe Microscopes"]

CONTENTS

Observation of Organic Molecules by AFM

936C1098A Tokyo JAPAN SURFACE SCIENCE SOCIETY in Japanese 25 Jun 93 pp 1-7

[Article by Horibumi Yamada, National Institute for Advanced Interdisciplinary Research, MITI]

[Text] **1. Introduction**

The atomic force microscope (AFM) is a scanning microscope that was developed in 1986 by G. Binnig, et al. It detects various kinds of forces that act between a probe and the surface of a specimen placed close to it, and obtains a three-dimensional image with spatial resolution on the atomic-molecular scale by mechanical scanning of the probe. It is also frequently called a scanning force microscope (SFM). Since forces necessarily act with each other between two adjacently placed materials, in principle there exist no restrictions on the specimens for AFM scanning, and high-resolution observations of organic molecules or biological specimens having weak electrical conductivity should be possible. Moreover, few restrictions exist as to sample atmosphere, so experiments are possible in the atmosphere, in a liquid, or in a vacuum.

2. Principle and Apparatus of AFM

In general, an attractive force such as a dispersive force acts between pieces of matter at a far distance, and a repulsive force due to exchange interaction acts at a near distance. When a leaf spring-like cantilever having a probe whose tip radius has a curvature of about 10 nm is made to approach the surface of the sample, the cantilever is bent convexly toward the sample due to the force from the surface when it is attractive, whereas the cantilever bends in the opposite direction when it is repulsive. By measuring the fine bending it becomes possible to learn about the local force that acts between the probe and the sample. Through two-dimensional scanning of the sample while measuring the force, it is possible to obtain a two-dimensional image of the force on the surface of the sample (variable force mode). By scanning the sample while controlling by feedback the position in the Z direction of the sample so as to keep the signal of the force constant, it also is possible to obtain the fine shape of the surface (constant force mode), similar to the STM. Since the value of the attractive force acting between a neutral atom and

a surface is typically in the range of 10^{-9}~10^{-10}N, it is considered possible to measure surface information due to the forces acting between atoms and molecules if a detection sensitivity less than this order of magnitude is attainable. The system for measuring the cantilever displacement is required to have a resolution smaller than 0.05 nm, and at present measurement by the light lever method is often employed. A schematic diagram of the apparatus currently used by the author's group is shown in Figure 1. This apparatus can operate in a liquid. The light lever method is used for displacement detection, and a laser diode is used for light source. AFM is combined with an optical microscope, and the sample can be observed by an objective lens with a relatively large numerical aperture through a chromatic beam splitter placed above the cantilever to facilitate the positioning of the sample and the probe.

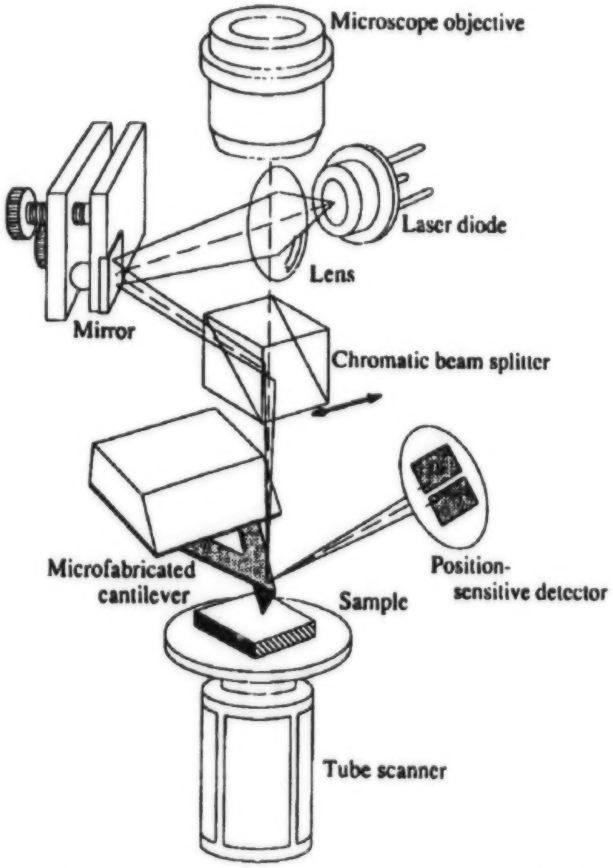

Figure 1. Schematic Diagram for AFM

The AFM's cantilever with a probe not only determines the sensitivity and resolution of the AFM, but also is extremely important in optimizing observation conditions (minimizing the set force) due to the fact that the adhesive force is proportional to the radius of curvature of the probe tip, as will be described later. At present, methods for producing an AFM include: 1) producing a pyramidal Si_3N_4 probe formed by transfer of an Si etch pit pattern, 2) a conical Si probe by utilizing undercutting in dry etching, and 3) a triangular cone Si probe obtained by the combination of dry etching and anisotropic etching. The Si_3N_4 cantilever having a pyramidal probe is commercially available. In our experiment, as described later, we used an Si_3N_4 cantilever with a triangular cone probe made of Si. It had a modulus of elasticity of 0.5 N/m, a resonance frequency of 110 kHz, and a tip radius smaller than 10 nm.

The operational region of an AFM may be divided into two parts, the repulsive force region (contact region) very close to the surface, and the noncontact attractive force region several nanometers away from the surface. Although the noncontact operation in the attractive force region has a very significant advantage in that damage to the sample and the probe can be avoided, the interaction region of the probe and the surface is extended due to the long distance nature of the attractive force, resulting in an inevitable deterioration of the transverse resolution. Actually, all of the high-resolution AFM

images obtained at present are due to contact operation. However, if the probe is made very sharp, there is a possibility of obtaining a resolution on the atomic-molecular level, even by the attractive force (noncontact) operation. In fact, Nonnenmacher, Geschmer, et al., succeeded in observing the 18 nm periodic structure of a two-dimensional protein crystal (HPI structure of *Deinococcus radiodurans*) in the attractive force mode using a very sharply pointed probe developed independently.

3. Examples of Organic Molecular Observation by AFM

In the past, AFM observations by repulsive mode have centered around the surface of organic monomolecular crystals and organic thin film samples. Measurement data with a resolution on the molecular level are being reported for single crystal surfaces such as the ab face of DL-leucine crystals, and pyrene crystals. Meanwhile, AFM observations of organic thin film samples, such as a self-assembled film (octadecyl-trichlor-silane (OTS)), an LB film (Cd-arachidate), a liquid crystal (octylcyanobiphenyl), DNA, purple film (Halobacterium halobium), and lipid molecule systems (Dlα-dimyristoylphosphatidylethanolmine (DMPE)), L-α-myristoylphosphatidylglycerol (DMPG), have been obtained by deposition on various kinds of substrates such as graphite and mica. Observation samples of polymers include a polymeric monomolecular level thin film of diacetylenic lipid deposited by the Langmuir-Blodgett (LB) method, which uses as a substrate Si with a thermally oxidized film in which a Cd-arachidate monomolecular film is deposited. A was sample obtained by depositing on single crystal graphite a 10-nm thin film formed by drawing poly (1-butene) in a fused state. Although structural observation of monomer units has not so far been made, observation of the molecular orientation on a subnanometric scale has been made. Observation of the cleavage surface of polymer crystals makes it possible to determine the side chain resolution for polydiacetylene crystals, as will be described below. As for "soft" samples like biological polymers, such as proteins, deformation, and damage due to contact cause problems, efforts are being made to reduce the contact force. However, a high resolution observation does not necessarily appear to be an easy task.

AFM Observation of Polydiacetylene Crystal

Polydiacetylene crystals have a very large third order nonlinear optical susceptibility. This is because they have a diacetylene conjugate principal chain along the polymerization direction. Thus it is expected that these crystals will be of use as a nonlinear optical material. Such crystals can be obtained by irradiating diacetylene monomer crystals with γ-rays or X-rays. Since this process makes it possible to polymerize the crystal in a solid state while keeping the molecular configuration of the monomer crystal, a polymer crystal with a very high degree of perfection can be obtained. For the future application to nonlinear optical elements, etc., the development of technologies for thin film crystal formation, and joining to other substrates are needed. Also, an accompanying analysis of the real space structure of surfaces and interfaces is becoming indispensable. Here, we will take up poly-PTS (polymerized 2,4-hexadiene-1,6-diol bis (p-toluene-sulfonate) (see Figure 2(a)) and poly-DFMP (polymerized bis-2,2′,5,5′-tetraxistrifluoromethyl-phenyl)

butadiene (see Figure 2(b)) whose bulk structure is known by X-ray structural analysis to be polydiacetylene crystals. We also will report on the result of AFM observation of their cleavage surfaces.

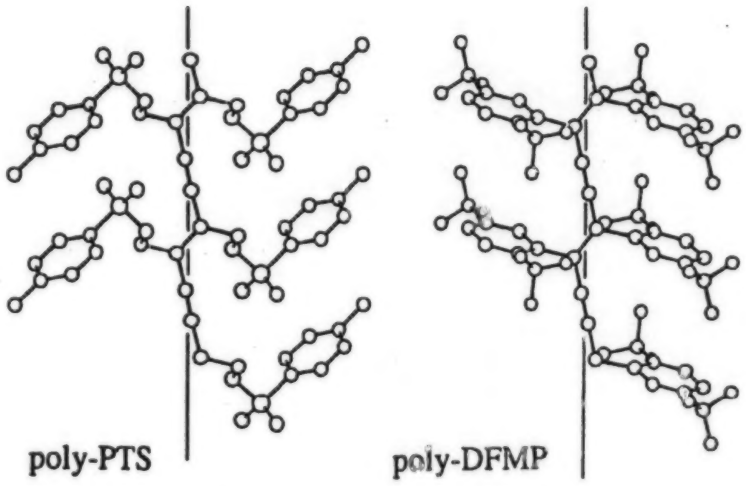

Figure 2. Molecular Structure of Diacetylene Molecule

These samples were obtained by multiple recrystallization, that is, formation into monomer single crystals by slow evaporation at room temperature, followed by solid phase polymerization by γ-ray irradiation. Poly-PTS has a principal polymerization axis in the b-axis direction, and has a toluene-sulfonate substituted group projected in a direction of about 45° with respect to the principal axis as a side chain on both sides of the principal axis. A relatively large plate-like crystal is obtainable, and this crystal can easily be cleaved along the bc face. The sample exhibits a metallic gloss due to polymerization. Its crystal structure is a monolithic system, and its crystal parameters are: a=1.449 nm, b=0.491 nm, c=1.494 nm, and β=118°. An AFM image in the vicinity of the step in the cleavage plane—the bc plane— of poly-PTS is shown in Figure 3. The range of scanning is 12 nm x 12 nm. The bright portions correspond to topographically elevated portions, and the step difference between the bright part on the left and the dark part on the right is about 0.5 nm, which corresponds to the thickness of two molecular layers. The step edge at the center is roughly parallel to the polymerization direction, or b axis, which is consistent with the results of observation by optical microscope. Microscopic inspection reveals a structural disturbance in the step edge near the center of the figure. Also, in the low flat area in the dark part on the left side, there are several microscopically observable defects.

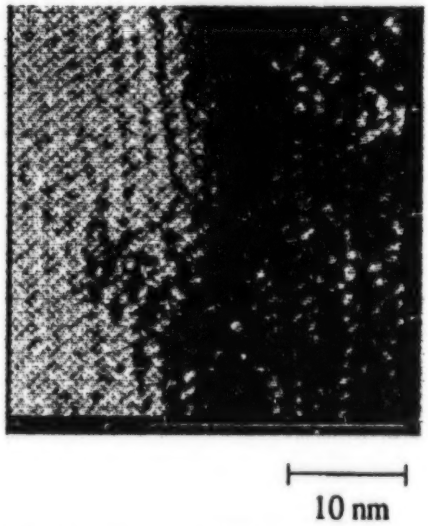

Figure 3. AFM Image in the Vicinity of Step of Poly-PTS Crystal

An AFM image of a micro region within a scanning range of 6 nm x 6 nm in the bc plane of poly-PTS, and a structural model for a bc cross section of the bulk crystal obtained by X-ray structural analysis are shown in Figures 4(a) and 4(b), respectively. The toluene-sulfonate side chain on one side of the principal axis has a structure in which it projects out obliquely upward

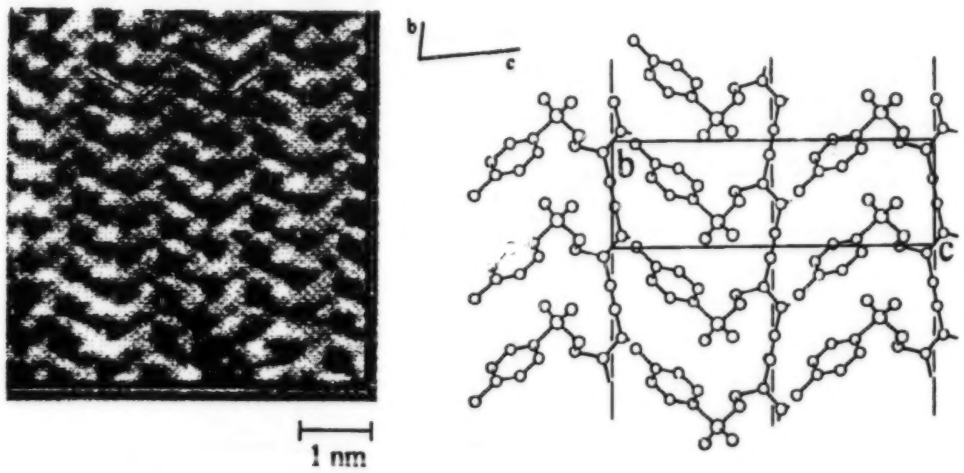

Figure 4.

(coming out of the plane of the paper) with an angle of about 30° with respect to the bc plane. By contrast, the other side chain has a structure in which it creeps underneath the side chain of the adjacent principal chain (it is not observable in Figure 4(b)). Moreover, in the bc projected plane, the side chain is tilted about 45° with respect to the principal axis. Corresponding to this, in the AFM observation image, adjacent principal chains appear as if they have side chains extending in different directions. The unit cell deduced from the AFM observation image is 1.5 nm x 0.5 nm, which agrees approximately with the bulk bc plane structure.

Poly-DFMP, meanwhile, is a molecule in which the conjugate π electron system possessed by the side chain group can be conjugated with the principal chain, and it is expected to have a still larger value of χ_3. It differs from the poly-PTS crystal in that it has a needle crystal several millimeters long and several hundred micrometers wide. Also, it has the ab plane as the cleavage plane, but it was difficult to obtain a clean cleavage plane. A crystal structure model based on an X-ray structural analysis is shown in Figure 5. The bulk crystal structure is a triclinic system. Its crystal parameters are a=0.489 nm, b=0.740 nm, c=12.81 nm, α=96.73°, β=91.84°, and γ = 92.27°.

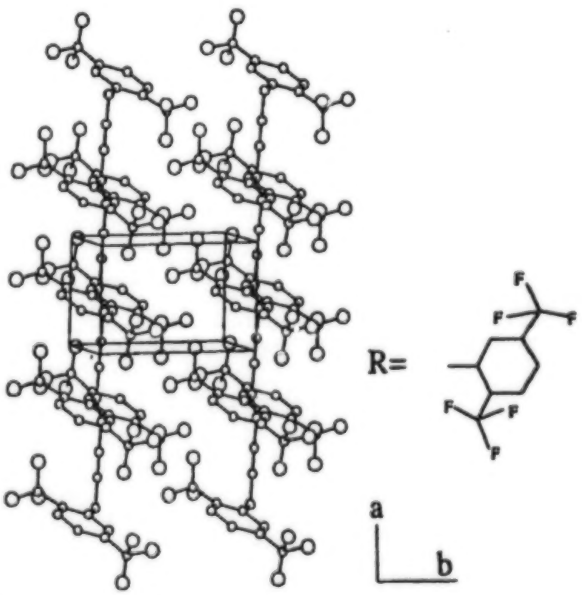

Figure 5. Crystal Structure of Poly-DFMP

Figure 6 is an AFM image of the cleavage plane, or ab plane, of poly-DFMP. The scanning range is 6 nm x 6 nm. For poly-DFMP it was not possible to obtain a clear image as in poly-PTS, but a periodic structure corresponding to the ab

cross section of bulk crystal structure was observed. The observed unit cell was 0.5 nm x 0.75 nm. In the lower central part of Figure 6, a defect can be observed. A periodic structure several times that of the fundamental period was also observed. This is probably due to the imperfect polymerization of the crystals, and singular structure caused by the coexistence with monomer crystals was produced.

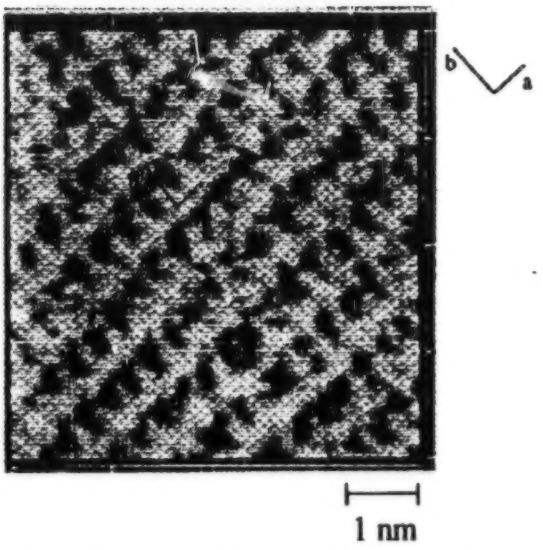

Figure 6. AFM Image of Poly-DFMP (6 nm x 6 nm)

4. Problems in AFM Observation

In AFM observations of organic molecular thin films and biological samples, one often encounters problems such as the impossibility of obtaining data with high reproducibility, the impossibility of obtaining high resolution, and abnormalities in that the initially scanned part of the observation image remains bright (or dark). These problems can be summarized into the following two points:

1) The resolution is not sufficiently high because of an insufficiently small radius of curvature at the tip of the probe.

2) The set force is too high.

The problem of set force can be reduced markedly through noncontact operation. Since, however, all of the high-resolution observations today are obtained by the contact mode, we will discuss the set force only in the case of contact mode. These problems will be further discussed below.

The Problem of Resolution

Apart from the problem of the sensitivity of the displacement measuring system, insufficient resolution seems to be caused by a radius that is too large at the tip of the probe. But, at present, a technology for producing probes having a sufficiently pointed tip with a high degree of reproducibility has not yet been established. However, due to the rapid progress of micromachining technology, the performance of AFM probes produced on the research level has advanced remarkably. We should like to expect the supply of sharply pointed probes produced by batch process in the near future.

Problem of Set Forces

In general, biological samples such as organic molecular thin films, proteins, etc., are not bound strongly to the substrate, and thus the samples are easily deformed by the force of the probe. Accordingly, in AFM observation of such a sample, reducing the set forces becomes a very important problem.

In particular, the most important problem for actual experiments is the presence of large attractive forces, such as the surface tension of the layer of adsorbed water that covers the surface of the probe, and van der Waals force. The repulsive force applied by the tip part of the probe, which can potentially damage the sample, apparently becomes an attractive force because of the shielding by these large attractive forces. One method for avoiding the problem of surface tension is to submerge the entire sample and the lever in a liquid. Thus the influence of the adsorbed surface layer can be avoided since the surface tension is inoperative under water. At the same time, water is a polar liquid with a high dielectric constant, so an underwater scanning mirror is also desirable for reducing the van der Waals force. Since these forces are proportional to the tip radius of the probe, it is necessary to further reduce the radius of curvature in order to decrease these forces. The production of probes with a small tip radius is extremely important, not only for the reason of the resolution, but also to reduce adhesion and the van der Waals force.

5. Future Problems

Concerning the detection process in AFM observation, there remain many unsolved issues related to the problem of the interaction between the probe and the surface of the sample. Regarding the interaction between the probe and the sample surface, research on the dynamic aspects of its microscopic process is progressing vigorously. In this connection, the future progress of experiments using AFM on interactions at the micro level at the interface is eagerly awaited. As mentioned in Section 4, in conducting AFM observations an organic thin film and biological samples, it is necessary to reduce the influence of the measurement forces on the sample, and to develop a cantilever for microforce measurement that has a finer probe in order to improve the spatial resolution.

Since the set force of the AFM probe ultimately is determined by the shape of the tip of the probe, a technology of forming a sharply pointed probe at the tip of the lever is very important.

In addition, for the future observation of organic molecular samples, identification of the molecular species of the samples to be observed is important. Accordingly, the development of an AFM combined with other scanning probe microscopes, which make it possible to effect such positioning, is desirable.

References

1. Binnig, G., Quate, C.F., and Gerber, Ch., PHYS. REV. LETT., Vol 56, 1986, p 930.

2. Israelachvili, J.N., "Intermolecular and Surface Forces," Chapter 7, Academic Press London, 1985.

3. Albrecht, T.R., Akamine, S., Carver, T.E., and Quate, C.F., J. APPL. PHYS., Vol 61, 1990.

4. Akamine, S., Barrett, R.C., and Quate, C.F., APPL. PHYS. LETT., Vol 57, 1990, p 311.

5. Nonnenmacher, M., Greschner, J., Walter, O., and Kassing, R., J. VAC. SCI. TECHNOL., Vol B9, 1991, p 1358.

6. Walter, O., Bayer, Th., and Greschner, J., Ibid., Vol B9, 1981, p 1353.

7. Gould, S., Marti, O., Drake, B., Hellemans, L., Bracker, C.E., Hansma, P.K., Keder, N.L., Eddy, M.M., and Stuckey, G.D., NATURE, Vol 332, 1988, p 332.

8. Overney, R.M., Howald, L., Frommer, J., Meyer, E., and Brodbeck, D., STM'91 Abstracts, 1991, p 265.

9. Weisenhorn, A.L., Egger, M., Ohnesorge, F., Gould, S.A.C., Heyn, S.P., Hansma, H.G., Sinsheimer, R.L., Gaub, H.E., and Hansma, P.K., LANGMUIR, Vol 7, 1991, p 8.

10. Meyer, E., et al., NATURE, Vol 349, 1991, p 398.

11. Yamada, H., Akamine, S., and Quate, C.F., submitted to STM'91 Proceedings.

12. Hansma, H.G., Weisenhorn, A.L., Gould, S.A.C., Sinsheimer, R.L., Gaub, H.E., Stuckey, G.D., Zaremba, C.M., and Hansma, P.K., J. VAC. SCI. TECHNOL., Vol B9, 1991, p 1282.

13. Butt, H.J., Prater, C.B., and Hansma, P.K., Ibid., Vol B9, 1991, p 1193.

14. Radmacher, M., Eberle, K., and Gaub, H.E., ULTRAMICROSCOPY, Vol 42-44, 1992, p 968.

15. Weisenhorn, A., Gaub, H.E., Hansma, H.G., Sinsheimer, R.L., Keldermann, G.L., and Hansma, P.K., SCANNING MICROSCOPY, Vol 3, 1990, p 511.

16. Eng, L.M., Fuchs, H., Jandt, K.D., and Petermann, J., ULTRAMICROSCOPY, Vol 42-44, 1992, p 989.

17. Yamada, H., Okada, S., Fujii, T., Kageshima, M., Kawazu, A., Matsuda, H., Nakanishi, H., and Nakayama, K., APPL. SURF. SCI, 1993, in printing.

18. Weisenhorn, A.L., Hansma, P.K., Albrecht, T.R., and Quate, C.F., APPL. PHYS. LETT., Vol 54, 1990, p 2651.

19. Yamada, H., APPL. PHYS., Vol 59, 1990, p 191.

Observation of Organic Molecules by STM

936C1098B Tokyo JAPAN SURFACE SCIENCE SOCIETY in Japanese 25 Jun 93 pp 9-19

[Article by Masahiko Hara, International Frontier System, Institute of Physical and Chemical Research]

[Text] 1. Introduction--Organic STM and Inorganic STM

Since the appearance of the scanning tunnel microscope (STM), research involving a structural analysis of the surface and the interface showed a remarkable expansion. Over the past several years, many attempts have been made to obtain a real image of organic molecules using STM. However, in the general organic STM, there is not yet available a sufficiently established technique. This is due partly to the fact that the objects to be observed are on the order of individual atoms and molecules, which has never been discussed in detail.

One object (model) that may be used in establishing organic STM as a technique for surface analysis will be an STM that uses inorganic substances as the objects. When one considers why an organic STM has not succeeded substantively, and remains not generally recognized, one has to conclude that organic molecules themselves, in particular in terms of structural analysis, have never been analyzed in terms of a well-defined surface and interface in a clean atmosphere, and under conditions that do not tolerate impurities, as is the case for inorganic semiconductors.

Normally, an ATM is classified according to the category of surface analysis. However, surface analysis itself is a field that grew up having mainly inorganic substance systems as the objects of observation. In that sense, it may be said that the approach itself, in which similar arguments are made from a viewpoint similar to those for inorganic substances, is not quite plausible. In fact, inorganic STM may be described as a field that grew up based on the surface analysis results and methodology accumulated in the past on inorganic substance systems. For organic molecular systems, meanwhile, development has taken place from a somewhat different viewpoint, and it could well be said that it lacks an exact background, such as in inorganic substance systems and arguments, as if finding peaks in an amorphous region, have been given. However, the frontal attack method, to be developed with inorganic STM as one of the goals based on an understanding of the characteristics of organic

molecules, which may seem to be handicaps at first glance (though they offer diverse advantages that cannot be realized in inorganic substances), is one of the important elements to be considered in parallel with an approach based on the arguments and techniques characteristic of organic molecules. In approaching STM from the organic molecule side, we feel that we have been weak in the frontal attack method, namely obtaining an exact background.

A point which needs to be considered in advancing the frontal attack method is that we have to extract from organic molecular systems ideal systems having a two-dimensional ordering of the surface and interface, which have been points of focus in the inorganic substance systems. In this article, we will draw on reports of research on organic STM that were conducted from a viewpoint close to that of inorganic STM, and will consider what kind of substance is needed in order to establish organic STM as a technique. Identifying a characteristic direction of organic STM, which is different from inorganic STM, will become possible only when discussions of such ideal systems, and the development of discussions on organic molecular systems come into contact.

In what follows, for convenience, we will classify organic molecular systems into various dimensional systems. These are: zero-dimensional systems comprising simple form condensed ring molecules that can be obtained by increasing the benzene ring starting from forms closest to inorganic atoms; one-dimensional systems comprising rod-like molecules obtained by extending alkyl chains represented by alkane and liquid crystal molecules; two-dimensional systems comprising surface-like molecules higher than coronene represented by porphyrin and phthalocyanine; and three-dimensional systems comprising solid spherical molecules represented by C_{60}. We will present representative examples of molecular systems that are considered promising for each dimension.

2. Zero-Dimensional Molecular System: Monatomic System to Condensed Ring System

STM observation of a zero-dimensional system, that is, fundamental molecules with simple shapes such as benzene, is positioned closest to inorganic atoms, and is therefore closest to inorganic STM. Examinations of the adsorption of single crystals of zero-dimensional molecules historically have involved primarily the use of low energy electron beam diffraction (LEED) developed by Somorjai, et al., since the 1970s.[1] Information obtained by LEED has been developed in more detail based not only on the adsorbed sites on the substrate, but also on intensity distribution. However, actual specific images have never been obtained by the use of any method.

STM research on the adsorption process of condensed ring molecules has been developed as one of the important fields in general STM research, including inorganic STM, where the research group of Chiang, et al., has reported many detailed results. Of these, STM images of the adsorbed condition of benzene and carbon monoxide on a rhodium (111) plane reported by Ohtani, et al., represent pioneering research in which the molecular adsorption structure that had so far been analyzed only in terms of electron beam diffraction was observed in real space (Figure 1).[2] Chiang, et al., carried out the adsorption

of condensed ring molecules on a single crystal substrate whose surface was revealed in an ultrahigh vacuum, analogous to LEED studies, and succeeded in obtaining real images with a high degree of reproducibility by using an ultrahigh-vacuum STM. In particular, an analysis of the way the molecular images appear due to differences in the superlattice structure in the vicinity of the atomic step in the substrate, or difference in the applied voltage, gives one the impression that they belong to the category of inorganic STM rather than to that of organic STM. These research efforts, which satisfy the fundamental conditions for epitaxial growth (commensurate structure) on a single crystal substrate whose surface is exposed in a clean atmosphere in an ultrahigh vacuum, occupy an important position in the examination of fundamental areas to be clarified in the development of an organic STM. The group is continuing its examination of the adsorption process of condensed ring molecules of naphthalene and beyond, with Hallmark, et al., as the center (Figure 2).[3]

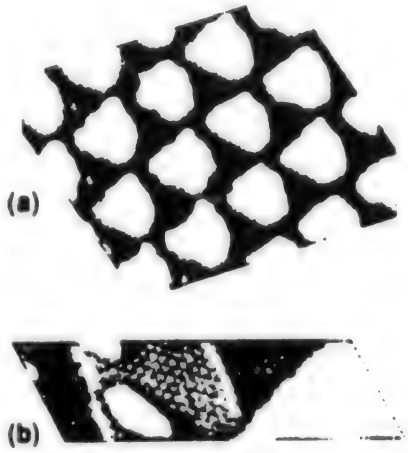

Figure 1. Benzene on Rhodium (111) (Oya, et al.)

In addition, Somorjai is engaged in the study of STM, and has issued a report on the adsorption mode of sulfur atoms on rhenium (Figure 3).[4]

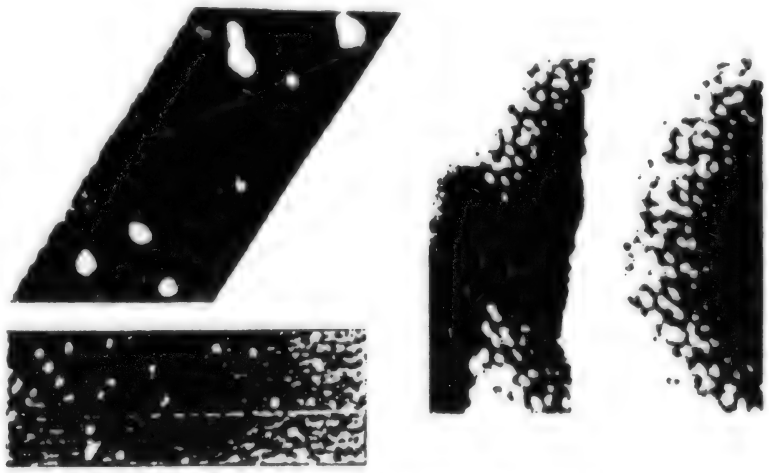

Figure 2. Naphthalene on Platinum (111) (Hallmark, et al.)

3. One-Dimensional Molecular System: Alkane System to Liquid Crystal System

Molecules that are important for organic STM in one-dimensional molecular systems are liquid crystal molecular systems. One reason for this is that the study of the structure (anchoring structure) of liquid crystal molecules in the vicinity of the substrate interface is one of the most closely watched research fields on materials research. Another reason is that, considering specific situations, they belong to one of a few organic molecular systems for which samples having a two-dimensional order, which are most important in STM observation, can be obtained relatively easily by thermal fluctuation of the molecules themselves. Figure 4 shows some examples of the observation of the

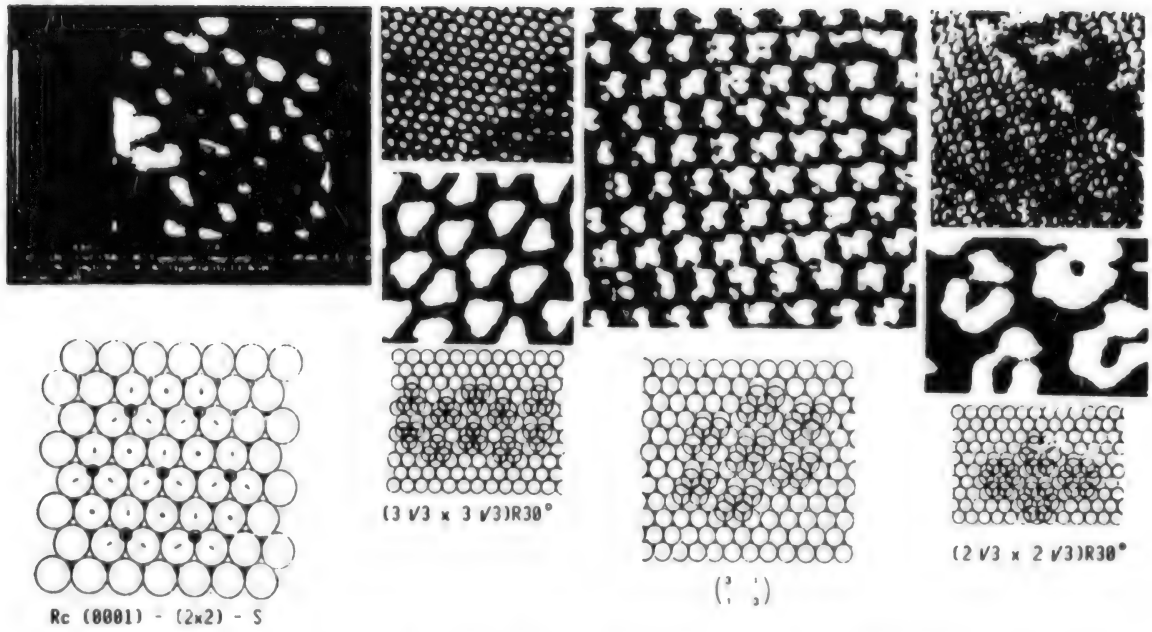

Figure 3. Sulfur Atoms on Rhenium (0001) (Somorjai)

anchoring structure on MoS_2 of cyanobiphenyl molecules of a homologous series in which the length of the alkyl chain is changed from 7 to 12.[5] This liquid crystal molecule series is a system in which molecules are diffused and rearranged in the air on a single crystal substrate cleaved in the air, and is observed by STM in the air. It represents one of a few materials systems in which the relationship between the configuration structure of homologous series molecules, and the bulk phase transition reported by Iwakabe, et al.,[6] and the difference in the formation of configuration structure on different substrates, etc., were examined systematically.

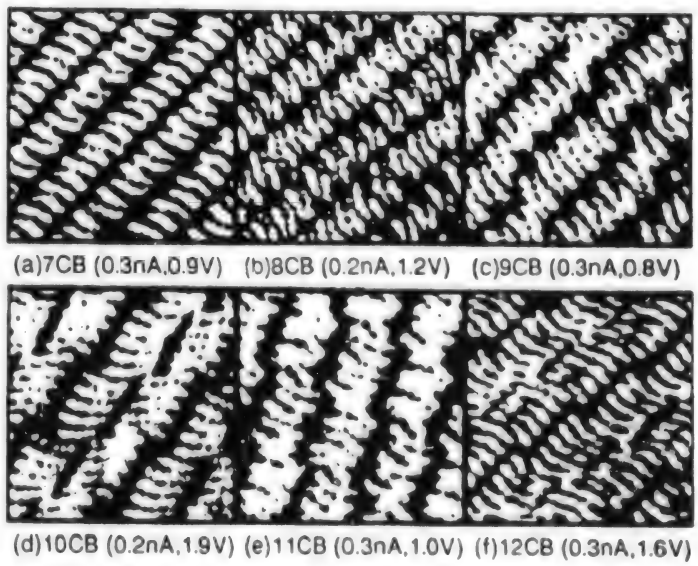

Figure 4. Anchoring Structure of Cyanobiphenyl Homologous Series (Iwakabe, et al.)

One reason this system permits relatively stable observation in spite of being in the air, is because this material system creates not a gas (air)/solid (anchoring structure) interface, but a liquid (isotropic molecular layer)/solid (anchoring structure) interface, and because the isotropic molecular layer creates a clean environment equivalent to a vacuum layer. Even though

samples are actually formed in the air, the configuration is that of a single crystal and annealing, which is an important process in sample preparation, also has a zone refining effect that excludes impurities.

STM images of the alkane system, as seen in the report by McGonigal, et al.,[7] represent a trial of examination based on the registry model on a graphite substrate using simple columnar molecules. These images have been regarded since then as an important one-dimensional molecular system for organic STM. This result not only presents the problem of how the alkyl chain is adsorbed relative to the graphite substrate, but also raises the question of what we are actually seeing in the real images obtained by STM. It is thought that when columnar molecules having many carbon atoms are used, there appears a moire structure in STM images which shows a transition from commensurate to incommensurate relative to the periodic structure of the substrate. A theoretical interpretation of this phenomenon is awaited.

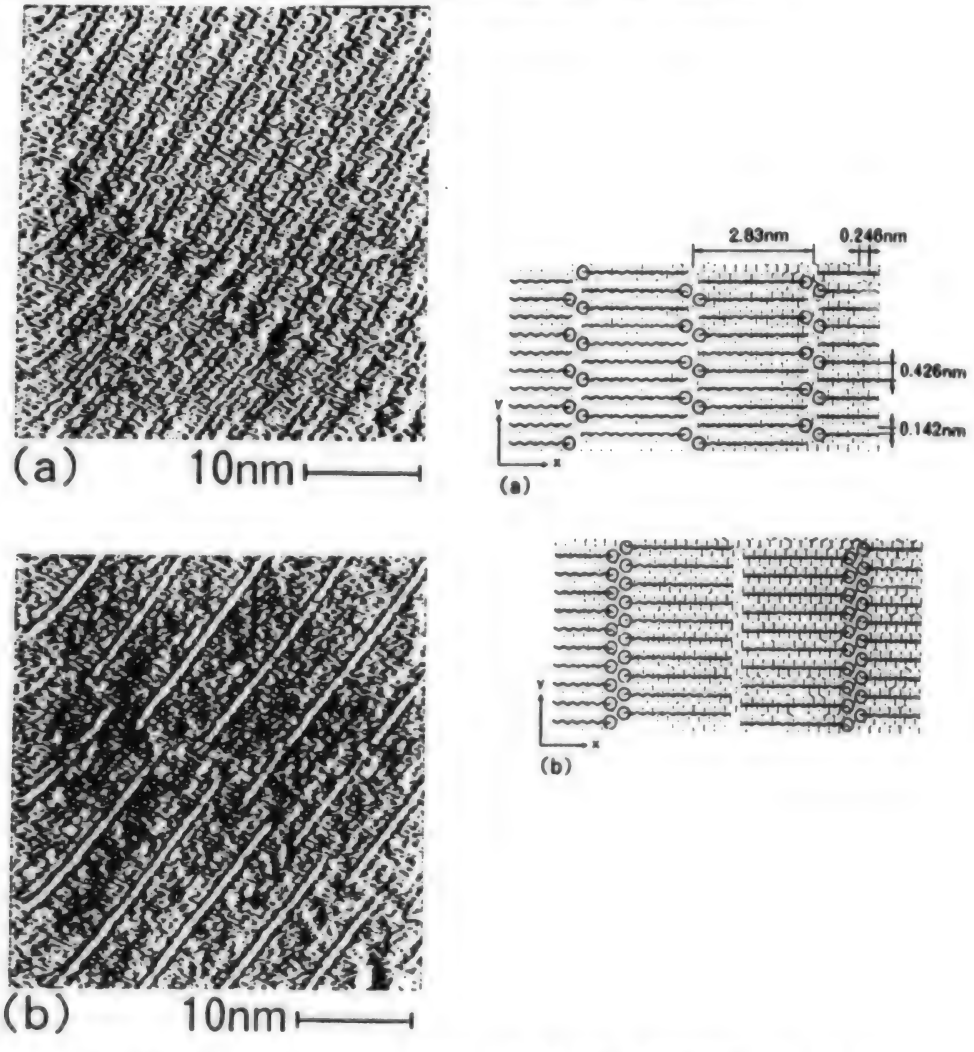

Figure 5. Aliphatic Acid LB Films (Kuroda, et al.)

This alkane system also includes those in which a benzene ring is introduced at an edge or near the center of the molecule. It can be said that this is a system suitable for a fundamental structural analysis similar to that of a zero-dimensional molecular system. Figure 5 shows STM images of aliphatic acid Langmuir-Blodgett (LB) films reported by Kuroda, et al.[8] They claim that the portions that appear as lines on STM images show the configuration at the molecular end. It is said that the LB film constitutes only a molecular layer placed on the substrate by the LB method, and is different from seeing an LB film directly. An important point for the observation of organic STM images will be the adsorption layer formation of a monomolecular level including the LB method. This is because it is difficult to realize the adsorption of a small amount of a controlled organic molecular system, such as in molecular beam epitaxy, which is used for inorganic substances. Although it is a simple problem, it contains an important key to the problem of sample formation that has to be solved in organic STM. In fact, all of the highly reproducible organic STM images reported so far are for systems in which adsorption and rearrangement control of a monomolecular layer were achieved successfully.

In addition, STM image recording of 10~40 screens per second became possible due to improvements in the sweeping rate of STM, and observations close to real time are becoming possible. One-dimensional molecular systems are being used as the object of STM, where dynamic observations, such as the movement of dislocation due to the sliding of molecules, are being tried.

4. Two-Dimensional Molecular System: Phthalocyanine System

A representative substance system for STM of a two-dimensional molecular system is phthalocyanine. This is because configuration control using molecular beam epitaxy in an ultrahigh vacuum, and structural analysis using electron beam diffraction are possible at the molecular level. Figure 6 shows examples of real images of copper phthalocyanine on single copper crystal reported by Wilson, et al.[9] This result was obtained by using the same apparatus as that used by Chiang, et al., for the adsorption of benzene, etc. In zero-dimensional molecular systems, STM images were made and compared with the electronic states anticipated by HOMO-LUMO computations within a molecule by which the internal structure of one molecule was obtained for the first time.

Figure 6. Copper Phthalocyanine on Copper (Lippel, et al.)

Phthalocyanine has a molecule that is relatively stable to heat, and has an interesting functionality. It is used frequently in the so-called organic molecular beam epitaxy. This author's group is performing STM observation by epitaxially growing copper phthalocyanine on the (111) plane of gold formed by molecular beam epitaxy while making in-situ observation of reflected

high-energy electron diffraction (RHEED). Figure 7 shows the commensurate growth on the substrate of individual copper phthalocyanine molecules, where the central metal—copper—can be clearly recognized. A feature of this image is that the organic molecules are depicted as negative images, which is the opposite of conventional organic STM images.

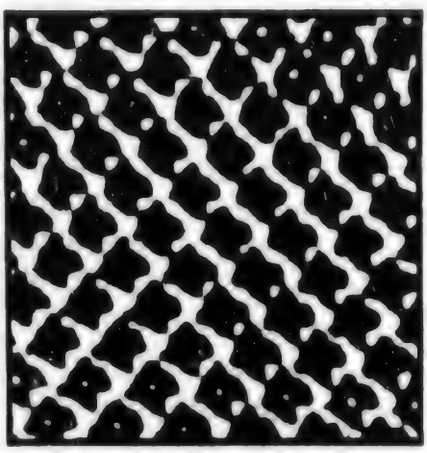

Figure 7. Phthalocyanine on Gold

5. Three-Dimensional Molecular System: C_{60} System

The third allotrope of carbon, Buckminster-Flaren C_{60}, has been attracting considerable interest because of its manifestation of superconductivity, thanks to its geometrical property. It has been an object material for STM for many years, and the first STM images of it were reported by Wilson, et al., using an ultrahigh vacuum STM (Figure 8).[11,12]

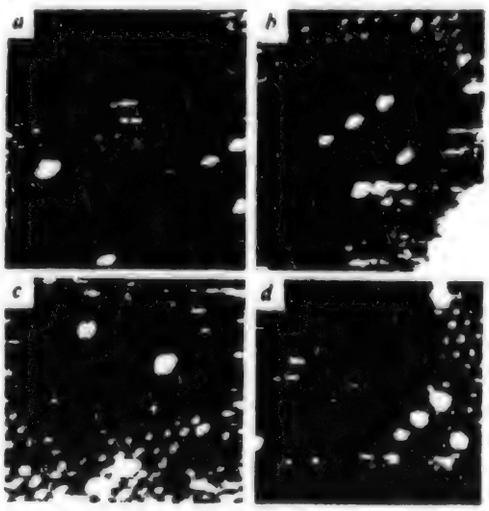

Figure 8. C_{60} on Gold (111) (Wilson, et al.)

Later, the C_{60} molecule was subjected to molecular beam epitaxy in an ultrahigh vacuum, and the study of epitaxial growth on a single crystal substrate was started. The first report was on one to two molecular layer STM images epitaxially grown on GaAs (Figure 9).[13] Subsequently, Sarid, et al., informally announced STM images in which molecular rotation is stopped. To date, however, the STM image of C_{60} reported by Sakurai and Hashizume is one of the best in the field (Figure 10).[14]

6. Future Developments

As noted above, systems with a relatively simple molecular form will be important elements in the future development of organic STM. In particular, it is expected that there are systems that obey the sense of conventional surface analytical techniques in the one-dimensional and three-dimensional molecular systems. For these molecules there is the possibility of obtaining exact solutions that are difficult to realize in general organic STM systems.

However, when one considers STM for broad general organic molecules, we do not think that exact interpretation and analysis such as for the zero- and three-dimensional molecular systems can be obtained in the near future. The fact that exact details are required in the microscopic regions represents the first task in research of organic molecules. Thus, if everything has to be established as in the case of inorganic STM, there is the possibility that what was achievable in the beginning will not be accomplished.

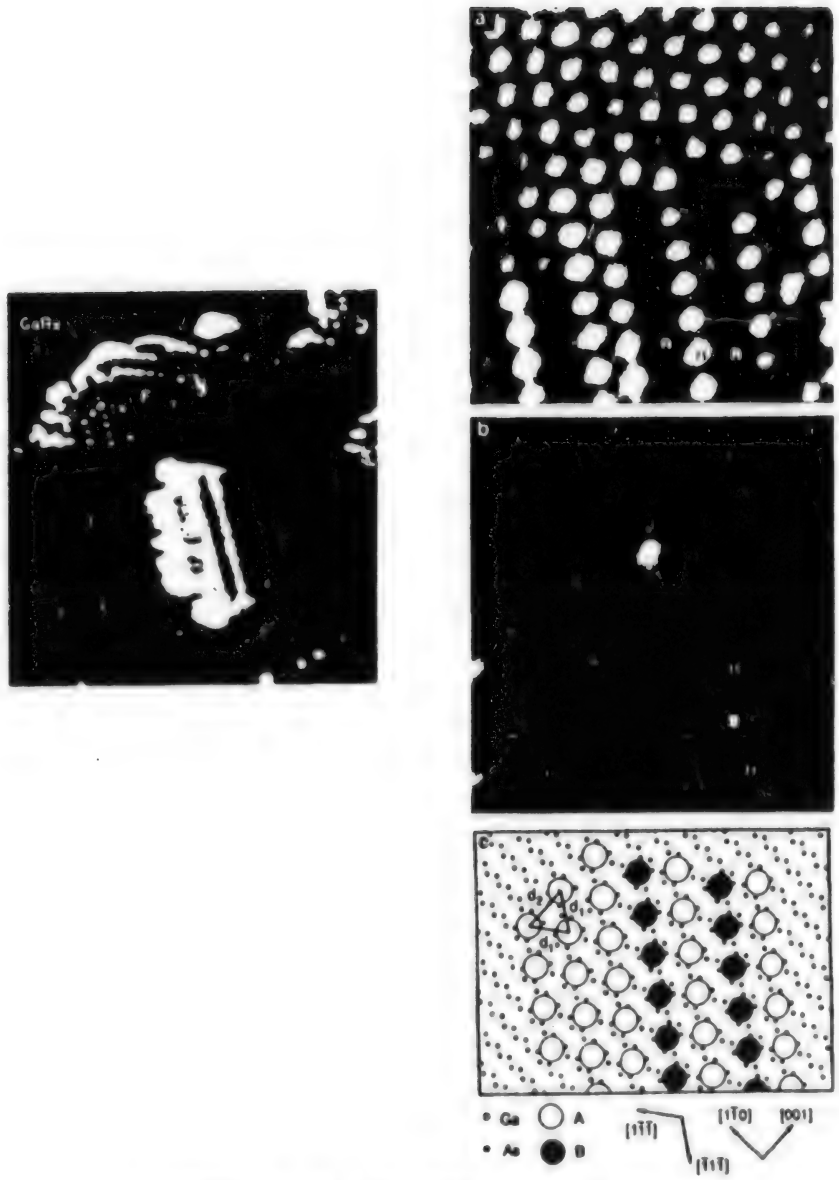

Figure 9. C_{60} on GaAs (Li, et al.)

Needless to say, many problems in organic STM have to be solved, but we feel that it will be possible to develop a methodology in parallel with work on ideal systems and organic molecular systems, while constantly seeking a juncture of the two. Even when an exact interpretation has not been obtained (in fact, it is premature in a worldwide sense in this case) there are many areas in which work can be started. In the history of unestablished techniques, as many new techniques initially were, one can sense the necessity for an era of artifact. It may be said that the era of artifact for organic STM will be completed in several years. We feel that regardless of discussions of ideal systems or organic molecular systems, organic STM should go back once more to the configuration of the samples, and try to find clues for reconsideration by examining the substrate, fixation, commensurate property, epitaxial property, and the like.

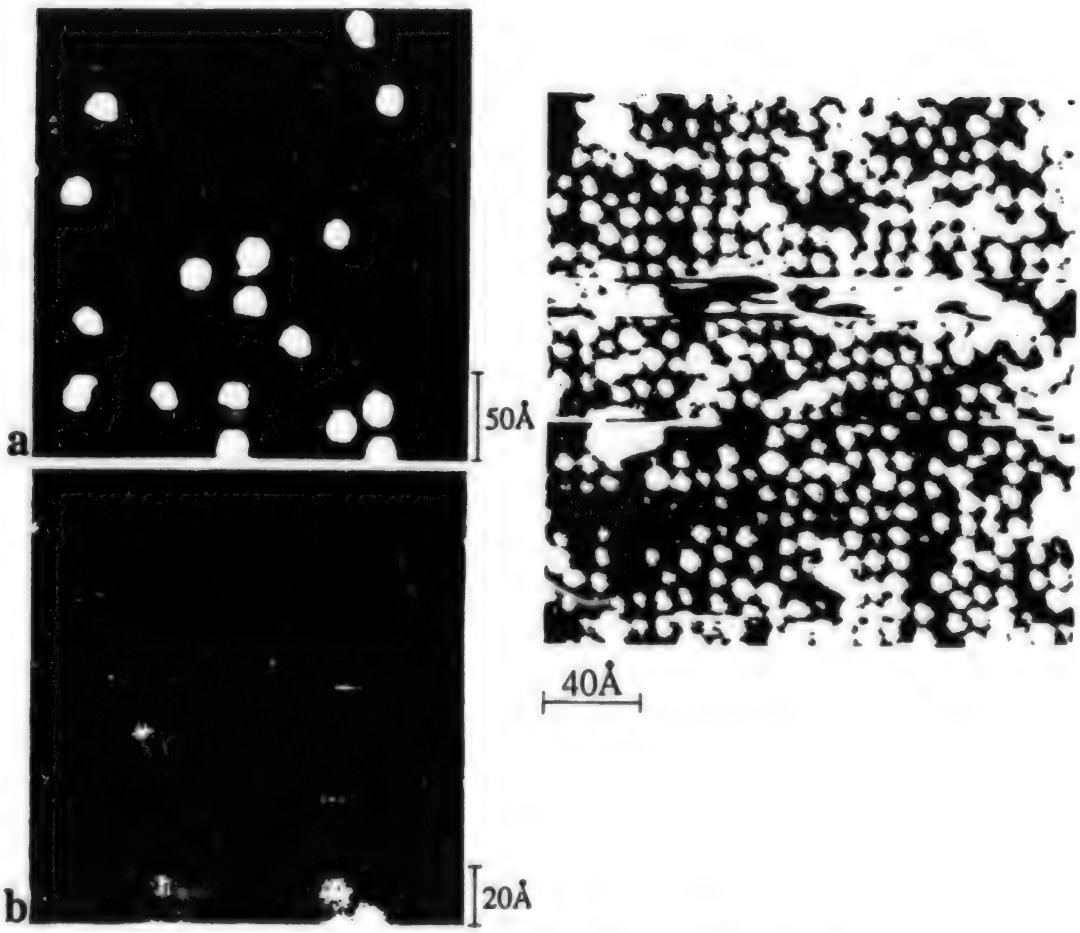

Figure 10. C_{60} on Si(100) (Hashizume, et al.)

References

1. Gland, J.L., and Somorjai, G.A., SURF. SCI., Vol 38, 1973, p 157.
2. Ohtani, H., et al., PHYS. REV. LETT., Vol 60, 1988, p 2398.
3. Hallmark, V.M., et al., J. VAC. SCI. & TECHNOL., Vol B9, 1991, p 1111.
4. Somorjai, G.A., LANGMUIR, Vol 7, 1991, p 3181.
5. Iwakabe, Y., et al., JPN. J. APPL. PHYS., Vol 30, 1991, p 2542.
6. Hara, M., et al., NATURE, Vol 344, 1990, p 228.
7. McGonigal, G.C., et al., APPL. PHYS. LETT., Vol 57, 1990, p 28.
8. Kuroda, R., et al., M. VAC. SCI. & TECHNOL., Vol B9, 1991, p 1180.
9. Buchholz, S., and Rabe, J.P., Ibid., Vol B9, 1991, p 1126.
10. Lipple, P.H., et al., PHYS. REV. LETT., Vol 62, 1989, p 171.
11. Wilson, R.J., et al., NATURE, Vol 348, 1990, p 621.
12. Wragg, J.L., et al., Ibid., Vol 348, 1990, p 623.
13. Li, Y.Z., et al., SCIENCE, Vol 252, 1991, p 547.
14. Hashizume, T., et al., JPN. J. APPL. PHYS., Vol 31, 1992, p 1880.

Scanning Probe Microscope

936C1098C Tokyo JAPAN SURFACE SCIENCE SOCIETY in Japanese 25 Jun 93 pp 21-28

[Article by Hiroshi Miyamoto, principal investigator, Chemical Technology Research Institute, Agency of Industrial Science and Technology]

[Text] **Abstract:** The principle of the scanning tunnel microscope (STM) is simple. The idea is to bring a sharply pointed probe close to a sample, and, when the tunneling current starts to flow, to scan the surface of the sample while controlling the distance to the sample so as to keep the current constant and to record the shape of the sample with a high degree of resolution. The distribution of the electron cloud on the surface of the sample is recorded by scanning the surface while keeping the probe height constant, and monitoring the tunneling current. At this time the space between the probe and the sample may be a vacuum, air, or a liquid. Control of the probe position is maintained by the voltage applied to a piezoelectric element. The great surprise is that a single atom can be seen by such a simple device. In particular, the fact that materials with poor electric conductivity, such as biological samples and organic molecules, were observed by STM shows a great potential for the future of this observation technology. Moreover, the atomic force microscope (AFM), which was developed later, is attracting attention as a microscope that is capable of recording the shape of a sample regardless of its electrical conductivity with a resolution of the order of an atom. Although the resolution of observations of these biological materials is not sufficiently high, observations by STM and AFM have just started, and it is expected that these methods will make marked advances in the future due to progress in the device itself, and to improvements in the methods for preparing samples.

1. Introduction

The tunnel effect—the word twice decorated the stage of the Nobel Prize in physics. The first was the occasion when Esaki, Giaever, and Josephson received the prize for their research on the tunnel effect in 1973. The second was the occasion when Binnig and R[illegible]hrer received the prize in 1986 for their research on the development of a microscope utilizing the tunnel effect that is the subject of this article. That the Nobel Prize was given only 5 years after discovery or invention is unusual, but that the Nobel Prize was given twice for the same principle of natural science is also unusual.

Starting with the success in the development of STM by Binnig and Rohrer in 1981, it became possible to see the arrangement of atoms on the surface of a silicon crystal. And in less than 10 years it was possible to see atoms not only on the crystal surface, but even materials with no electrical conductivity, like adsorbed molecules, and organic molecules such as phthalocyanine and cyanobiphenyl. The ability to see their structure was not anticipated at all in the beginning, but now it was possible to observe them with a resolution far surpassing the original expectation, to the extent that the atomic position can nearly be specified. Stimulated by this move, it was reported that the double helix of DNA, which is a biological substance, and other proteins could be observed. In the past couple of years, the front cover of NATURE carried a series of photographs taken by STM that had a great impact on society.

Following the development of STM in 1981, AFM was developed in 1986. AFM also drew attention as a new microscope that could discriminate one atom in the air. It has been used mainly for the surface analysis of metals and inorganic crystals. Since about 1988 observations of organic molecules and biological molecules by AFM has been active, and AFM images of LB films and biological membranes, DNA, proteins, etc., were published one after another. For proteins, however, resolution better than a nanometer (nm), which is the intrinsic resolution of STM and AFM, has not yet been realized. The development of this technique, which has the possibility of clarifying the three-dimensional structure of proteins, ideally even for a single molecule, would be of great significance not only for clarifying the three-dimensional structure of proteins, but also for probing their dynamic action mechanism.

2. Principle of STM

The STM is designed to measure the surface form of a sample, and the distribution of the electron cloud, by scanning its surface. In doing so, the STM utilizes the phenomenon of electron flow, in which it overrides a potential barrier by virtue of the effects of quantum mechanics, usually the tunnel effect, in a system where the space between two very closely situated electrodes is filled with a vacuum or some kind of dielectric material. In other words, a sharply pointed probe is used as one electrode, and a sample constitutes the other electrode. The probe is brought to a distance of about 1 nm from the sample, and an electric current of several millivolts to several volts is passed between the two electrodes. According to tunnel effect theory, the current flow can be expressed as follows:

$$I = (A\sqrt{\phi}\,V/S)\ \exp\ (-B\sqrt{\phi}\,S)$$

In this expression, V is the bias voltage between the electrodes; S is the distance between the electrodes; ϕ is the work function of each electrode, which is determined by the distribution of electrons in the electrode material; and A and B are constants. From this it can be seen that the tunneling current decreases exponentially with the increasing distance S. Actually, it is said that it decreases by about one-tenth for every separation of 1 Å (0.1 nm). Here, we would like to remind the reader that the tunneling

current, because it is not due to superconductivity, suffers from resistance. Accordingly, Joule's heat is generated along with the flow of the current.

The STM has two measurement modes. One is a constant current mode in which the surface of the sample is scanned while applying feedback to keep the tunneling current constant. The surface form of the conductive sample is measured by recording the displacement in the Z-axis direction at each position of the probe. Biological samples are generally measured by this mode. The other is the mode used for analysis of the surface of a very flat crystal, etc. Here, the sample surface is scanned by keeping the height of the probe in the Z-axis direction constant, and measuring the tunneling current at each position. In either case, scanning with the probe is done by controlling the voltage, ±150~200 V, which is applied in the X, Y, and Z directions of a piezoelectric element. Since a displacement of several nanometers can be controlled by 1 V, the accuracy of the piezoelectric element is sufficient to realize a resolution at the atomic level, and the actual resolution is often determined by the shape of the probe tip, and by the electrical conductivity of the sample.

Another type of measurement mode is scanning tunneling spectroscopy. There is no example of applying this technique to biological samples, but it is possible to measure the local tunneling property of the sample by adding perturbations to the applied bias voltages while carrying out normal STM scanning.

3. Principle of AFM

The AFM was developed by Binnig and Gerber of IBM, and Quate, et al., of Stanford University in 1986. Its principle is similar to that of STM, and it can be said that the AFM is a sister microscope to the STM. The difference is that with the AFM, the molecular force acting between two pieces of matter, instead of the tunneling current, is detected and imaged. In general, when molecules are brought very close to each other, an attractive force represented by the van der Walls force is created, and when they are brought still closer, an opposite repulsive force starts to act. The potential at this time can be represented as a Lennard-Jones potential, as can be expressed as follows:

$$E = \frac{\mu}{S^6} + \frac{\nu}{S^{12}}$$

where μ and η are constants, and S is the intermolecular distance. The force corresponding to this potential is measured from a minute bending in a cantilever. A pyramidal or triangular cone-shaped crystal of silicon nitride (Si_3N_4) 4 μm on a side is attached at the tip of an SiO_2 cantilever as a probe, and the tip interacts with the sample. The bending of the cantilever is detected by receiving the reflected light of a laser beam irradiating the tip by means of a bipartite photodiode. Actually, the sample surface is scanned by feedback control so as to keep the bending constant, and the three-dimensional shape of the sample is determined from the displacement in the Z-axis direction of a piezoelectric element at each point.

In the currently available apparatus, control is possible only to a force of about 10^{-9}N, but the atomic image of even a soft biosample, such as a protein, can be determined in principle if the radius of curvature of the tip of the probe is 1 nm, and if the force applied to the cantilever can be controlled to 10^{-11}N.[1]

4. Technological Underpinning of STM and AFM

The technological developments that made it possible for these scanning microscopes to become available as relatively simple devices, and to make the observation of atomic images a simple process, include: 1) the position control down to 0.1 Å was made possible by the availability of high-performance piezoelectric elements, 2) a control system for measuring the extremely small currents used for patch clamping was developed, 3) the availability of a high-precision cantilever utilizing semiconductor processing technology, 4) the availability of a compact and stable semiconductor laser, and 5) the downsizing of computers and advances in image processing technology, etc. Finally, one might add that the IBM Zurich Laboratory gave free rein to two workers, Binnig and Rohrer, who had been deeply involved in the manufacture of an obscure new microscope, without interrupting their work.

5. What Can Be Seen by STM?

The occasion on which the newly-developed STM demonstrated its full power came when it showed the arrangement of atoms on a silicon crystal surface (111), thereby resolving a long-standing argument concerning its surface structure. In addition, the atomic image of the cleavage face of highly-oriented thermally decomposed graphite, which is frequently used as a substrate on which to place the sample, also can be observed with relative ease. In these cases, individual atoms can clearly be observed in samples that are electrically conductive, have a flat surface, and have a certain degree of mechanical strength. That it is possible to see where lattice defects and deficiencies on the level of individual atoms occur in the sample surface is a remarkable advancement. The surfaces of other similar samples, such as various kinds of semiconductors, metals, and evaporated thin films are being analyzed by STM. What is more surprising is the fact that organic molecules, which do not seem to have much electrical conductivity to begin with, also can be observed by STM.[2] Noteworthy in this regard are 8CB, 10CB, etc., which are cyanobiphenyl liquid crystal molecules; s-MDOPEFB, which is a ferroelectric liquid crystal; BEDT-TTF, which is a kind of organic superconductor; and phthalocyanine. The hydrocarbon chains of these molecules do not have too strong a contrast, but portions with many π electrons, such as phenyl, can be recognized as bright portions. That the biphenyl part of 8CB is seen with two hexagonals linked together is a very impressive sight. Observation of these liquid crystal molecules ordinarily is made by placing a few drops on a substrate such as graphite, and by scanning with the probe dipped in the liquid to see only those molecules that are firmly adsorbed on the substrate's surface. Accordingly, the molecular arrangement changes with different substrates, as has been shown by Hara, et al., of the Institute of Physical and Chemical Research.[3] That atomic images, or images with a similar degree of resolution, of nonconductive or weakly conductive organic molecules could be observed by

the use of STM had a big impact on the observation of biosamples. With new ideas, improved methods of sample preparation, and better measurement conditions, double helix DNA, single helix DNA, left-wound DNA--called Z type--bacteriophage ϕ29, RNA polymerase, tobacco mosaic virus, LB film, microtubules, F-actin, myocin, and phosphotransferase have been measured and imaged.[4] Some of these samples are given a carbon or metallic coating, while others are replica films. Further, some are chemically fixed by some means, or seen as is in a naturally dried condition. In many cases, samples dispersed on a highly oriented graphite are used. However, after it was pointed out that an artifact that looks like a spiral filament might arise due to the fact that the graphite surface tends to make it hard for proteins to be adsorbed there or to some defects,[5] substrates obtained by evaporating gold or platinum on mica, or evaporating metal on glass are being employed. Regarding the observation of biosamples, only in the case of seeing DNA in an ultrahigh vacuum was the resolution close to that of an atomic image.[6] In other cases, it has not been possible to attain such a resolution, and efforts aimed at improvements are in progress. In what follows, we will describe the observation by STM of a replica film of the ripple structure on a phospholipid membrane that was done in our laboratory jointly with a group headed by Professor Yata of the Applied Physics Department, Faculty of Engineering, Nagoya University. We will also describe the observation of unfixed and unstained raw microtubule that was done in our laboratory.

6. Structure of Lipid Membrane

It has long been known that when a phospholipid is dispersed in water, a so-called bilayer structure is formed in which hydrophobic hydrocarbon chains are faced with each other. This structure has been widely studied as a model for biomembranes. In a phospholipid membrane, as the temperature rises from the low temperature side, there appear crystal phase structures (sub-gel phase), gel phase, ripple phase, liquid crystal phase (fluid phase), etc. The transition from the crystal phase to the gel phase is called subtransition (T_s), the transition from the gel phase to the ripple phase is called pretransition (T_p), and the transition from the ripple phase to the liquid crystal phase is called main transition (T_m). Also, a very characteristic ripple structure appears in the Pβ phase between the pretransition and the main transition.[7] In this temperature range, the phospholipid membrane exhibits an undulatory periodic structure with a wavelength of 13~15 nm that resembles the ridges in a field.

This ripple structure has been analyzed by rapidly freezing a phospholipid membrane emulsion sample, obliquely evaporating platinum and carbon on a surface cut at a low temperature, evaporating carbon on top of it as a reinforcement to obtain a replica film, and observing the film with a transmission electron microscope (TEM) (Photograph 1(a)). However, the TEM has a very large focal depth and thus the information obtained is only estimated based on the nonuniform distribution of platinum particles evaporated from the oblique direction. In order to examine the structure three-dimensionally in more detail, the replica image of a frozen cut cross section was observed using STM.[8]

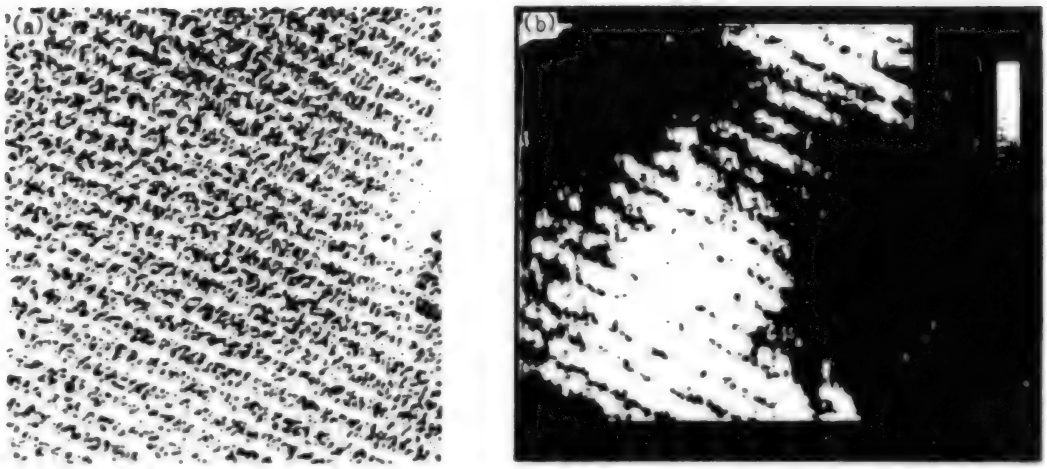

Photograph 1. (a) Electron Microscopic Image of Phospholipid Membrane Showing Ripple Structure
(b) STM Image of Phospholipid Membrane Showing Ripple Structure

DPPC liposome that had been kept at 38°C was rapidly frozen, and shadowing and reinforcing were given after cutting using platinum and carbon. This replica was scooped by a grid for electron microscopy, and observed by TEM. AT the same time, the same grid was fixed by a silver paste to a conductive substrate for observation by STM. At this time, to prepare an ordinary sample for electron microscopy one needs only to scoop the replica floating at the air and water interface from down below with a grid. In this case, however, the surface, which was in contact with the replica sample, comes to the lower side. Therefore, the replica film was scooped from the top down to mount it on a grid for electron microscopy. By so doing, it was possible to observe and compare a single sample by both TEM and STM. The STM observation conditions were a bias voltage on the sample side of +440 mV, a tunneling current of 1.2 nA, and the use of a commercially available platinum-iridium probe. The result of observation by STM confirmed a periodic structure identical to that seen by TEM observation, with an identical pitch, as shown in Photograph 1(b). Information in the depth direction can only be estimated by a TEM. However, the manner in which shadows appear, the depth of ripple grooves, long wavelength undulation on the membrane surface, and fine projections and recesses on the surface can be read from the image produced by STM.[7] The depth of the ripple grooves was 2-5 nm, although there were some local variations. The sample used for the measurement was a replica film made of platinum and carbon, but the STM probe did not discriminate platinum from carbon in terms of conductivity, and the ruggedness of the surface was believed to faithfully reflect the actual shape of the sample. In addition, the replica film was placed on a grid made of copper, but there was no problem regarding conductivity and position fluctuation, and an image with a high degree of reproducibility was obtained.

7. Direct Observation of Microtubule by STM

Microtubules are tubular fiber with a diameter of about 25 nm. Such fibers play an important role in a living body, such as in the morphogenesis of

cells, axonal transport of nerve cells, ciliary movement in protozoa and mucosa, and the division and segregation of chromogenes in cell division. They are formed by protein tubulins, which assemble themselves into tubular fibers with a diameter of about 25 nm, and a molecular weight of about 50,000. One microtubule consists of 13 protofilaments, and its composition unit is a heterodimer consisting of α tubulin and β tubulin with partly different amino acid sequences.

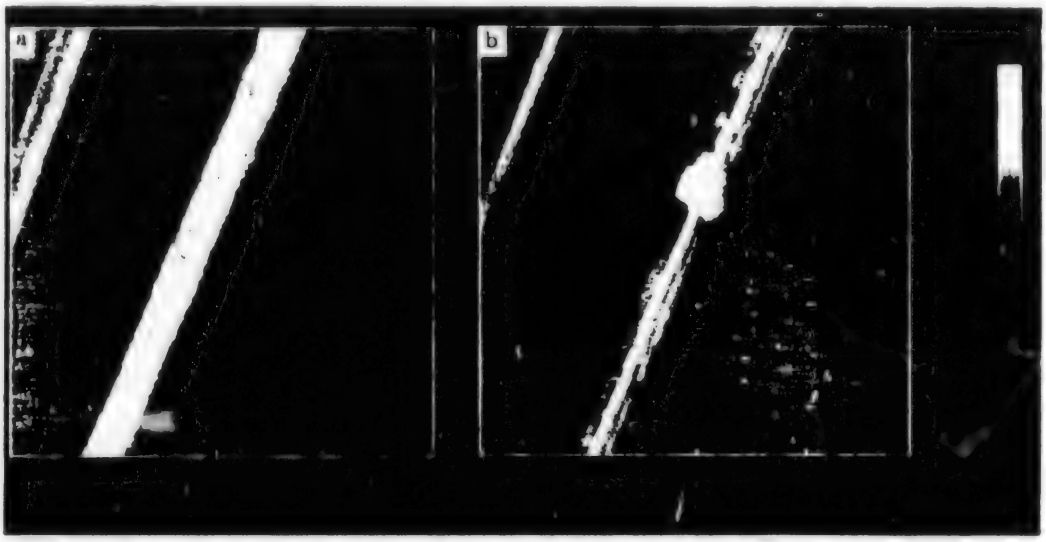

Photograph 2. (a) STM Image of Microtubule Polymerized on Graphite Substrate
(b) STM Image of Microtube Modified and Coaggulated by Electric Pulse

The structure of a microtubule is estimated from TEM observation of a negatively stained sample, or by microscopic observation at extremely low temperatures of an unstained frozen sample.[9] In order to clarify the fine structure of the microtubule, a single microtubule was observed by STM in the air without fixing and without staining. Refined tubulin protein extracted from cow brains was polymerized on a highly oriented graphite substrate to form a microtubule. After washing for 10~15 minutes with ultrapure water twice, it was naturally dried in the air to be used as a sample for observation. Observation conditions were a sample bias voltage of 200~1300 mV, a set tunneling current of 0.5~1.0 nA, and the use of commercially sold platinum iridium as the probe. As a result, a single filament with a thickness of about 30 nm lying straight on the graphite substrate was observed as shown in Figure 2(a). When using a tunneling microscope, steps, flaws, or lattice defects on the graphite substrate often appear in the image as if they were real images of the sample, so it is important to exclude the possibility of such artifacts. In our experiment, during the scanning of the filament the bias voltage between the probe and the sample was suddenly raised to about 5 V, and the same field of vision was observed again by returning the bias voltage to the original value. As a result, the filament under observation shrank to a point, as shown in Figure 2(b), and the original position of the filament showed only a very slight adhesion. Based on this result, we can confirm that

the filament we were observing was not the effect of some kind of defect, but was an easily destroyed piece of matter that is deformed by a small electric pulse. Second, there is a high probability that the filament is a protein since it is deformed by electric pulses, and we can assume that an actual microtubule was placed as the sample. Third, this operation represents a kind of micromanipulation using STM, and shows that it is possible to induce a chemical change in a very small region.

Photograph 3. Enlarged STM Image of Single Microtubule

Not much information can be obtained from the filament in Photograph 2(a) about the internal structure of a single fiber. Photograph 3, however, reveals that fibers lie in the form of one-half of a split cylinder, with several grooves running on the surface in the direction of the axis. This is regarded as the top half of the microtubule, and the size of the total fiber is about 25 nm. A microtubule consists of 13 protofilaments, and six to seven of them on the top side are thought to be arranged in a cylindrical form running parallel along the axis of the microtubule. Summarizing the above, there is no doubt that the image obtained shows the microtubule itself, which consists of proteins.

The STM scans and records an image by detecting tunneling current, so the question why an STM image is obtainable for a collection of proteins which are not conductive, cannot be fully answered at present. One interpretation is that even when a microtubule is naturally dried on the substrate, water molecules may remain in relatively large numbers between the protein molecules, or on their surface, and that these maintain their conductivity.

8. Observation of Biosamples by AFM

The AFM is a scanning microscope similar to the STM. It shows the fine structure of the surface as a three-dimensional image by detecting the force acting between the probe and the sample. It differs from STM in that an AFM makes it possible to observe the surface of crystals or organic molecules with a resolution on the order of an atom, and does not necessarily require a special measurement environment such as a vacuum, as is also the case for STM. Thus a wide range of applications can be considered. The AFM also can produce atomic images of the cleavage face of mica, and the surface of salt, gypsum, and inorganic crystals such as PbTeO. Experiments are being conducted on a large number of biosamples, but the resolution obtained is not very good. These samples include red blood cells, LB films, bacteria bodies, liposomes, bacteriorhodopsin membranes, plasmid DNA, etc., but a resolution that would enable one to discriminate an individual molecule has not yet been obtained.

In the author's laboratory, we have observed several biosamples without fixation of staining, and under conditions close to the live state. We have

succeeded in observing a microtubule, the body of B-coli, a flagellum, the body of thermophilic blue-green algae, and a thylakoid membrane whose photosynthesis function had been extracted and refined from the former.[10] Photograph 4 shows B-coli at the terminal phase of cell division, showing the form of the bacterial body which is about to become two entities. The sample is a K-12 strain of B-coli at the terminal phase of the logarithmic multiplication period which had been washed thoroughly with water and naturally dried on a substrate. A slight undulation on the surface of the body can be seen. It can also be seen that two flagella are growing from the side of the body. The above-mentioned examples of observation are advantageous compared with electron microscope observation, even though the resolution remains somewhat unsatisfactory in that neither fixation nor staining is applied at all, and the observation is done in the air under naturally dried conditions relatively close to the living state. However, the resolution is still not quite satisfactory. The causes for this include the fact that the force of the cantilever is too great to extract the soft and accurate structure of proteins as information, and because observation is done in the air, adsorbed water causes a capillary phenomenon between the cantilever and the sample. This gives rise to a strong force that makes observation with a weak force difficult. Recently, it was reported that Hansma, et al., carried out an AFM observation in water, and obtained a resolution which makes it possible to individually discriminate the head group of the surface of an LB film.[11]

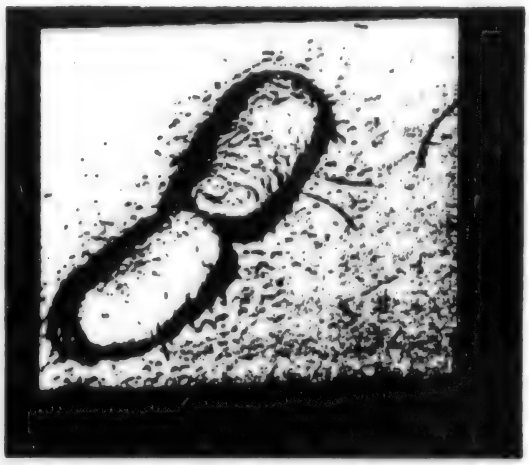

Photograph 4. AFM Image of B-Coli Body and Flagella

9. Conclusion

Immediately after the fine structure of matter became observable with a resolution far surpassing that of optical microscopes due to the invention of the electron microscope, many people tried hard to apply the technique to biological materials. In observing biosamples with electron microscopes, persevering despite various criticisms, we are now seeing the results of our efforts spread before us as we begin to observe biosamples with a higher resolution under conditions closer to natural ones. It is a goal that researchers have sought since the invention of the electron microscope.

When the elemental processes of each and every living body are traced back, all the reactions and changes taking place can be reduced to interactions between atoms and molecules. Thus it would be a very powerful tool to be able to directly observe the behavior of molecules which are alive and functioning, in order to eventually understand the very processes of life. More specifically, it would be a wonderful thing if one could directly observe the cutting of a substrate by an enzyme, the process of DNA duplication by DNA polymerase, and the conversion of chemical energy to mechanical energy by a locomotive

protein. It will also open unlimited possibilities for understanding and finding new applications for life functions. STM and AFM seem to contain the possibility of developing into powerful techniques for that very purpose.

(It should be noted that this article is based on a paper reported in the Special Issue "Functional Structural Design of Life at the Atomic Level" in SCIENCE AND TECHNOLOGY OF JAPAN, Vol 32 No 262, 1991, published by the Japan Science and Technology Promotion Corporation.)

References

1. Persson, B.N.J., CHEM. PHY. LETT, Vol 141, 1987, p 366.

2. Special Issue on Progress of STM (Scanning Tunnel Microscope), CHEMISTRY, Vol 45, October 1990.

3. Hara, M., Iwakabe, Y, Tochigi, K., Sasabe, H., Harito, A.F., and Yamada, A., NATURE, Vol 344, 1990, p 228.

4. Engel, A., ANNU. REV. BIOPHYS. CHEM., Vol 20, 1991, p 79.

5. Clemmer, C.R. and Beebe, T.P., Jr., SCIENCE, Vol 251, 1991, p 640.

6. Driscoll, R.M., Youngquist, M.G., and Baldeschwieler, J.D., NATURE, Vol 346, 1990, p 294.

7. Hatta, I., PARITY, Vol 02, 1990, p 560.

8. Miyamoto, S., and Miyamoto H., BIOPHYSICS, Vol 30 No 3, 1990, p 590.

9. Mandelkow, E.M. and Mandelkow, E., J. MOL. BIOL., Vol 181, 1985, pp 123-135.

10. Azumi, R., et al., CHEM. LETT., 1991, p 1925.

11. Weisenhorn, A.L., et al., LANGMUIR, Vol 7, 1991, p 8.

Measurement of Self-Assembled Monolayer by Nonlinear STM, STM/FM

936C1098D Tokyo JAPAN SURFACE SCIENCE SOCIETY in Japanese 25 Jun 93 pp 41-48

[Article by Wataru Mizutani, National Institute for Advanced Interdisciplinary Research]

[Text] **Abstract**: Various local probe methods were applied to investigate local electronic and mechanical properties of self-assembled monolayers (SAM) formed on gold (111) surfaces. Characteristic depressions of 3~7 nm in diameter and 0.2~1.0 nm deep were found in scanning tunnel microscope (STM) images of the SAM. A high-resolution constant current image of the SAM shows periodic structures with the molecular spacing expected from the sulfur adlattice on the gold surface.

A combined STM/scanning force microscope was used to measure force and compliance together with the constant current topography. The three measured data sets were used to compensate for the mechanical deformation of the layers induced by the probe, indicating that the depressions are mechanically induced by the probe due to the reduction of conductivity.

Tunneling current response to vertical modulation of the probe, dI/dz image shows rows rotated by 20 degrees from that in the STM image, and with wider spacing. In the depressions, the ordered structures disappear in both images.

A combined STM/surface harmonic instrument was used to measure nonlinear properties of the SAM. The ratio of current versus generated third harmonic signal changes little in the depressions, suggesting that the electron transfer mechanism is the same as that for the flat part of the film. It is proposed that the molecular packing is loose and disordered in the area, reducing the electronic conductance and hence appearing as the depressions in the constant current STM images.

1. Introduction

Organic thin films are materials that have diversified applications since they exhibit a variety of electronic, optical, chemical, biological, and mechanical properties. In particular, self-assembled monolayers (SAMs) have a fundamentally very interesting film formation process together with practical utility, for example, for controlling surface properties by changing the functional

group at a terminal part of the molecule. The physical properties of SAMs are being studied by such techniques as infrared spectroscopy, contact angle, ellipsometry, X-ray photoelectric spectroscopy, and second harmonic generation. In addition, the order of molecular arrangement within the film is being clarified by computer simulation.

In recent years, the local properties of a film at the molecular level are being studied by local probing methods such as the scanning tunnel microscope (STM). For example, as will be described in detail later, in an STM image of a SAM prepared on a gold surface, one can observe a characteristic recessed structure with a diameter of 3~7 nm and a depth of 0.2~1 nm which is not observable when a gold substrate alone is examined. This is in addition to the monatomic steps and screw defects of the underlying gold substrate, as shown in Figure 1(a). By way of explanation, various theories have been proposed. These include, for example, a hole in the film, a structure caused by a mismatch in the disposing of the gold substrate and molecules, a point at which part of the gold in the substrate is dissolved into the solution during film formation, and a deformation due to structural changes (kink, trans, gauche, etc.) in the molecular interior.

In order to investigate the internal structure of a SAM, we will consider the recess on the surface of a SAM based on measurements taken from many angles, using STM/force composite microscope (STM/FM), the current-gap characteristic (dI/dz), and microwave nonlinear STM.

2. Experiment

2.1 Sample Preparation

A SAM can be produced by a soaking gold (111) substrate in a solution for one to two days. The substrate is obtained by vacuum-evaporating gold on cleaved mica to 200 nm, and the formation of a flat terrace having a monatomic step is observed by STM. The atomic image of gold, and a $23 \times \sqrt{3}$ reconstructed long period structure are also observed. The solution used is an 0.2 mol 11-mercaptoundecanol ($HS-(CH_2)_{11}-OH$) ethanol solution, and a monolayer is formed by the bonding of sulfur occupying one end of the molecule and gold. After taking out the substrate, it was washed with a solvent, and dried by blowing argon gas on it. The contact of a drop of water on the surface of the produced film was very small, showing that the surface is covered with hydrophilic OH group.

After drying, the sample was observed immediately by STM in the air.

2.2 STM/FM

In a measurement made with a commercially available AFM, the characteristic recessed structure was not observed, and when the scanning region was broadened, film elements pushed aside by the probe were observed deposited in the periphery of the previously scanned region. The fact that these deposits disappeared as the scanning continued led us to conclude that normal AFM operation destroys the film.

In order to carry out a simultaneous measurement of the mechanical properties of the sample surface, an AFM cantilever and probe with a high degree of rigidity (150 nN/m) was coated with gold to enhance its electrical conductivity, and it was devised so as to permit the measurement of the force (f) exerted on the probe by controlling the tunneling current. In addition, compliance (df/dz) was also measured by oscillating the sample in the z direction. In the STM operation, if the tunneling current is reduced (50 pA), f can be brought into the attractive region without spoiling the lateral resolution. In this case, the measured attractive force is considered to be a local one due to capillary force, but the fluctuation of the magnitude of the force from one place to another is nearly equivalent to the resolution due to the tunneling current. This fact suggests that the measured force is the result of a nearly constant large attractive force and a small repulsive force that acts locally at the tip of the probe.

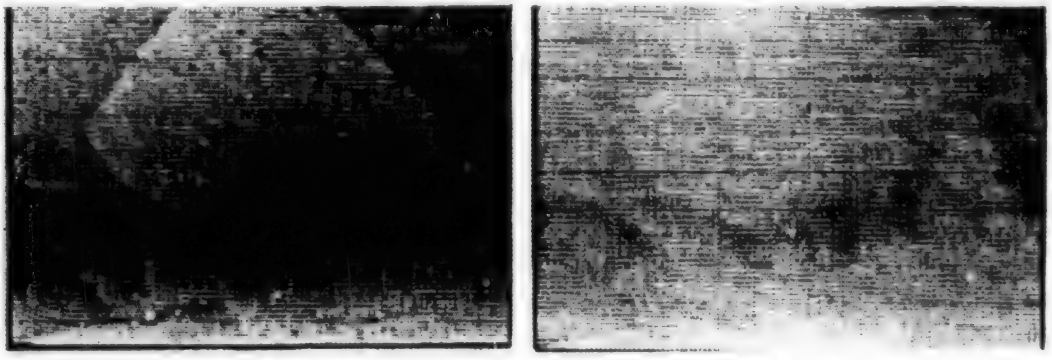

(a) (b)

Figure 1. Examples of SAM Measurement by STM/FM

(a) Constant current STM image, 150 x 100 nm. 100 pA, 0.5 V sample +). In addition to monatomic step due to underlying gold substrate, screw defects, a characteristic recessed structure with a diameter of 3~7 nm and a depth of 0.2~1 nm can be seen.

(b) Image of (a) corrected by determining film deformation from force (f) and compliance (df/dz) measured at the same time. The step of the underlying gold substrate remains, but the recessed structure is gone.

Figure 1(a) is a constant current STM image of a SAM. In the recessed structure, f increased but df/dz remained approximately constant. It is possible to correct the deformation of the film generated by the measurement using f and df/dz, which are measured on the assumption that the attractive force is constant. The result of the correction showed a flat surface free from any recessed structure, as shown in Figure 1(b).

2.3 STM and dI/dz Measurement

The image of a SAM with the best resolution was obtained with a simple STM that does not use a cantilever. In our experiment, the STM image was obtained by the constant current mode, and dI/dz was measured simultaneously by

oscillating the probe in the z direction at 50 kHz. The width of the oscillation of the probe (dz) was 0.05 nm, and the corresponding current variation (dI) was recorded simultaneously with the STM image using a lock-in amplifier. When dI/dz is measured in this manner, it contains electronic information on the work function of the surface, as well as mechanical information on the form of surface deformation generated by the oscillation of the probe.

Figure 2(a) is an STM image showing an enlargement of the SAM surface, and part of the recessed structure can be seen in the lower right-hand part. The pattern seen in the part of the surface other than the recessed part can be explained as sulfur atoms arrayed on the gold (111) surface, and molecules are all arrayed in a transconfiguration.

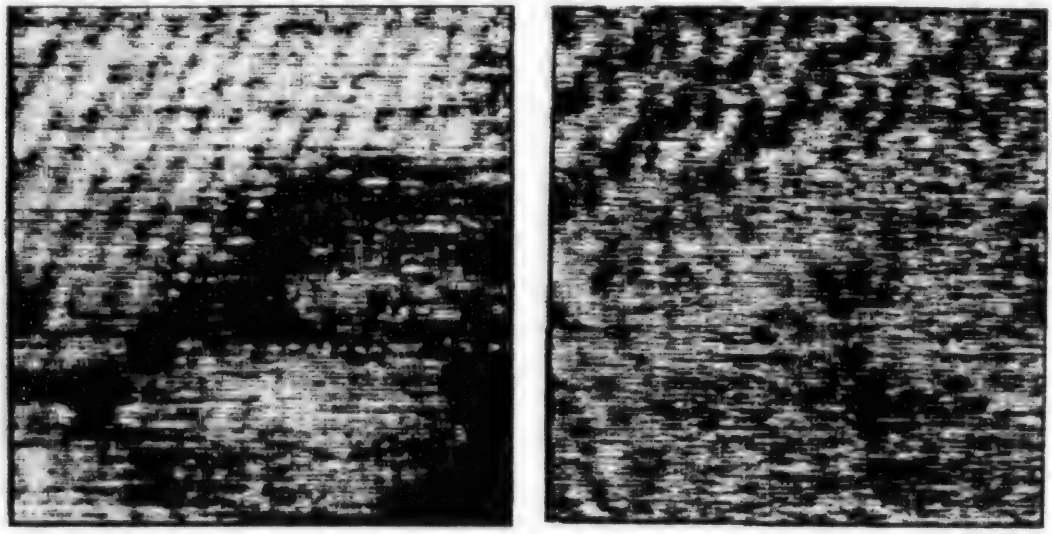

(a) (b)

Figure 2. Surface of SAM

(a) Constant current STM image. 6 x 6 nm. Part of the recessed structure is seen at the lower right. Measurement conditions: 300 pA, 0.3 V (sample +). Gray scale of height is 1 nm. The spacing of 0.41 nm of the periodic structure at the upper left corresponds to molecular strings.

(b) dI/dz image measured simultaneously. Period of the upper left structure is 1.1 nm, and is tilted by 20° from the structure in (a).

Local variations of dI/dz measured simultaneously are shown in Figure 2(b). The periodic line structure seen in this image has a broader spacing than, and is inclined by 20 degrees to, that seen in Figure 2(a). In both Figures 2(a) and (b), the periodic structure disappears in the recessed structure, but there is no change in the signal intensity for dI/dz.

2.4 Nonlinear Microwave STM

By arranging a sample and a probe in the interior of a microwave resonator, and using an STM to measure the local nonlinearity of the surface, the third harmonics (THs) signal generated by the molecules within the gap can be measured. Microwaves at a frequency of 900 MHz were applied to the sample, and the 27 GHz resonance frequency signal from the resonator was taken out by an antenna. The gold substrate itself has a weak nonlinearity, and almost no TH signal was detected when a gold probe was used. However, the TH signal increases when covered by a SAM. This suggests that the nonlinearity was generated either by the adsorbed molecules or the interface.

Figure 3(a) is a SAM image obtained by holding the TH signal, instead of the tunneling current, constant. The tunneling current at this time has a large value of about 10 nA, but a recessed structure similar to that obtained in the case of controlling by the tunneling current was observed.

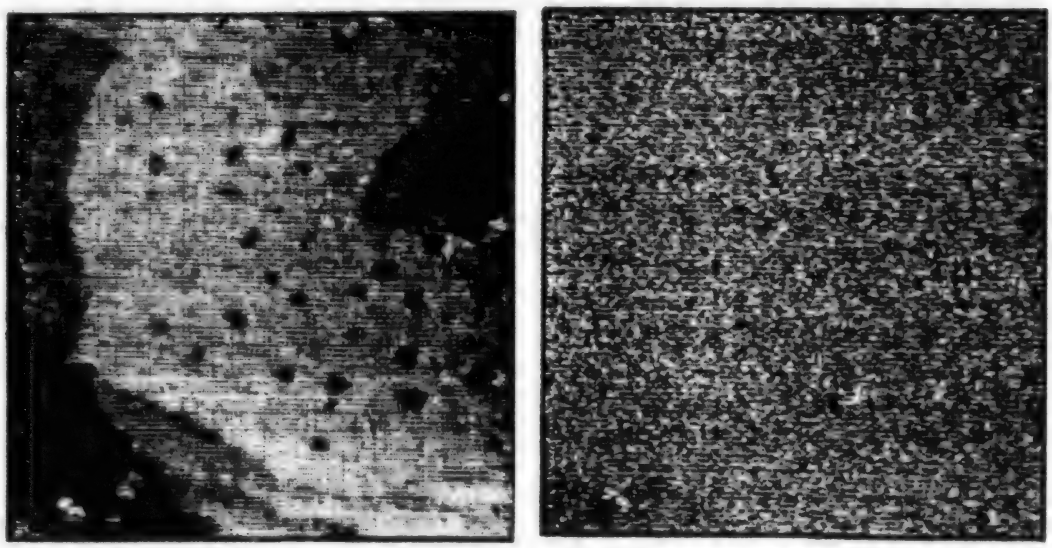

(a) (b)

Figure 3. Measurement by Nonlinear STM

(a) Image obtained by scanning with TH signal kept constant. 80 x 80 nm. 900 MHz, 1.3 Vp-p, dc bias 0.1 V applied. TH signal level is −134 dBm (4×10^{-17}W). Depth of recess is 0.5-1.0 nm.

(b) Image by dc current measured at the same time as (a). Current level is about 10 nA without change even in the recessed part.

Figure 3(b) is the simultaneously measured dc current, but there is hardly any change in the recessed part. In other words, above the recessed structure the dc tunneling current does not change if the TH signal is kept constant. Based on the model which shows that a higher harmonic current is generated from the nonlinearity of the I-V curve, and is radiated to the interior of the resonator using the probe as an antenna, it can be said that there is no change in the third order component of the I-V relation within the recessed structure. Note, however, that among the SAM structures there are some which change their nonlinearity locally.

3. Discussion

Among the possible explanations mentioned at the beginning of the recessed structure, structural changes within the molecules such as kink, transposition, and gauche can be excluded, since a similar structure is also found in films that use mercaptoethanol ($HS-(CH_2)_2-OH$) which has a smaller molecular length. Moreover, what is important is the fact that, based on the results of STM/FM measurement, the recessed structure was created by the approach of the probe due to the electrical property, namely, the phenomenon of electrical conductivity, of the film. In other words, in reality this structure is not depressed. Thus it can be said that it is neither a hole in the film nor a depression in the base. Furthermore, in the nonlinear STM measurement there is no change in the nonlinearity, and it can be assumed that there is no essential change in the conduction mechanism. Thus the possibility of it being a hole in the film or a structure due to impurities is rather low.

The line-form periodic structure observed in the high resolution STM image of the SAM surface can be said to correspond to the molecular arrangement in the film. The difference in the spacing and the direction of the periodic structure seen in the dI/dz image led us to generate a model in which the OH groups at the terminals of molecules form by hydrogen bonding a superstructure in which four to six molecules are bound together, resulting in an increase in mechanical rigidity. If it is assumed that electrical properties do not change at this time, one can argue that apparent differences appear without corresponding changes in the current image.

An irregularity in the molecular arrangement is observed within the recessed structure. This means that the molecules are loosely packed. These experimental results can be explained by a model in which the conductivity of the film depends on the density of the molecules, the nonlinearity is little changed by the density, and the recessed structure is a deformation generated by the approach of the probe. It is brought about by the phenomenon of a tunneling current generated by the change in the molecular density of the film.

4. Conclusion

Using STM/FM and dI/dz measurements, and a microwave nonlinear STM, the local electric and mechanical properties of the SAM surface, in particular the recessed structure, were assessed. Based on the results of the measurements, a model was proposed in which no change in the thickness of the recessed structure occurs, but the density is low due to irregularities in the molecular arrangement of the film. As a result, during STM measurement, the probe comes nearer due to a lack of ease in the flow of the tunneling current.

Acknowledgements

This research was done at IBM's Zurich Laboratory jointly with B. Michel and D. Anselmetti. For the preparation of self-assembled monolayers, the cooperation of H. Wolf of Mainz University is appreciated. Much advice and many ideas on the analysis and interpretation of data were offered by Ch. Gerber and H. Rohrer, to whom the author is very grateful.

This article is based on the contents of Reference 19. Regarding the figures used here, approval was granted by the publisher.

References

1. Laibinis, P.E., Whitesides, G.M., Allara, D.L., Tao, Y.T., Parikh, A.N., and Nuzzo, R.G., J. AM. CHEM. SOC., Vol 113, 1991, p 7152.

2. Bain, C.D., Troughton, E.B., Tao, Y.J., Evall, J., Whitesides, G.M., and Nuzzo, R.G., Ibid., Vol 111, 1989, p 321.

3. Bain, C.D., Biebuyck, H.A., and Whitesides, G.M., LANGMUIR, Vol 5, 1989, p 723.

4. Buck, M., Eisert, F., Fischer, J., Grunze, M., and Träger, APPL. PHYS., Vol A53, 1991, p 552.

5. Siepmann, J.I., Thesis, "Physical Chemistry," Robinson College, Cambridge, 1991; Siepmann, J.I. and McDonald, I.R., MOLECULAR PHYSICS, Vol 75, 1992, p 255.

6. Häussling, L., Michel, B., Ringsdorf, H., and Rohrer, H., ANGEW. CHEM. INT. ED. ENGL., Vol 30, 1991, p 569.

7. Widrig, C.A., Alves, C.A., and Porter, M.D., J. AM. CHEM. SOC., Vol 113, 1991, p 2805.

8. Kim, Y.T. and Bard, A.J., LANGMUIR, Vol 8, 1992, p 1096.

9. Edinger, K., Gölzhäuser, A., Wöll, Ch., and Grunze, M., "Abstracts of Raster-Nahfeld-Mikroskopien and Organische Materialien," Martinsried, 1992, p 12.

10. Anselmetti, D., Gerber, Ch., Michel, B., Rohrer, H., and Güntherodt, H.J., REV.SCI. INSTR., Vol 63, 1992, p 3003.

11. Anselmetti, D., Gerber, Ch., Michel, B., Wolf, H., Güntherodt, H.J., and Rohrer, H., submitted to PHYS. REV. LETT.

12. Travaglini, G., Rohrer, H., Amrein, M., and Gross, H., SURF. SCI., Vol 181, 1987, p 380.

13. Anselmetti, D., Erdelen, Ch., Häussling, L., Michel, B., Mizutani, W., Ringsdorf, H., Wolf, H., and Yang, J., submitted to LANGMUIR.

14. Kochanski, G.P., PHYS. REV. LETT., Vol 62, 1989, p 2285.

15. Seifert, W., Gerner, E., Stachel, M., and Dransfeld, K., ULTRAMICROSCOPY, Vols 42-44, 1992, p 379.

16. Michel, B., Mizutani, W., Schierle, R., Jarosch, A., Knop, W., Benedickter, H., and Rohrer, H., REV. SCI. INSTR., Vol 63, 1992, p 4080.

17. Mizutani, W., Michel, B., Schierle, R., and Rohrer, H., submitted to APPL. PHYS. LETT.

18. Krieger, W., Suzuki, T., and Völcker, M., PHYS. REV., Vol B41, 1990, p 10229.

19. Mizutani, W., Anselmetti, D., and Michel, B., "Local Probe Investigation of Self-Assembled Monolayers," in "Computations for the Nano-Scale," edited by P.E. Bloechl, A.J. Fisher, and C. Joachim (Proc. NATO ARW on Computations for the Nano-Scale, Aspet, France, 12-16 October 1992) (Kluwer Academic, Dorrecht, in press).

Development of Photon Scanning Tunneling Microscope

936C1098E Tokyo JAPAN SURFACE SCIENCE SOCIETY in Japanese 25 Jun 93 pp 49-57

[Article by Motoichi Ohtsu, Research Institute of General Science and Engineering, Tokyo Institute of Technology]

[Text] 1. Introduction

A widely known representative property of light is the fact that, "it propagates in free space, and does not exist localized in a region with a dimension smaller than its wavelength." Let us consider instrumentation and control of objects using such "ordinary" light. First, in an optical microscope, a representative device for measurement, the measurement limit in the observation of fine objects, the resolution, is determined by the diffraction property of the microscope. Because of this diffraction limit, images of objects smaller than the wavelength cannot be observed. This is due to the above-mentioned spatial nonlocal property of light. It is well known that microscopes that employ electron beams instead of light are used in order to obtain a better resolution, and that resolutions at the atomic level have been realized in recent years by the scanning tunnel microscope (STM), which makes use of tunneling electrons.

Next, let us consider control, especially control of the motion of an object. That light possesses a force is confirmed by the fact that the tail of a comet that passes near the sun flows away from the sun. By using this force, deceleration, capture, etc., of particles, atoms, and ions by laser beams have been tried in recent years.

It has recently become known that novel techniques for measurement and control are possible by the use of different forms of light contained in a minute space rather than the ordinary light. This light is called evanescent light according to traditional optical terminology. It is said that an idea about a measuring method using this light was noted by Einstein in a letter to one of his friends, but so far no rigorous theory describing the entity of the light has even been presented. In this article the author would like to present the results of research in this unexplored field, which he has found to be challenging.

2. Measurement Using Evanescent Light

Light radiated from the surface of an object includes evanescent light, which exists localized on the surface of the object, in addition to the ordinary light mentioned at the beginning. Evanescent light has the property that "it does not propagate in free space, and exists localized in a region with a dimension smaller than its wavelength." Therefore, it is possible to measure the shape of an object by preparing the topography of scattered light power when the evanescent light localized on the surface of a minute object is scattered while scanning with an optical probe, as shown in Figure 1.

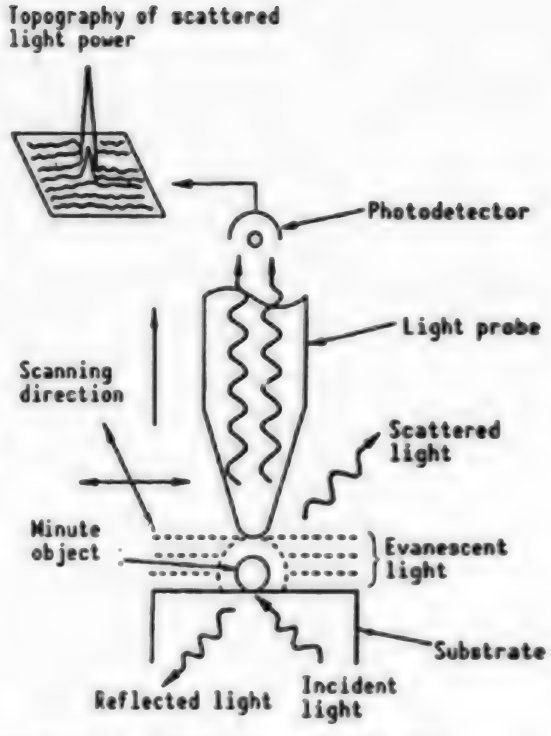

Figure 1. Principle of Photon Scanning Tunneling Microscope

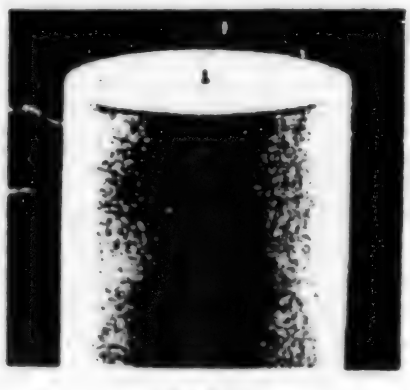

(a)

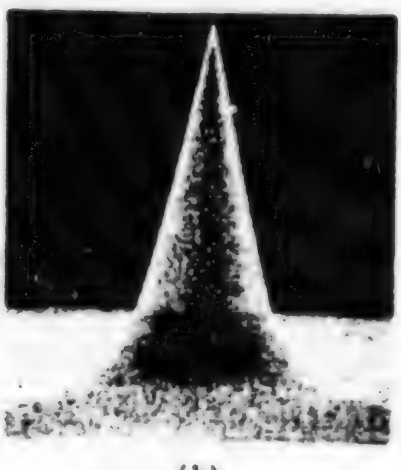

(b)

←Figure 2. Electronmicrograph of Optical Fiber With Sharpened Core Center
(a) General view of optical fiber end. Outer diameter: 90 μm.
(b) Enlargement of tip part. Width of the photograph corresponds to 5.6 μm.

Since the resolution is determined by the size of the tip of the light probe, it is possible to realize an ultrahigh-resolution optical microscope that far exceeds the diffraction limit of ordinary light if the tip size can be made smaller than the wavelength of the light. This is the principle of the photon scanning tunnel microscope (STM).

For an actual optical probe, it is important that reproducibility, which is related to the sharpness of the tip, be high, and that the scattered evanescent light can be guided and condensed efficiently.

In order to achieve this, the author and his collaborators are using optical fibers like those used in optical communications. An example of an electron micrograph of the tip of an optical fiber processed by chemical etching using a hydrofluoric acid solution is shown in Figure 2. We have achieved a conic angle for an optical fiber core, and the minimum value of the radius of curvature of the tip is less than 20 and 5 nm, respectively.[8] This method of using optical fibers makes it possible to realize a resolution that is about one order of magnitude superior to that of the conventional method,[9] which uses a pipette, etc.

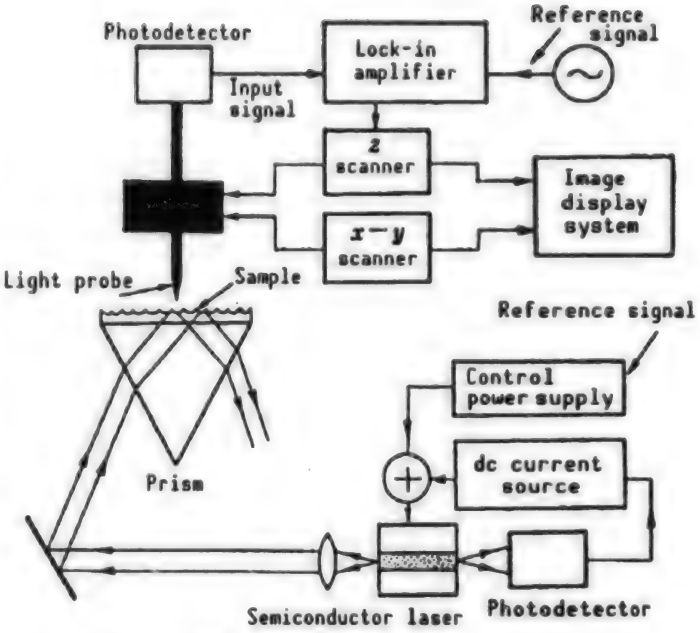

Figure 3. Photon STM Apparatus

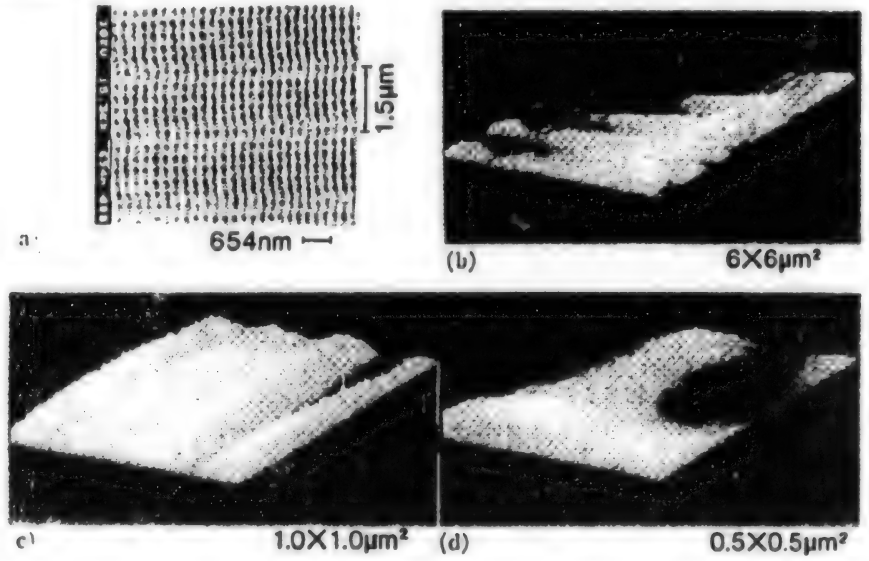

Figure 4. Measurement of Surface Shape of Butterfly-Type Optical Disk
(a) Measurement by electron microscope. (b)-(d) Measurement by photon STM. Numbers at lower right are longitudinal and lateral lengths.

Figure 3 is a block diagram of the measurement apparatus used by the author's group.[10] A semiconductor laser with a wavelength of 0.8 μm is used to ensure the compactness and high reliability of the device. Figure 4 is the result of the surface measurement of a butterfly-type optical disk with a diameter of 300 nm and a depth 80 nm placed at the intersections of an orthogonal grid with periods of 1.5 μm and 0.22 μm.

Figure 5 shows an image in which two T4 bacteriophages with a head diameter of 100 nm, a tail width of 9 nm, and a length of 100 nm are observed in the air.

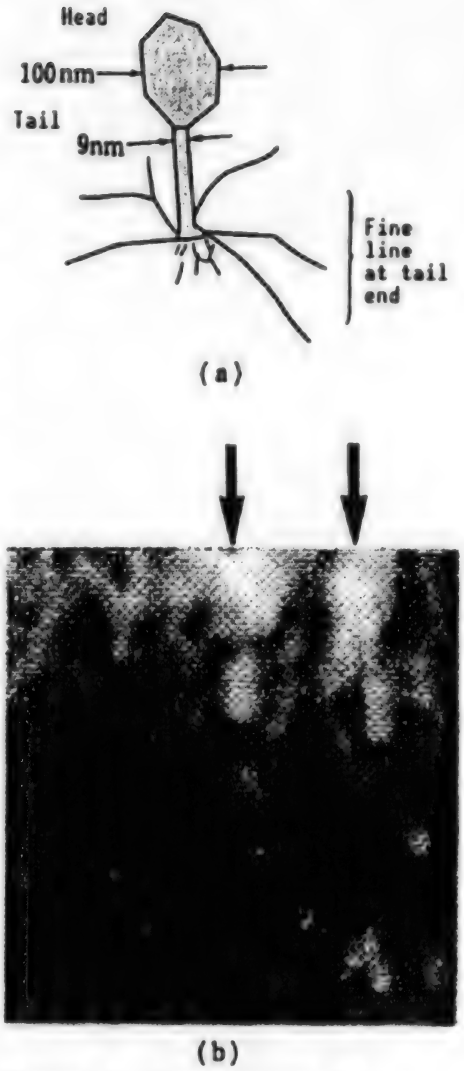

Figure 5. Measurement of Bacteriophage T4
(a) Diagram for explaining the shape
(b) Measurement of result
Images are seen at tips of arrows. One side of photograph is 0.6 μm

Both images were taken in the air in a non-contact and nondestructive manner. From a series of these experiments it is estimated that the resolution in the sample direction is less than 2 nm, and the resolution in an in-plane direction is less than 5 nm. Although these resolutions are limited by acoustic vibrations and temperature drifts of the optical probe, it should be possible to reduce these values to 0.1 nm if these influences can be reduced by future system improvements, and if resolution determined by optical detection noise can be achieved. In other words, a resolution on the atomic scale level can be expected. The basis for this expectation will be described in the next section.

3. Resolution of a Photon STM

Let us consider the case when a minute object to be measured having a radius far smaller than the wavelength of light is placed on a substrate. According to Heisenberg's indeterminacy principle $\Delta x \cdot \Delta p \sim h$ (h is Planck's constant), the field of evanescent light generated in the vicinity of the minute object has a spread of $\Delta x \sim a$ and a momentum of $\Delta p \sim h/a$. Since this momentum is parallel to the surface of the minute object and is greater than the momentum of ordinary light, the momentum in the normal direction is imaginary according to the dispersion relation. In other words, evanescent light cannot propagate in free space, and is localized in the vicinity of dimension $a \ll \lambda$ of the minute object. If one regards the field of evanescent light having a complex momentum as a virtual photon (heavy photon) having a Compton wavelength corresponding to the size of the minute object, and if one represents its propagation using the Yukawa potential, not only is understanding the phenomenon facilitated, but also it becomes possible to estimate the field of the evanescent light by omitting the perturbation calculations concerning many-body interaction.

The distribution of evanescent light is called the "wave function of the evanescent field" having a complex momentum. In order to obtain a photon STM

image by detecting scattered evanescent light in the vicinity of the minute object, the following conditions have to be satisfied:

(1) That a mutually matching component exists in the wave function of the evanescent field of the minute object and that of the optical probe.

(2) The component spread beyond the wave function of the evanescent field of the minute object should not be scattered.

In order to satisfy these conditions, the following restrictions have to be imposed on the shape of the optical probe to be used in a photon STM:

(A) That the radius of curvature at the tip of the optical probe be as small as the radius of the minute object.

(B) That the conical angle at the tip of the optical probe be sufficiently small.

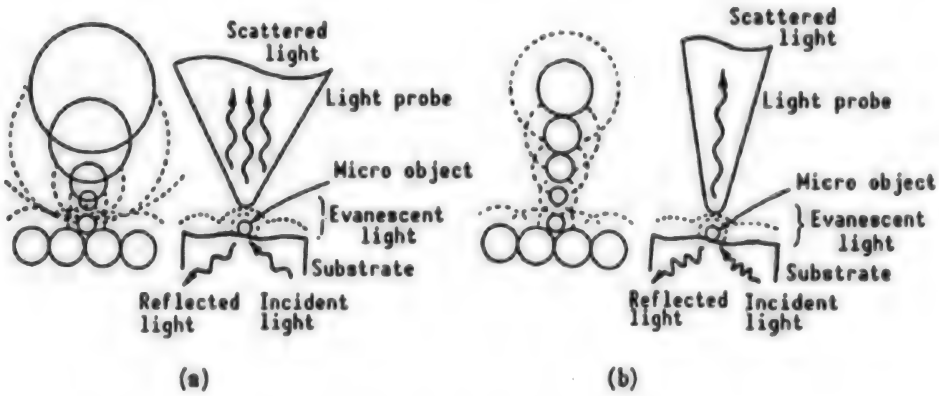

Figure 6. Explanation of Resolution of Photon STM

Parts (a) and (b) denote cases where a large and a small light probe is used, respectively. Schematic picture on the left side of each part is an explanatory diagram in which the micro object to be measured, substrate, and light probe are regarded as collections of minute spheres.

Condition (A) corresponds to (1) above. It shows that the evanescent light of the minute object can be scattered efficiently at the tip of the optical probe, and is converted to an ordinary light component. Condition (B) corresponds to (2). It shows that the evanescent light expanded corresponding to the roughness of the substrate surface is not scattered because it does not match the wave function of the evanescent field for the thick part of the optical probe. This can readily be understood if the optical probe is regarded as a collection of minute spheres with different diameters (Figure 6). In other words, matching the wave functions corresponds to the momentum consecration law in the tunneling process between the minute object and the tip of the optical probe.

From the above conditions it can be seen in order to obtain the high level of resolution that is necessary not only does the radius of curvate of the tip have to be small, but also the conical angle must be small. In order to satisfy conditions (A) and (B) the most effective method available at present is to sharpen the optical fiber by chemical etching. If an optical probe satisfying conditions (A) and (B) is swept while keeping a distance on the order of the tip radius, the component of evanescent light with a small attenuation distance generated by the still finer structure on the surface of the minute object will not be scattered, either. As noted above, a photon STM is a device that selectively extracts, like a bandpass filter, a component having a fineness that corresponds to the radius of curvature of the tip of the optical probe from among the spatial frequencies of the fine unevenness of the surface of the object to be measured, and its resolution is determined by the radius of curvature and the conical angle of the tip of the optical probe. If the tip of the optical probe can be observed by enlarging the tip of the optical probe, what determines the smallest degree of unevenness is the size of an atom. Accordingly, if the tip of the optical probe and the surface of the minute object are brought to a distance on the order of atoms, a resolution at the atomic level can be realized.

The measurement apparatus described above is also called a near field microscope.[11] As is clear from the discussion, this piece of apparatus utilizes light that is bound to the surface of an object and is localized, having a resolution that is determined by Heisenberg's uncertainty principle. It is similar to the STM in that it uses tunneling electrons. Therefore, the author and his collaborators call it a "photon STM."

4. Control of Movement of a Single Neutral Atom

By going one step further from the measurement as described in the preceding sections, we will try to process a new material by controlling the motion of the minute object. As mentioned in Section 1, the capture of a minute object by using ordinary light already has been realized, but this applies only to a collection of neutral atoms, an ion, or a particle whose size is of the same order or greater than the wavelength of the light, and the capture of a neutral atom has not yet been achieved. In this section we will show that it is possible if one utilizes an optical probe like that shown in Figure 2.

As illustrated in Figure 7, evanescent light is made diffuse out from the tip of an optical probe placed in vacuum. At this time, a neutral atom that came flying in a direction tangential to the tip with a velocity v loses momentum and is decelerated by the recoil effect at the time of collision with an evanescent photon due to the large tangential component of momentum possessed by the photon. The velocity after deceleration v_m (=h/2ma, where m is the mass of the atom) is estimated to be several tens of centimeters per second. With this velocity, the atom executes a gentle Brownian motion along the surface of the tip of the optical probe. The atom also receives a dipole force due to evanescent light power, which rapidly decreases in the axial direction of the optical probe. When the light frequency is smaller than the atomic resonance frequency, the atom receives this in the form of an attractive force toward the direction of the surface of the optical probe. Meanwhile, the atom also

receives a repulsive force due to the centrifugal force from the Brownian motion. Due to the equilibrium of these two forces, the atom is captured in a state where it is levitating at the tip of the optical probe. The position of capture is where the rate of change of the light power is the maximum, that is, where z = a. In addition, since the spread of the wave function of the evanescent light is less than several tens of nanometers, multiple atoms will not be captured in such a small region, because of the repulsive force among atoms.[12]

Even when the energy of the incident light on the optical probe is as low as 10 mW, the density of the evanescent light power per unit cross-sectional area is larger than 100 W/cm^2, and a deep capture potential is formed. Figure 8 shows the result of calculations of the relationship between the optimum value of the radius of curvature of the fiber

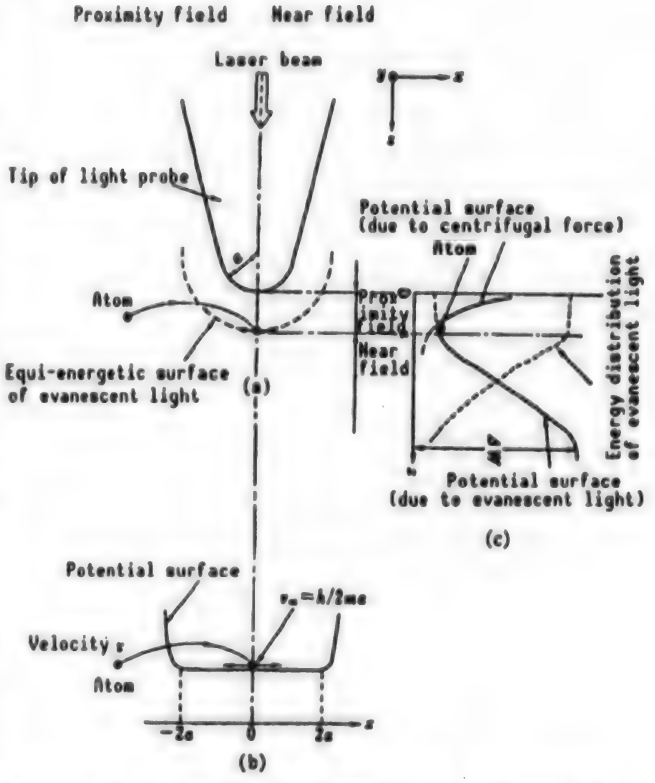

Figure 7. Explanatory Diagram for Single Neutral Atom Capture by Evanescent Light at the Tip of the Light Probe

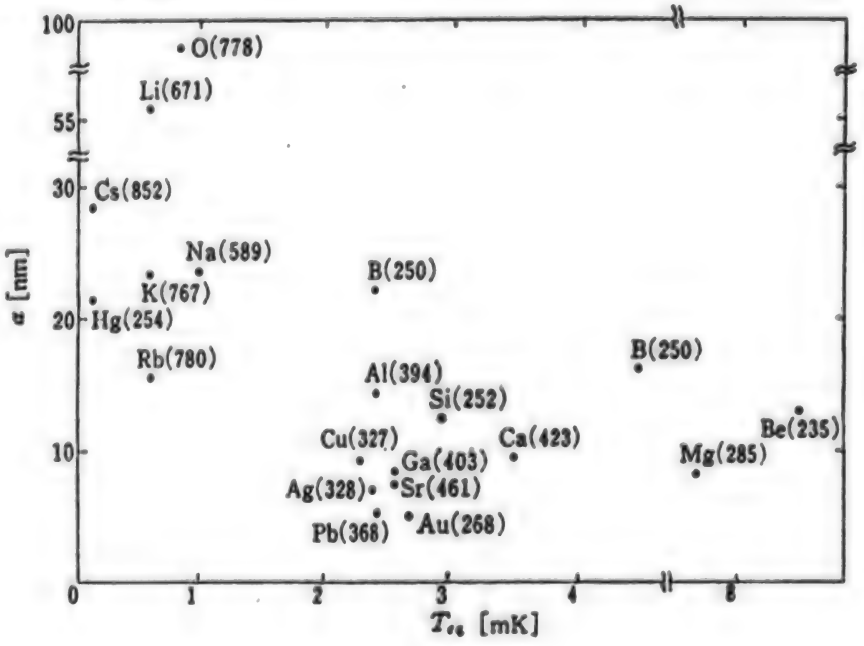

Figure 8. Equivalent Temperature T_{eq} Representing Potential Depth for Capture of Various Atoms and Calculated Value for Optimum Value of the Tip Radius of Curvature of a Light Probe
Numbers in ( ) are wavelength in nm of light used.

tip for the capture of various kinds of atoms, and the equivalent temperature T_{eq} (W/k_e where k_e is Boltzmann's constant) representing the depth of the capture potential.[12] Although these equivalent temperatures are several tens of milli-Kelvin, it can be seen that these potentials are sufficiently deep since a single atom can be captured from a collection of atoms that are precooled to several micro-Kelvin. It is estimated that atoms can be captured at the rate of one about every second if one waits with the optical probe for atoms that come by in free fall from such a precooled collection of atoms. For example, silicon atoms can be captured if one uses an evanescent light with a wavelength of 252 nm, but a coherent laser source containing these various kinds of wavelengths can be supplied by our laser beam frequency sweeping system.[13]

After capturing the atoms, by shifting the optical frequency to a value higher than the atomic resonance frequency, the dipole force can be changed to a repulsive force to the atom, so the atom can be pushed out and heated. By blowing the atom onto a substrate and cooling it with the van der Walls force or some other chemical binding force, crystal growth at the monatomic level becomes feasible.

In addition, ultrahigh-density optical recording in photon mode, manipulation of bioparticles, driving micromachines, etc., will become possible by utilizing the large energy density and force possessed by evanescent light.

5. Conclusion

Research on measurement and control by photon STM is being advanced based on Japan's superior optical fiber technology and laser technology. This research should lead to the creation of new forms of photons localized in space, and new forms of micromatter by measurement and control on atomic level using the photons, and, further, to the birth of microcrystal technology. However, in order to execute this research, it is necessary to escape from conventional optical theory, and to deal with fundamental problems based on field theory, the theory of elementary particles, etc., to construct a new scientific system of "microspace local optics."

References

1. Shimizu, "Laser Cooling and Its Peripheral Technology," APPLIED PHYSICS, Vol 60 No 9, 1991, pp 864-874.

2. Ohtsu, "Coherent Photon Engineering," Asakura Publishing House, 1990.

3. Ohtsu, "Photo Scanning Tunneling Microscope," CATALYST, Vol 32 No 8, 1990, pp 548-550.

4. Jiong, Tomita, and Ohtsu, "Photon Scanning Tunneling Microscope," OPTICS, Vol 20 No 3, 1991, pp 134-141.

5. Ohtsu, Jiang, and Ohsawa, "Movement Control of Single Atom by Light," JOURNAL OF PRECISION TECHNOLOGY, Vol 19 No 8, 1991, pp 839-848.

6. Ohtsu, "Movement Control of Single Atom by Light," Ibid., Vol 58 No 3, 1992, pp 410-414.

7. Hori, "Photon Scattering Tunneling Microscope and Its Theoretical Interpretation," APPLIED PHYSICS, Vol 61 No 6, 1992, pp 612-616.

8. Jiang, S., Ohsawa, H., Yamada, K., Pangaribuan, T., Ohtsu, M., Imai, K., and Ikai, A., "Nanometric Scale Biosample Observation Using a Photon Scanning Tunneling Microscope," JAPAN JOURNAL OF APPLIED PHYSICS, Vol 31 No 7A, 1992 (in press).

9. Redick, R.C., Warmack, R.J., and Ferrel, T.L., "New Form of Scanning Optical Microscopy," PHYS. REV. B., Vol 39, 1989, pp 767-770.

10. Jiang, S., Tomita, N., Ohsawa, H., and Ohtsu, M., "A Photon Scanning Tunneling Microscope Using an AlGaAs Laser," JAPANESE JOURNAL OF APPLIED PHYSICS, Vol 30 No 9A, 1991, pp 2107-2111.

11. Fischer, U.Ch., Durig, U.T., and Pohl, D.W., "Scanning Near Field Optical Microscopy in Reflection or Scanning Optical Tunneling Microscopy," SCANNING MICROSCOPY, Vol 3, 1989, pp 1-7.

12. Hori, H., Jiang, S., Ohtsu, M., and Ohsawa, H., "A Nanometer-Resolution Photon Scanning Tunneling Microscope and Proposal for Single Atom Manipulation," TECHNICAL DIGEST OF THE 28TH INTERNATIONAL QUANTUM ELECTRONICS CONFERENCE, Vienna, Austria, 14-19 June 1992; American Physical Society/European Physical Society, Paper No. MoM7.

13. Ohtsa, Sing, Kuzuzawa, Koro, and Suzuki, "Frequency and Phase Control of Semiconductor Laser," JOURNAL OF THE SOCIETY OF ELECTRON INF. COMM., Vol J73-C-1/5, 1990, pp 277-285.

Observation of Inorganic Materials by AFM

936C1098F Tokyo JAPAN SURFACE SCIENCE SOCIETY in Japanese 25 Jun 93 pp 59-68

[Article by Hitoshi Shindo, Department of Applied Chemistry, Faculty of Science and Engineering, Chuo University]

[Text] **Section 1. Scanning Tunnel Microscope**

A scanning tunnel microscope (STM), which is used for measuring surface shape, made a rapid advance in the 1980s. It is possible to investigate the arrangement of surface atoms, unevenness, and the atomic state with a resolution of the size of an atom by scanning the surface of a sample with a metallic probe. Since it does not require a periodic structure, the STM differs from methods that use diffraction phenomenon, and it is possible to examine discontinuous structures such as lattice defects and steps.

This section will describe the STM, and other scanning probe microscopes (generically called SPM or SXM) will be presented in the following sections. The reader is referred to Reference 12 for details of experimental techniques and various experimental examples.

1.1 Principle and Apparatus for Measurement

First, we will show Figure 1.1. It is the heart of the STM. A dc voltage is applied between a conductive sample, such as a metal or a semiconductor, and a sharply pointed metallic probe, and both are gradually brought close to each other. As they are brought to a distance of about 1 nm (one one-billionth of a meter) the electronic orbits of the atoms that constitute the sample and the probe overlap, and

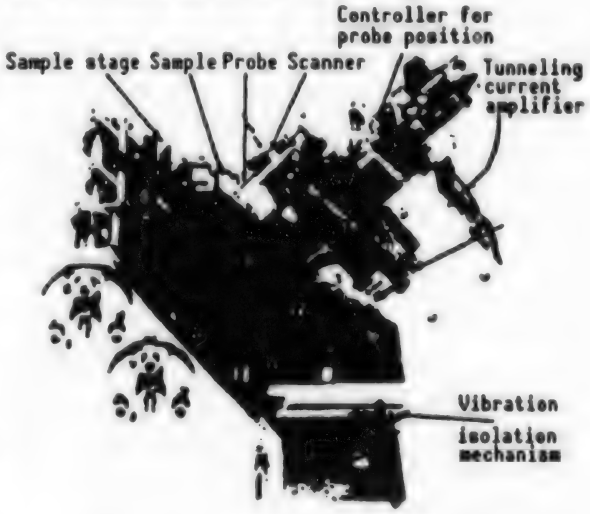

The STM part of a device compounded with SEM. An arbitrary point of a sample is observed by STM while watching from above by SEM.

Figure 1.1 Example of STM Measurement Unit
(Source: Hitachi, Ltd.)

a minute current (tunneling current) based on a quantum mechanical effort (tunnel effect) starts to flow. Since the current is extremely sensitive to distance, it is possible to investigate the unevenness of the surface by moving the probe along the sample surface while measuring the current. The most important point in the basic STM technique is to move the probe quickly while precisely controlling the probe positive relative to the sample surface, and an accuracy on the order of the size of an atom. By the use of a piezoelectric element that elongates and contracts according to the applied voltage, it is possible to move the probe independently both parallel (X and Y directions) and perpendicular (Z direction) to the sample surface.

In order to isolate mechanical vibrations from the surroundings, various kinds of vibration isolation mechanisms are employed. In the case of Figure 1.1, a system formed by stacking several layers of dampers is used. Sometimes the entire apparatus is suspended by springs or pieces of rubber.

Furthermore, it is also necessary to increase the mechanical resonance frequency by making the whole STM measuring unit hard and compact. Figure 1.2 is a photograph of an STM/AFM apparatus used to conduct measurements in the air. It can be seen that the measuring unit (AFM in this case) is relatively small.

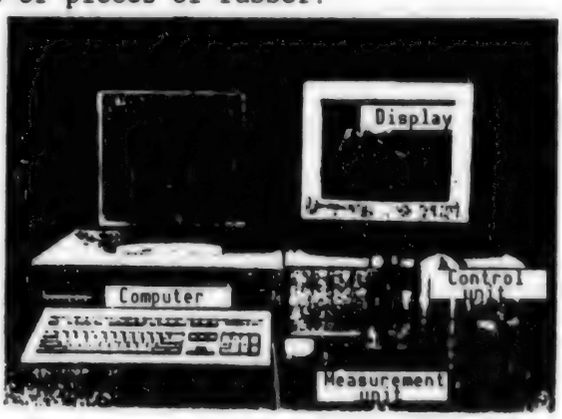

Figure 1.2 Example of STM/AFM Device for Use in Air (Commercially available)
(Source: Toyo Technica Co.)

The control unit in Figure 1.2 contains electronic equipment for taking in data at high speed while controlling probe movement. Since there are many measurement modes, as will be described later, the circuits are complicated. High-level functions are required for the computer and the software for controlling the measurement parameters. They also must process large quantities of data obtained along the sample surface, and image them. Although the basic configuration of the STM apparatus is as shown in Figure 1.2, various measuring units have been devised depending on the specific purposes. For example, the one shown in Figure 1.1 is for use in a vacuum in combination with a scanning electron microscope (SEM) which is installed in the upper part of the figure. Figure 1.3 shows examples of measurements. First, a broad range is surveyed, then STM observation is carried out by leading the STM probe to an arbitrary position. In a measuring system in the air, there is one combined with an optical microscope.

For samples whose surface tends to be oxidized in the air, it is necessary to take measurements in a vacuum. In this case, a coarse movement mechanism for the probe, a method for exchanging broken probes, etc., have to be devised. The materials to be used also must be limited in order to avoid deterioration of the vacuum due to the infiltration of air.

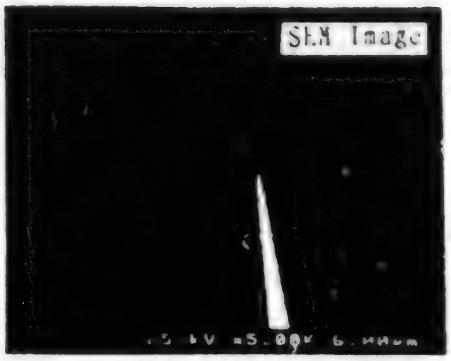

(a) SEM image

STM probe is also measured at the same time. Measurement of STM of the part in square is shown in (b)

(b) STM image

Full scale is 2.6μm×2.6μm×0.2μm

Figure 1.3 SEM Image and STM Image of Optical Disk Surface
(Source: Hitachi, Ltd.)

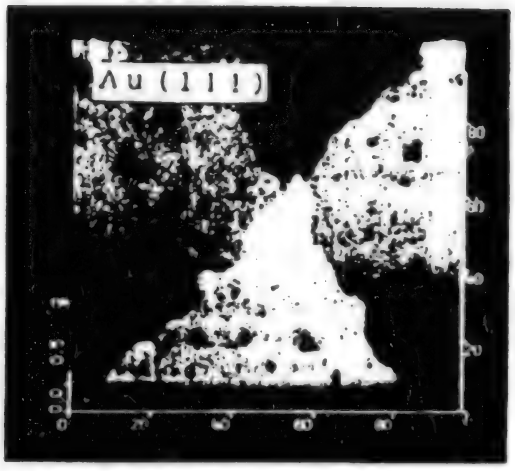

Figure 1.4 StM Image of Gold Single Crytal 9111) Surface in Perchloric Acid Aqueous Solution
(Source: K. Itaya,
Tohoku University)

In an electrolytic solution, though not in vacuum, it is possible to define a metallic surface satisfactorily at the atomic level. Figure 1.4 is an STM image of the (111) surface of a gold single crystal measured in an aqueous solution of perchloric acid. In addition to many pits, steps of monatomic layers that run in a specified direction are observed. When the step moves with time, it can be tracked in real time. No other method can provide direct atomic-level information in a solution better than this method.

It is difficult to perform STM measurements in experiments that involve changes in temperature. This is because fluctuations due to the expansion and contraction of the probe and other parts caused by the vibrations in temperature are large. Another reason is the deterioration of the performance of the probe due to high and low temperatures. Nonetheless, measurements at extremely low temperatures where the part to be measured was completely immersed in a coolant, and measurements up to about 800°C by ensuring a uniform heat dissipation from the sample were carried out.

1.2 Measurement Modes

There exist several STM measurement modes. The most basic of these is the constant current mode. In this mode, the sample surface is scanned by maintaining the bias voltage between the probe and the sample, and during this time the piezoelectric element for the Z axis is subjected to feedback so as to keep the measured current at a set value. By recording the voltage required to raise and lower the probe voltage, a topographic image of the surface can be obtained.

An STM image of graphite measured in the air by this method is shown in Figure 1.5. Since graphite is a layered compound and readily gives a flat surface on the atomic level when cleaved, it is used as a substrate on which to place other samples, or for checking the performance of the device as a standard sample.

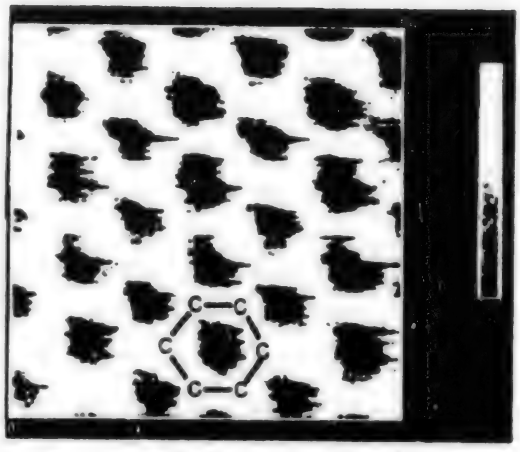

Bias voltage: ±30 mV (sample). Tunneling current: 1.5 nA. Height in full scale: 0.38 nm. Two kinds of images with different electronic conditions are generated in atoms of the first layer depending on the overlap condition with the carbon atoms of the second layer, and they are arranged alternately.

Figure 1.5 STM Image of Graphite Surface Measured by Constant Current Mode

For samples with flat surfaces on the atomic level, there is also a method for finding the surface topography by recording the changes in the tunneling current during scanning while keeping the probe height constant. This is called the "constant height mode." Although it makes quick measurements possible, it cannot be used for samples with a rugged topography because of the collision of the probe with the sample. The locations where carbon atoms are thought to be present are indicated in Figure 1.5, but a careful inspection reveals that the brightness given by the carbon spots varies. This is not due to a shift of the carbon nucleus in the vertical direction. What is measured by STM is the spread of the electron orbit, not the position of the nucleus.

In the case of graphite, two adjacent layers are staggered, and the carbon atoms in the first layer are alternately arranged so that one atom overlaps vertically with one carbon atom in the second layer, while the next atom does not do so. The brightness of the images for the two cases differs due to the difference in the electronic states. In Figure 1.5, the sample side has a positive potential, so the electrons are considered to be flowing from the filled electron orbits of the metal atoms at the probe tip to the empty orbits of the carbon atoms. A detailed understanding can be obtained by making measurements while changing the direction of the bias voltage and the set value.

An STM image obtained of the surface of a single silicon crystal measured by an ultrahigh-vacuum STM apparatus is shown in Figure 1.6. Cleaning the Si (111) surface by heat treatment produces a (7 x 7) reconstructed surface. A rhombus obtained by connecting the four holes (corner holes) is the unit lattice. The reason for the difference in figures (a) and (b) is the observation of the filled electron orbits and the empty electron orbits of Si depending on the direction of the voltage.

Next, the current image tunneling spectroscopy (CITS) mode will be described. This is a method for recording the value of the tunneling current when the voltage is separately set for each point while scanning the probe so as to keep the distance from the sample according to the constant current mode. An example is shown in Figure 1.7.

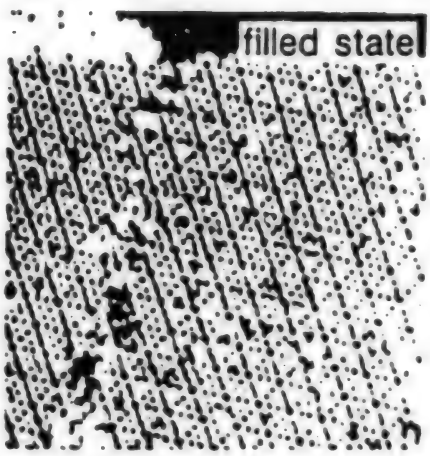

(a)

Image of filled electron orbit observed by +2 V (sample and 0.5 nA

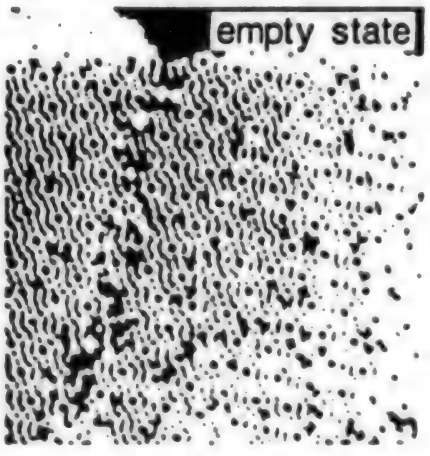

(b)

Image of unfilled electron orbit observed by +2 V (sample) and 0.5 nA

Figure 1.6 STM Image of Si (111)-(7x7) Reconstructed Surface (Source: NEC Corp.)

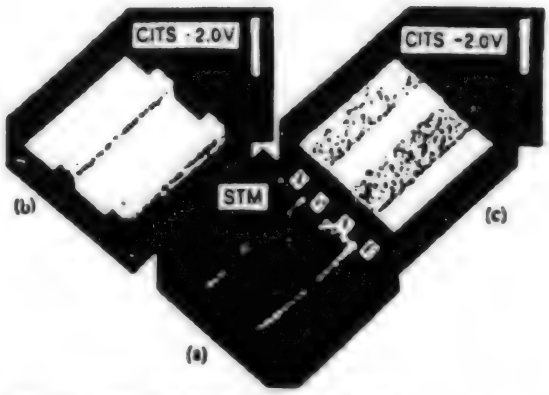

(a) Topography (4.5μm×4.5μm×40nm)
(b) Current image for +2 V; current flows only in the p-type part
(c) Current image for -2 V; current flows only in the n-type part

Figure 1.7 Image of Si P-N Junction by CITS Mode (Source: Hitachi, Ltd.)

The figure shows a simultaneously measured topography image and a current image of the P–N junction formed by implanting arsenic ions in a p-type silicon surface. Since the voltage for taking the current image was smaller than that at the time of taking the topography image the tunneling current is observed only in the p-type parts for positive potential, and in the n-type parts only for negative potential.

Going one step further, the scanning tunnel spectroscopy (STS) mode is one in which the current-voltage curve is obtained by fixing the probe position for each point on the surface and sweeping the bias voltage. By the use of this mode it is possible to investigate the chemical state and physical properties at each point. For example, there is reported a case in which the bonding state of oxygen atoms on the surface of the Si (111) surface in the ultrahigh-vacuum apparatus. In addition, local differences in the conductive property in high-critical temperature superconductors are investigated. Although element discrimination is not possible by STM, it is possible to some extent by STS. Although the cases are limited, element discrimination was performed based on differences in current response in an STS measurement under the irradiation of light.

1.3 Probe

Tungsten and a platinum-iridium alloy, both of which are very rigid, are used as the material for the STM probe. The tip of a wire made of such a metal is sharpened by electropolishing or a similar technique, which yields a radius of

curvature of the tip of about 50 nm at best. It is a wonder how an atomic resolution like that shown in Figures 1.5 and 1.6 is obtainable with such a radius. The reason for this is thought to be that the majority of the tunneling current concentrates only one atom situated closest to the sample. In fact, an atomic resolution can be obtained even with a probe with poor symmetry, such as one obtained by snapping a wire with a pair of sharp scissors.

However, aside from flat layer compounds, most of the practical samples have steep, rugged surfaces, and thus an exact topography of the surface cannot be obtained unless the shape of the tip of the probe is good. This is because a current flows even from the side faces of the probe.

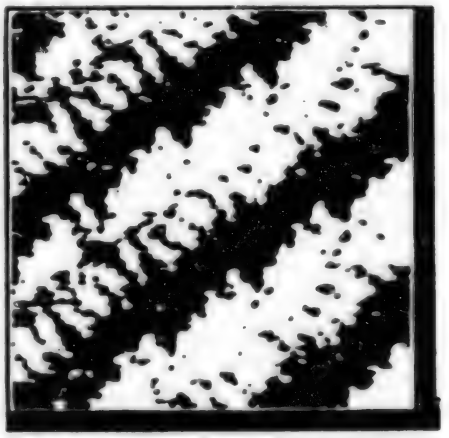

Constant current mode: -0.71 V (sample), 1.3 nA
Bright parts are biphenyl. A lamella structure is formed with two molecules facing each other.

Figure 1.8 STM Image of Liquid Crystal Molecule 8Cb Arranged on Graphite Surface
(Source: Y. Miura, Tokyo College of Science)

1.4 Measurement Examples

Some measurement examples will be presented here. Since graphite provides a flat plane by cleavage, as mentioned earlier, it is often used as a substrate on which to place other samples for observation by STM. Figure 1.8 is an STM image of smectic liquid crystal molecules 8CB (4'n-octyl-4-cyanobiphenyl) a thin layer of which was applied to a graphite surface. Since the probe goes into the liquid crystal layer and comes close to the graphite surface until the tunneling current flows, the arrangement of the adsorbing molecules in the first layer of the surface can be observed. The bright portions of the figure are places where the current flows easily. These are thought to represent biphenyl groups having a π electron system. Because of the polarity of the cyano group, this molecule takes on a lamella structure in bilayer units in which head and head are brought to face each other. The alkyl chain runs in the dark part. The semiconductor molybdenum bisulfide (MoS_2) is also a layered material that can be used as the substrate for molecular arrangement, but it is more hydrophilic than graphite. Even for the same liquid crystal, a completely different molecular arrangement is sometimes obtained by changing the substrate.

Figure 1.9 is an STM image obtained by abrading the graphite surface by irradiating it with an ultraviolet laser (KrF 248nm), and observing it after several hours.

Immediately after abrasion the roughened surface begins to lose its ruggedness, and gradually with the lapse of time, by the movement of carbon atoms, it changes to a flat surface. Since, however, there remain banks with a height of about 20 nm at the boundaries of the flat region, these are thought to be collections of carbon atoms expelled from the planar structure. For this observation, use is made of a scanner having an extremely side region of measurement.

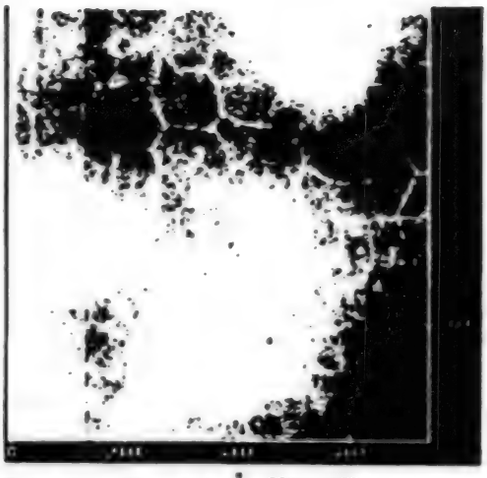

0.8 V (sample), 2.0 nA. 75μm×75μm.
The boundary of the flat region is a bank of height of about 20 nm.

Figure 1.9 STM Image of Laser Abraded Graphite Surface After Self-Restoration
(Source: H. Shinno, Chemical Technology Research Institute)

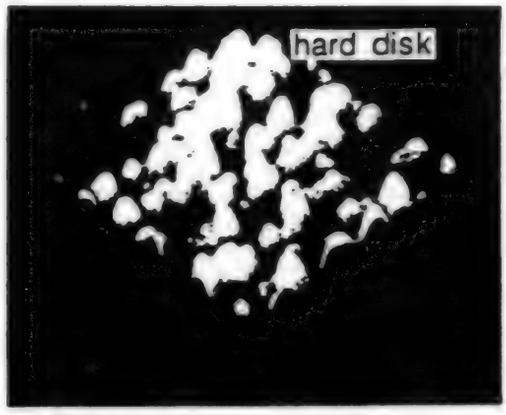

Figure 1.10 STM Image of Magnetic Recording Hard Disk
(Source: Hitachi, Ltd.)

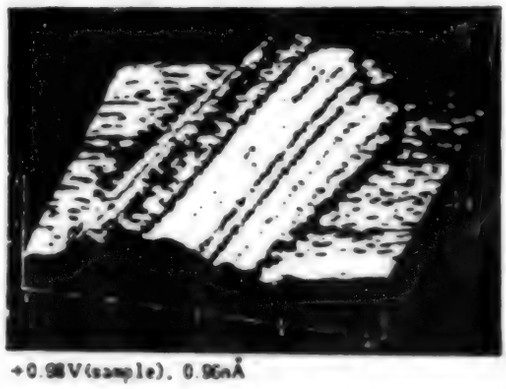

+0.98V(sample), 0.96nA

Figure 1.11 STM Image of Microtubule Protein Tubulin on Graphite
(Source: H. Miyamoto, Chemical Technology Research Institute)

Figure 1.10 shows an STM image of the surface of a hard disk used for magnetic recording. The surface is roughened so that it will not stick to the surface of the head for read and write. It is difficult to measure this topography by SEM. Figure 1.11 is an STM image of a protein tubulin like those that form microtubules in living bodies, that has been polymerized on a graphite substrate. The fibrous structure is interpreted to be showing six or seven of 13 proto filaments that form the microtubule. The outer diameter of the microtubule is about 24 nm. Since no conductivity treatment by metal evaporation is provided, it is thought that the current flow is mediated by the moisture content.

In observing biosamples by STM, it is necessary to carry out particularly thorough blank experiments in order not to erroneously observe the substrate structure as the image of the object.

1.5 Surface Treatment

STM can be used not only to measure the surface shape, but also for the fine treatment of the surface. For example, Figure 1.12 shows how characters can be written by forming grooves through the removal of surface atoms along lines. This is accomplished by applying a high-bias voltage to the probe for a single silicon crystal surface using an ultrahigh-vacuum STM apparatus.

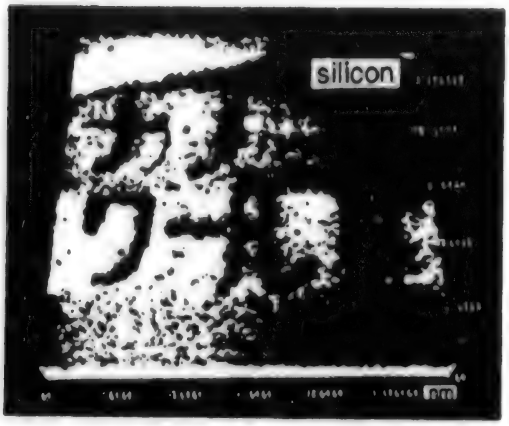

Figure 1.12 Characters Written on Single Si Crystal Using STM Probe (Source: Japan Electron Optics Laboratory Co., Ltd.)

Figure 1.13 STM Image of Pyramid Formed on Si (100) Under High Temperature and Large Current Measurement at 600°C, +2.0 V (Sample: 0.2 nA)

By contrast, Figure 1.13 shows a pyramid built in a Si (100) surface. This structure was obtained by heating a sample to 600°C, and causing a large current to flow between one point of the sample and the probe. A similar experiment done on the Si (111) surface shows that a hexagonal cone structure is obtained. In addition, an experiment on electrodepositing a metallic wire pattern on the surface in an electrolytic solution was carried out. As eventual cases, there are examples in which a desired arrangement was obtained or operated as a switch by manipulating and moving individual atoms by the probe. Such attempts will increase in the future.

Section 2. Atomic Force Atmosphere (AFM)

2.1 Principle and Apparatus for Measurement

One drawback of the STM is the fact that it is difficult to apply it to electrically insulated samples. For the atomic force microscope (AFM), however, the electrical conductivity of samples is not a problem since it measures the interatomic repulsive force (based on Pauli's exclusion principle concerning electron orbits) and the van der Walls attractive force that act between the atoms constituting the probe and the surface of the samples.

Figure 2.1 is an SEM image of a cantilever used in AFM measurement. Its thickness is about 0.3 μm. The image is looking at the tip of the cantilever formed on the Si (100) surface by utilizing the same microlithography technique as that used in fabricating integrated circuits. A pyramidal needle is formed at the tip. This part is formed of hard and chemically stable silicon nitride. It is formed by utilizing anisotropic etching of single silicon crystal face. When the sharpened end receives an attractive or repulsive force through interaction with the atoms on the solid surface, the thin leg of the cantilever bends. By keeping a narrowly controlled laser beam

Figure 2.1 SEM Image of Cantilever for AFM Formed by Microlithography
(Source: H. Miyamoto, Chemical Technology Research Institute)
(a) When the tip of the pyramidal needle receives a force from the solid surface, the leg part behind bends. By keeping a light projected from the rear on the part marked with a cross, bending can be measured from the change in the optical path, which in turn gives the sample topography.
(b) Enlargement of the needle part. The white line in the figure is 1 μm long. The needle is made of hard and chemically stable silicon nitride, and other parts are made of silicon.

projected on the rear side of the vicinity of the area marked with an X, it is possible to determine the bend from the change in the optical path of the reflected ray. In addition to this "optical lever method" there is a method of measuring the bend of the cantilever by STM. As in the case of STM, it is necessary in AFM to make the needle tip sharp. To that end, growing a whisker crystal on top of the projection has been tried. However, as the load per unit area becomes large, the sample surface tends to become damaged accordingly. Particular care has to be exercised for soft samples.

AFM measurements in a vacuum are not yet common, but they will gradually become popular since there is no difficulty in principle. At present, the majority of cases are done in the air or in a liquid.

Measurements in a liquid carry an important meaning. A careful examination of the change in the bending of the cantilever when it is moved in the air perpendicular to the surface of the sample reveals that the force acting between the two is not only the force between the atoms at the tip of the needle and the atoms on the surface. Due to the existence of a very small amount of water, etc., there are cases in which a large attractive force acts between the periphery of the needle and the sample. If measurement is performed by immersing the entire probe and the sample in a liquid, the attractive forces act in all directions and cancel each other out. Thus, it becomes possible to measure the actual force acting between the atoms of the needle tip and the surface. By the use of such a method a molecular image was obtained for the surface of a soft lipid membrane.

2.2 Measurement Examples

First, a layer formed from potassium niobate will be presented as an example of AFM measurement with an atomic resolution. The structure off this compound is shown in Figure 2.2(a), and cleavage can occur between two kinds of layers that have different structures and properties. When the cleavage took place gently in the air, the AFM image shown in Figure 2.2(b) was obtained. A comparison with the model structure of a cut crystal plane led to the conclusion that cleavage occurred between the I layers. The configuration structure of the interlayer I potassium ions that are known to be readily exchanged by alkyl ammonium ions, etc., was also confirmed by AFM measurement.

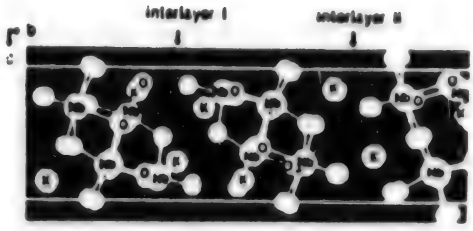

(a) Between layers of niobic acid sheets there is the complicated interlayer I and the flat interlayer II, the former tending to be hydrated in air.

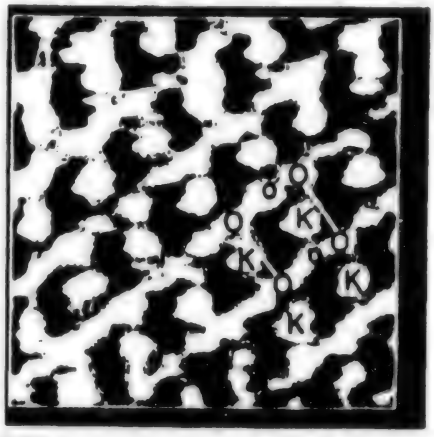

(b) AFM image when cleaved gently in air. (Corresponds to cleavage surface at (constant bend mode) interlayer I. Oxygen atoms labeled "O" and "o" are coordinated to the same niobium atom, but the former is at a higher position. (Taken under approval from Reference 12, LANGMUIR, Vol 8 No 2, 1992, p 353. © 1992 American Chemical Society.)

Figure 2.2 AFM Images of the Structure of a Layered Niobate ($K_4Nb_6O_{17}$) and Its Clevage Surface

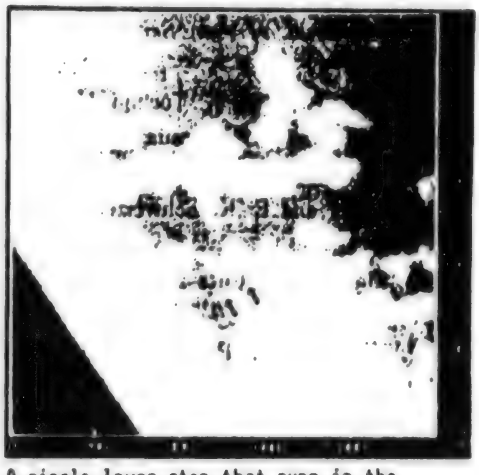

A single layer step that runs in the crystal axis direction is located along a line marked by arrows. When cleaved in air, the step was tilted against the crystal axis, but the axis direction becomes stable in NH_4Cl aqueous solution. Measurement was made in air.

Figure 2.3 AFM Image of Part of One (Pearly Gloss Surface) Cleavage Surface of Gypsum

In addition, clear atomic images on the cleavage plane were observed for gypsum dihydrate ($CaSO_42H_2O$) and anhydrite ($CaSO_4$). Figure 2.3 is an AFM image obtained by immersing the plane in a pearly gloss. This is the one that shows the most complete cleavage property of the three kinds of cleavage planes of anhydrite. It is immersed in an aqueous solution of a salt to partly dissolve its surface, and is then measured in the air. Steps with the height of a $CaSO_4$ monolayer are running at the locations indicated by the arrows. The fact that the direction differs from that in the plane immediately after cleavage in the air led us to conclude that the stability of the cleavage plane is changed markedly by the cancellation of the electric field generated by the ions on the crystal surface by the electrolyte ions.

Enlargement of the flat part readily produced an atomic image. With regard to the ionic crystal surface, a powerful measuring tool for the direct investigation of atomic level structures has been lacking, but with the appearance of the AFM, research in this field is expected to accelerate at once. Since the crystal step can be measured relatively accurately, the method will be extremely effective for monitoring crystal growth.

Figure 2.4 shows the surface structure of cuticles of hair. Although this is an example of biological molecules, measurement of the surface structure of synthetic polymers is also an important application for the AFM. In comparison to the use of a transmission electron microscope where segmentation of the sample thin film is laborious, sample preparation is easy for AFM. Therefore, when measurements of a large number of samples are required in materials research, the experimental efficiency will be high. However, obtaining atomic resolution may not be easy.

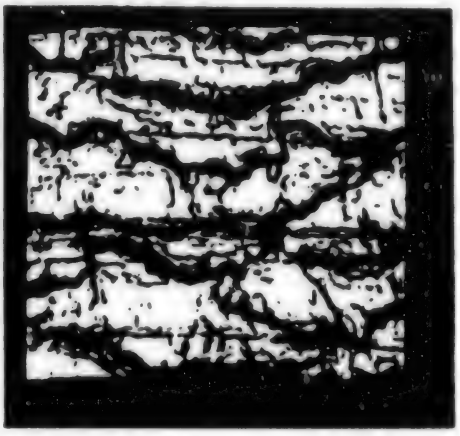

Figure 2.4 AFM Image of Hair Cuticles
(Source: Toyo Technica)

The AFM is also widely used for the measurement of biosamples. Since it does not require conductivity, as is the case for STM, measurement in the living state is possible. Figure 2.5 is an AFM image of red blood cells. The reader is referred to Reference 1 for measurement examples of biosamples.

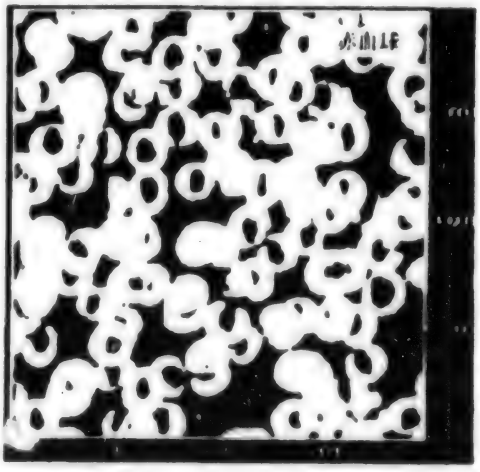

Figure 2.5 AFM Image of Red Blood Cells
(Source: Toyo Technica)

Section 3. Other Scanning Probe Microscopes (SPMs)

The basis of all scanning probe microscopes is a technology for precisely controlling the position of the probe relative to the sample. By measuring changes to the probe, it is possible to measure the distribution of various kinds of physical properties on the surface. Some representative types will be described below.

3.1 Frictional Force Microscope (FFM)

In the AFM, the vertical component of the force received by the cantilever from the sample is measured. If the horizontal component of the force generated by rubbing the tip of the cantilever is measured, it is possible to map the friction between the needle tip and the sample surface. This is the frictional force scanning mirror. Since it is possible to know the difference between the materials, even when contrast cannot be recognized from the topography of the surface, this will be useful for the evaluation of practical materials.

Examples in which a resolution at the atomic level was obtained for the surface of graphite and mica have been reported.

3.2 Magnetic Force Microscope (MFM)

A scanning-type magnetic force microscope is being developed for the purpose of investigating the distribution of magnetism on the surface of magnetic recording materials. Using a ferromagnetic body such as nickel or iron as the needle tip of a cantilever the same as that used in AFM, it is designed to measure the magnetic force that acts between the tip and the sample surface. If the distance between the surface is chosen to be greater than 1 nm, the effect of the force between the atoms can be made small, and it is possible to find the distribution of the magnetic force on the surface from the bending of the cantilever. An example in which the gradient of the magnetic field on the surface was investigated with a resolution of about 100 nm was reported by scanning the surface while electrically vibrating the cantilever.

3.3 Scanning Ion-Conductance Microscope (SICM)

This microscope uses a micropipette containing an electrolytic solution. When the probe is made to approach the surface of a sample, which is also in an electrolytic solution, the cross section effective to the electrical conduction between the electrolytes is decreased. By utilizing this effect it is possible to investigate the shape of the surface. Differing from the case of the AFM, it is considered effective for the observation of soft surfaces such as biosamples, because no force is applied to the surface. Further, it can be used to investigate the distribution of ionic channels on a membrane. A resolution of about 200 nm was obtained in an investigation of the surface of a membrane filter.

3.4 Others

In addition to what has been described above, there is one microscope that investigates the charge distribution by means of electrostatic force (localized charge force microscope (LCFM)), one for finding the temperature distribution by means of thermoelectromotive force (scanning thermal profiler (SThP)), etc. Furthermore, other microscopes are being tested that are designed to detect light or ultrasonic waves.

References

1. Nozoe, S., et al., "New World of Atoms and Molecules Opened by STM" edited by the Association of Organic Electronics, Bronshin Publishing, 1993, in press.

2. "Special Issue: Advances of STM," CHEMISTRY, Vol 10, 1990.

3. Sakashita, K., Furuya, N., and Itaya, K., J. VAC. SCI. TECHNOL., Vol B9, 1991, p 457.

4. Kitamura, S., Sato, T., and Iwatsuki, M., NATURE, Vol 351, 1991, p 215.

5. Avouris, Ph. and Lyo, I.W., SUR. SCI., Vol 242, 1991, p 1.

6. Kazmerski, L.L., J. VAC. SCI. TECHNOL., Vol B9, 1991, p 1549.

7. Hara, M., Iwakabe, Y., Tochigi, K., Sasabe, H., Garito, A.F., and Yamada, A., NATURE, Vol 344, 1990, p 228.

8. Eigler, D.M. and Schweizer, E.K., Ibid., p 524.

9. Eigler, D.M., Lutz, C.P., Rudge, W.E., Ibid., Vol 352, 1991, p 600.

10. Weisenhorn, A.L., Hansma, P.K., Albrecht, T.R., and Quate, C.F., APPL. PHYS. LETT., Vol 54 No 26, 1989, p 2651.

11. Weisenhorn, A.L., Egger, M., Ohnesorge, F., Gould, S.A.C., Heyn, S.P, Hansma, H.G., Sinsheimer, R.L., Gaub, H.E., and Hansma, P.K., LANGMUIR, Vol 7, 1991, p 8.

12. Shindo, H., Kaise, M., Kondoh, H., Nishihara, C., Hayakawa, H., Ono, S., and Nozoye, H., Ibid., Vol 8 No 2, 1992, p 353.

13. Ibid., J. CHEM. SOC. CHEM. COMMUN., Vol 16, 1991, p 1097.

14. Shindo, H. and Nozoye, H., J. CHEM. SOC. FARADAY TRANS., Vol 88 No 5, 1992, p 711.

15. Hawley, M., Raistrick, I.D., Beery, J.G., and Houlton, R.J., SCIENCE, Vol 251, 1991, p 1587.

16. Mate, C.M., McClelland, G.M., Erlandsson, R., and Chiang, S., PHYS. REV. LETT., Vol 59 No 17, 1987, p 1942.

17. Erlandsson, R., Hadziioannou, G., Mate, C.M., McClelland, G.M., and Chiang, S., J. CHEM. PHYS., Vol 89 No 8, 1988, p 5190.

18. Sáenz, J.J., Garcia, N., Grütter, Meyer, E., Heinzelmann, H., Weisendanger, R., Rosenthaler, L., Hidber, H.R., and Guntherodt, H.J., J. APPL. PHYS., Vol 62 No 10, 1987, p 4293.

19. Martin, Y. and Wickramasinghe, H.R., APPL. PHYS. LETT., Vol 50 No 20, 1987, p 1455.

20. Rugar, D., Mamin, H.J., Guethner, P., Lambert, S.E., Stern, J.E., McFadyen, I., and Yogi, T., J. APPL. PHYS., Vol 68 No 3, 1990, p 1169.

21. Hansma, P.K., Drake, B., Marti, O., Gould, S.A.C., and Prater, C.B., SCIENCE, Vol 243, 1989, p 641.

Ultrahigh-Vacuum STM, Single Electron Tunneling

936C1098G Tokyo JAPAN SURFACE SCIENCE SOCIETY in Japanese 25 Jun 93 pp 77-86

[Article by Kiyohiko Uozumi, Faculty of Science and Engineering, Aoyama Gakuin University]

[Text] 1. Introduction

As a way to explain the fact that the electrical conductivity of metallic island-like thin films show negative temperature dependence, as shown in Figure 1, and have an activation energy on the order of 0.1 eV, Neugebauer and Webb[1] have proposed an activation tunneling mechanism. That is, if the diameter of the particles is on the order of 10 nm, the charging energy of a single electron to the particle is no longer negligible. Thus they propose that an activation energy corresponding to the charging energy is required for the electron to tunnel through the particles. In the process of investigating the size dependence of superconductivity by producing an M-I-M junction that includes particles in an insulating film, as shown in Figure 2, Zeller and Giaever[2] observed a conspicuous temperature dependence, as shown in Figure 3, in the region of low bias voltage. However, these authors regarded this finding as a "trivial" classical effect in which the charging energy is playing an active role.

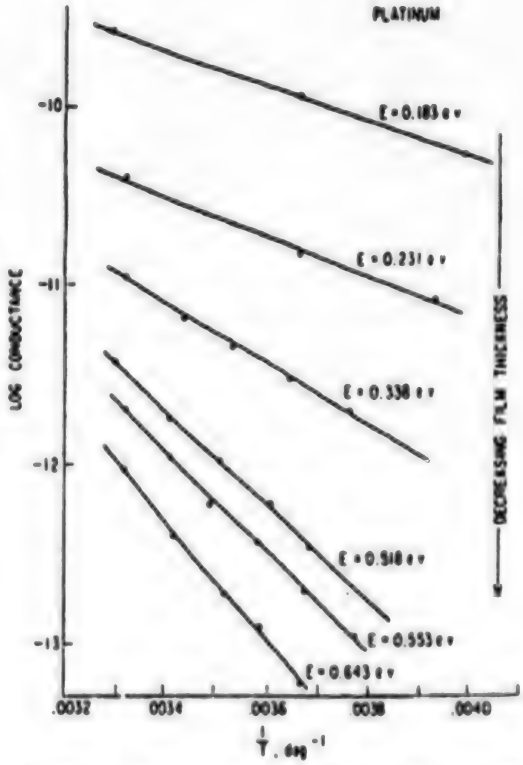

Figure 1. Temperature Dependence of Electric Conductivity of Island-Like Pt Film

In the process of discussing the electrical conduction of such an island-like thin film, we derived an equation for representing electrical conduction through particles as an elemental process. It has been nearly 10 years since we started to manufacture an scanning tunnel microscope (STM) in order to

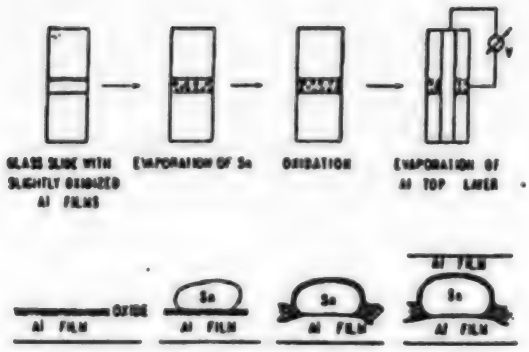

Figure 2. M-I-M Structure Containing Particles

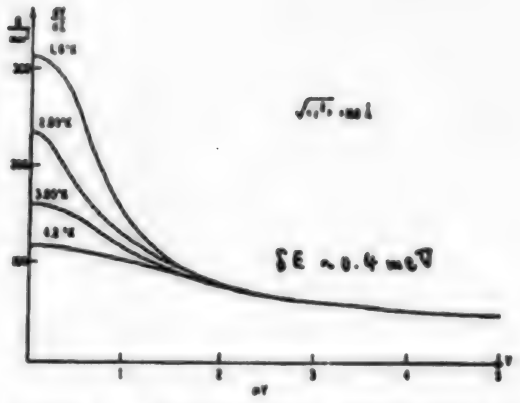

Figure 3. Temperature Dependence of Differential Resistance of M-I-M Structure

demonstrate this theory. Since an STM can be used even in liquid He, low-temperature observations are frequently carried out by placing the STM unit directly in a crystal of liquid He, as shown in Figure 4. Considering the fact that we are looking at the electronic state of the sample surface using a probe, we are undoubtedly looking at a surface on which something is adsorbed. Accordingly, there a requirement for an STM that is capable of cleaning the surface in an ultrahigh vacuum, and yet is capable of operating at low temperatures. In recent years in STM appeared that is capable of cooling a sample in an ultrahigh vacuum. In this article, we will present an STM for low-temperature observation that cools the sample by the use of an ordinary exchange gas, and an STM for use in ultrahigh vacuums and at low temperatures developed by our group. Following that, the present status of the beautiful observation of single electron tunneling by STM will be presented in conjunction with our calculations and experiments.

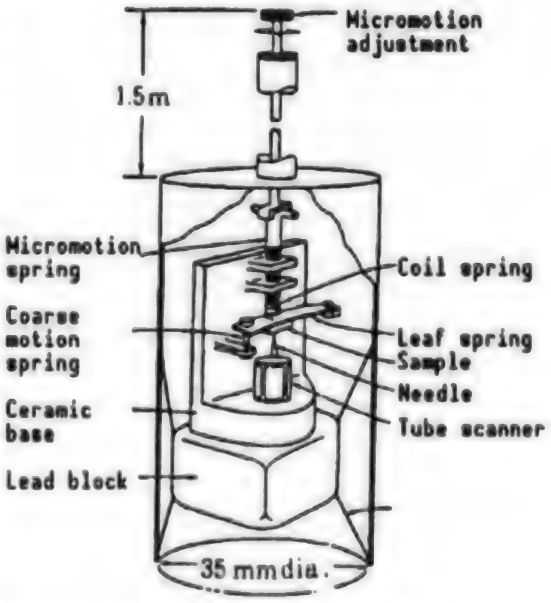

Figure 4. Low-Temperature STM Utilizing Diffential Spring

2. STM for Low-Temperature Observation

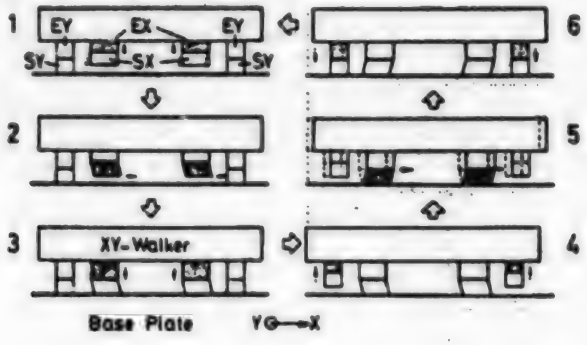

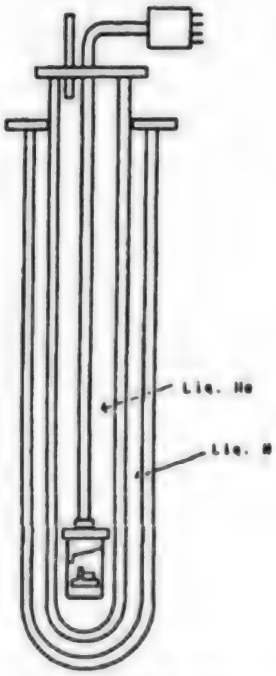

Figure 5. Diagram for Explaining Walker Utilizing Shear Deformation and Elongational Deformation of Piezoelectric Body

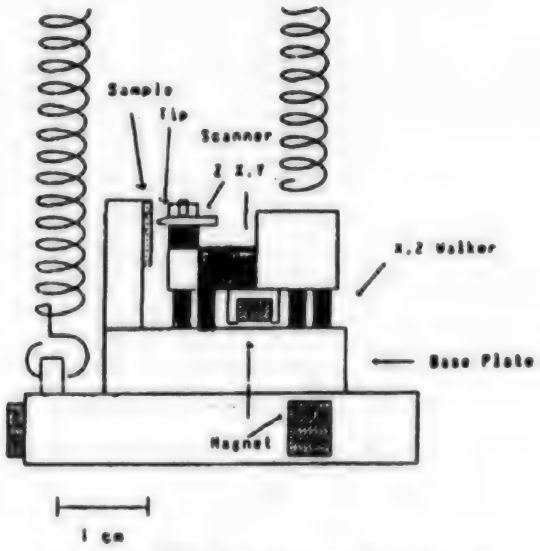

Figure 6. STM Utilizing Ordinary Cryostat

3. STM for Ultrahigh-Vacuum and Low-Temperature Observation

A completely loaded lock-type ultrahigh-vacuum STM with a spare chamber that we developed is shown in Figure 8. For the STM unit, an inertial drive system utilizing shear deformation was employed to provide operational stability at low temperatures.

As shown in Figure 9, this STM has a mechanism for sample exchange, probe exchange, and evaporation, and in cooling the sample the entire STM unit is lowered to bring it into contact with the low-temperature part. It is possible to cool the sample to about 20 K.

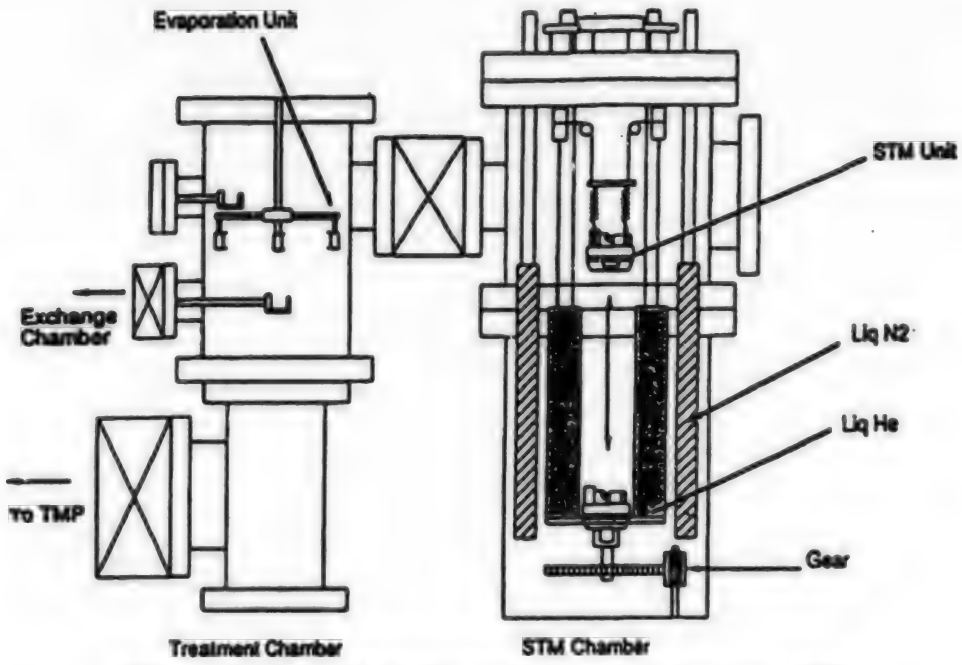

Figure 7. Ultrahigh-Vacuum, Low-Temperature STM

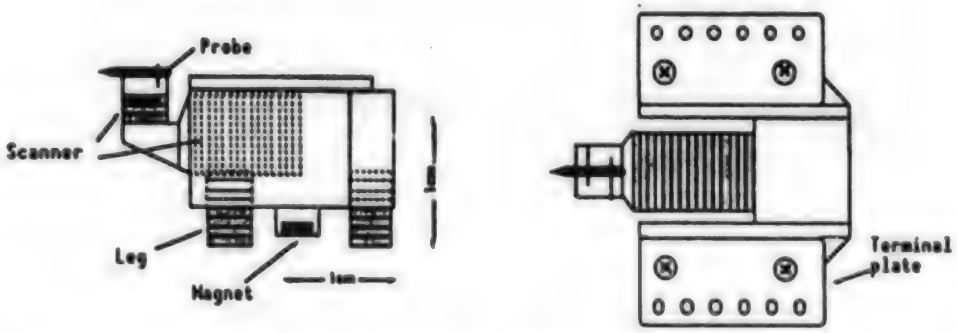

Figure 8. Inertially Driven Two-Dimensional Walker STM Unit

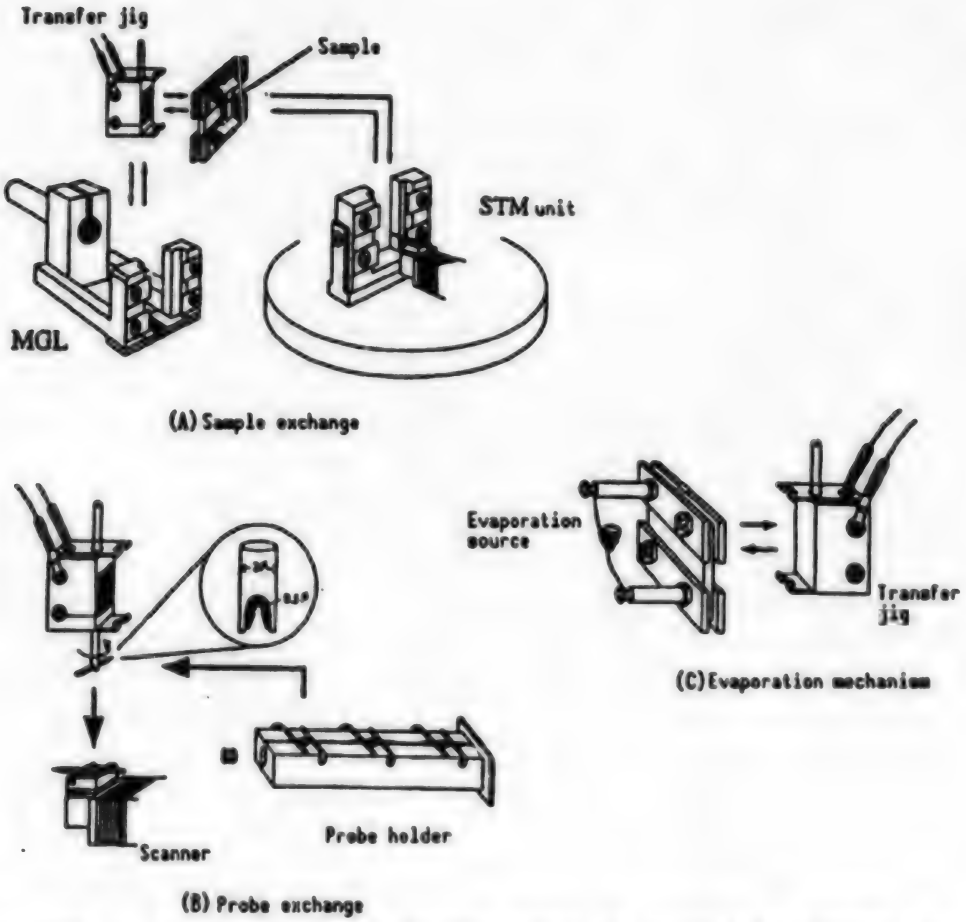

Figure 9. Description of Various Parts of Ultrahigh-Vacuum STM

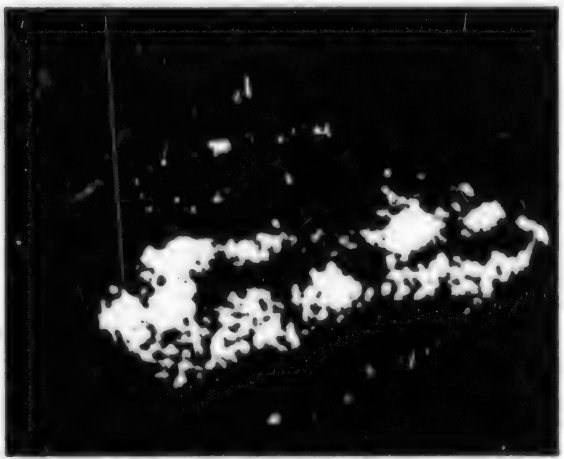

Figure 10. STM Image (8 nm square) of Island-Like Pt Film

4. Electron Tunneling Via Particles in Insulating Film

4.1 Monte Carlo Method

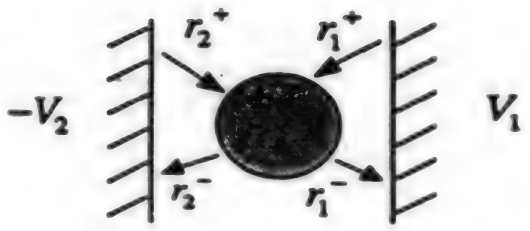

Figure 11.

Probability of Tunneling

$r_1^+(j)$: Electrode 1 ⟶ No. of electrons becomes (j+1)

$r_1^-(j)$: Electrode 1 ⟶ No. of electrons becomes (j−1)

$r_2^+(j)$: Electrode 1 ⟶ No. of electrons becomes (j+1)

$r_2^-(j)$: Electrode 1 ⟶ No. of electrons becomes (j−1)

When a current I flows, if the average time in which a single electron undergoes tunneling is t, and the number of electrons that undergo tunneling per second is n, one has

$$I = ne = \frac{e}{\Delta t} \quad , \quad n = \frac{1}{\Delta t} \tag{1}$$

Then,

$$P_1^+(j) = \frac{I_1^+(j)}{I_1^+(j)+I_1^-(j)+I_2^+(j)+I_2^-(j)} \quad , \quad P_1^-(j) = \frac{I_1^-(j)}{I_1^+(j)+I_1^-(j)+I_2^+(j)+I_2^-(j)}$$

$$P_2^+(j) = \frac{I_2^+(j)}{I_1^+(j)+I_1^-(j)+I_2^+(j)+I_2^-(j)} \quad , \quad P_2^-(j) = \frac{I_2^-(j)}{I_1^+(j)+I_1^-(j)+I_2^+(j)+I_2^-(j)} \tag{2}$$

$$P_1^+ + P_1^- + P_2^+ + P_2^- = 1$$

The average time ΔT(j) during which one of the above changes occurs is given by

$$\Delta T(j) = \frac{e}{I_1^+(j)+I_1^-(j)+I_2^+(j)+I_2^-(j)} \tag{3}$$

Random numbers are generated (0<P<1), the processes that have occurred are made to correspond to the changes for one electron, and the time required for a change to occur is set to be equal to ΔT.

The set number n_2 of electrons that went out from particles to electrode 2, and the net number n_1 of electrons that entered the particles from electrode 1 are equal, and the current 1 is given by

$$I = \frac{n_1 e}{\sum \Delta T_1(j)} = \frac{n_2 e}{\sum \Delta T_1(j)} \tag{4}$$

By using this setting, it is possible to use random numbers effectively without fixing the time increment, and 100,000 instances of random number generation can be made to correspond to 100,000 electron transfers.

4.2 Analytical Method

If the time during which the number of electrons existing in an island per second is j is called t_j, then

$$\sum_j t_j = 1 \tag{5}$$

The component due to transitions during this time contributing to the total current is

$$\begin{aligned} I_j &= \sum t_j (I_1^+(j) - I_1^-(j)) \\ &= \sum t_j (I_2^-(j) - I_2^+(j)) \end{aligned} \tag{6}$$

The total current I is given by

$$I = \sum I_j = \sum t_j (I_1^+(j) - I_1^-(j)) \tag{7}$$

Let us now consider a stationary state. Since the frequency of $j+1 \to j$ is equal to $j \to j+1$, one has

$$t_j (r_1^+(j) + r_2^+(j)) = t_{j+1} (r_1^-(j+1) + r_2^-(j+1)) \tag{8}$$

Now, there exist

J_{max}: for which the probability of tunneling to the particle is (or can be) regarded as 0, and
J_{min}: for which the probability of tunneling from the particle to the electrode is (or can be regarded as) 0, namely:

$$\begin{aligned} I_1^+(J_{max}) + I_2^+(J_{max}) &= 0 \\ I_2^-(J_{max}) + I_2^-(J_{min}) &= 0 \end{aligned} \tag{9}$$

Actually, if $V_1 > 0$, $V_2 < 0$, and the charge is positive, there exists J_{max} for which

$I_1^+(J_{max}) = 0$, and J_{max} for which $I_2^-(J_{min}) = 0$.

Therefore, from the equation for the stationary state, equation (8), one obtains

$$t_{J_{max}} (r_1^-(J_{max}) + r_2^-(J_{max})) = t_{J_{max-1}} (r_1^+(J_{max}-1) + r_2^+(J_{max}-1)), \tag{10}$$

$$t_{J_{min-1}} (r_1^-(J_{min}+1) + r_2^-(J_{min}+1)) = t_{J_{min}} (r_1^+(J_{min}) + r_2^+(J_{min}))$$

Since one can obtain $J_{max}-J_{min}$ equations for $J_{max}-J_{min}+1$ unknowns $t_{j_{max}}$, $t_{j_{max-1}}$, ···, $t_{j_{min+1}}$, $t_{j_{min}}$, the ratios among the unknowns can be determined.

At $t_{j_{min}}$ there are $(j_{max}-J_{min})$ equations for an arbitrary t_j, namely,

$$\begin{cases} t_{j_{min+1}} = \dfrac{r_1^+(J_{min})+r_2^+(J_{min})}{r_1^-(J_{min+1})+r_2^-(J_{min+1})} \cdot t_{j_{min}} \\ \vdots \\ t_{j_{max}} = \dfrac{r_1^+(J_{max-1})+r_2^+(J_{max-1})}{r_1^-(J_{max})+r_2^-(J_{max})} \cdot \dfrac{r_1^+(J_{max-2})+r_2^+(J_{max-2})}{r_1^-(J_{max-1})+r_2^-(J_{max-1})} \cdots \dfrac{r_1^+(J_{min})+r_2^+(J_{min})}{r_1^-(J_{min+1})+r_2^-(J_{min+1})} \cdot t_{j_{min}} \end{cases}$$

Since there are $J_{max} - J_{min} + 1$ variables, by normalizing them by

$$t_{j_{max}} + t_{j_{max-1}} + \cdots + t_{j_{min+1}} + t_{j_{min}} = 1$$

all of them can be determined.

The time over which the charge of the particle per second is j can be determined, and the current is determined by Equation (7) for I (current for 1→2).

$$I = \sum t_j (I_1^+(j) - I_1^-(j)) \quad \textit{(net current from electrode 1 to the island)}$$

$$= \sum t_j (I_2^-(j) - I_2^+(j)) \quad \textit{(net current from the island to electrode 2)}$$

The time-averaged number of electrons residing on the particle is given by

$$\sum j \cdot t_j, \tag{11}$$

and the charge fluctuation σ_j is given by

$$\sigma_j = [\langle (j \cdot t_j - \langle j \cdot t_j \rangle)^2 \rangle]^{1/2} \tag{12}$$

4.3 Example of Calculation

If the charging energy is called E_j^*, then the tunneling current is given by

$$\Gamma_j^+(n) = \frac{1}{R_j e^2} \left[\frac{-\Delta E_j^+}{1-\exp(\Delta E_j^+ / \kappa_B T)} \right], \tag{13}$$

We are looking for an exact label which represents the current that is flowing via the particles.[5] The use of such a formula makes it possible to replace the so-called tunneling resistance by a specific work function and gap, and to carry out calculations that take into account the non-ohmic nature of the tunneling current. An example of calculations which use the parameters obtained by Wilkins, et al.,[6] that showed a typical step-wise I-V characteristic is shown below.

Figure 11 shows the temperature dependence for charging energy 37 meV. Figure 12 is an example of calculations taking non-ohmic property into account.

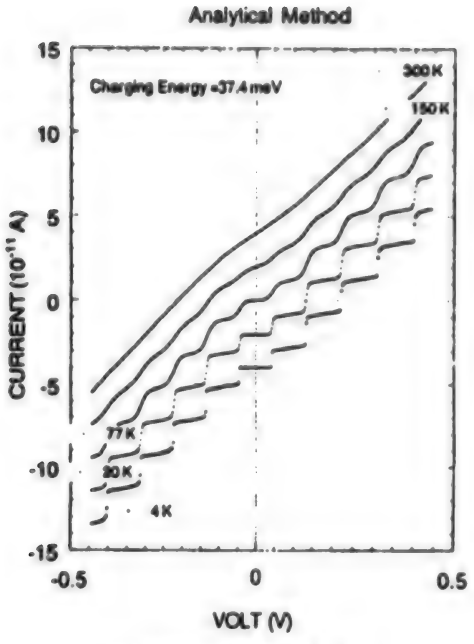

Figure 11. [sic]

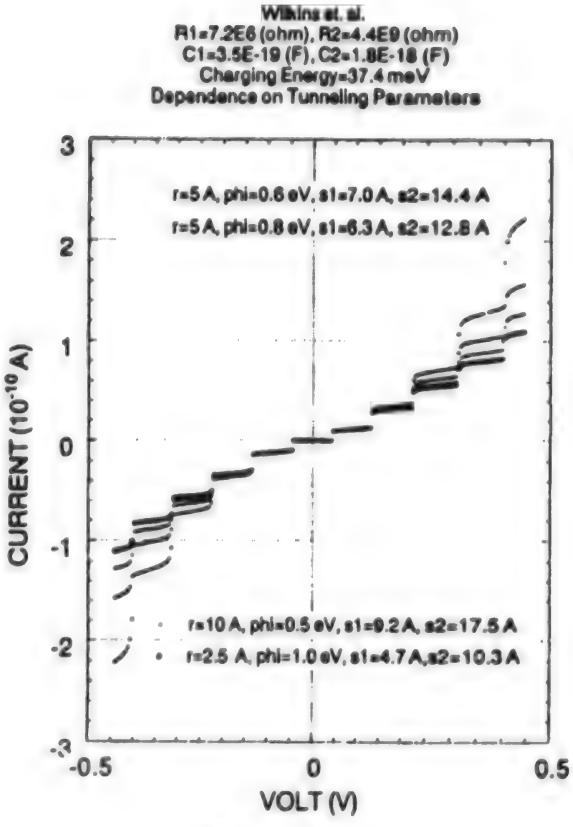

Figure 12.

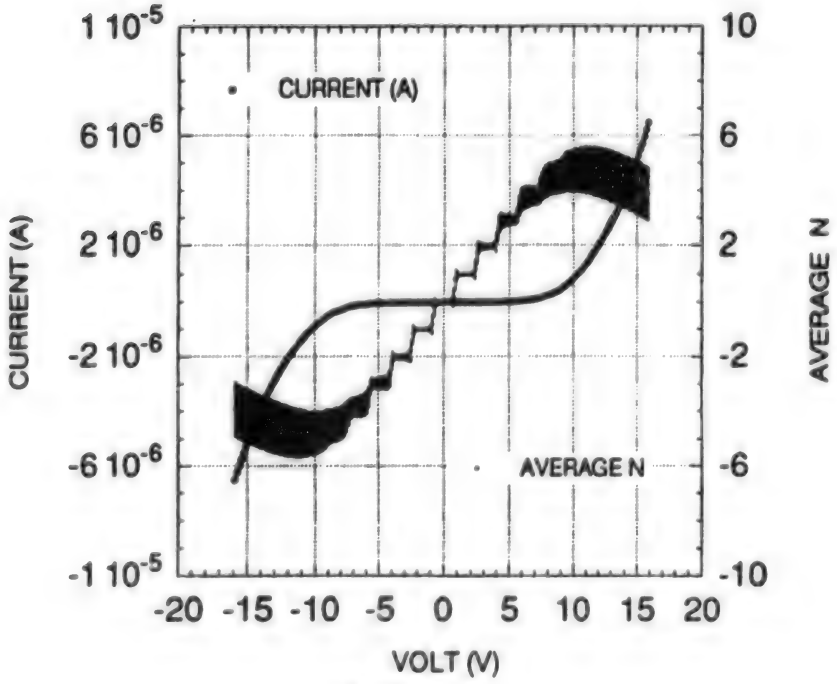

Figure 13.

Figure 13 shows the I-V characteristic at room temperature when the charging energy is large (0.4 eV).

4.4 Results Obtained by Hanna and Tinkham

$$\Delta E_1^* = \frac{e}{C_\Sigma}\left[\frac{e}{2} \pm (ne - Q_0) \pm C_2 V\right]$$

$$\Delta E_2^* = \frac{e}{C_\Sigma}\left[\frac{e}{2} \pm (ne - Q_0) \pm C_1 V\right]$$

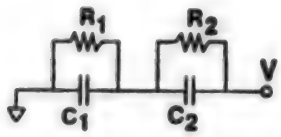

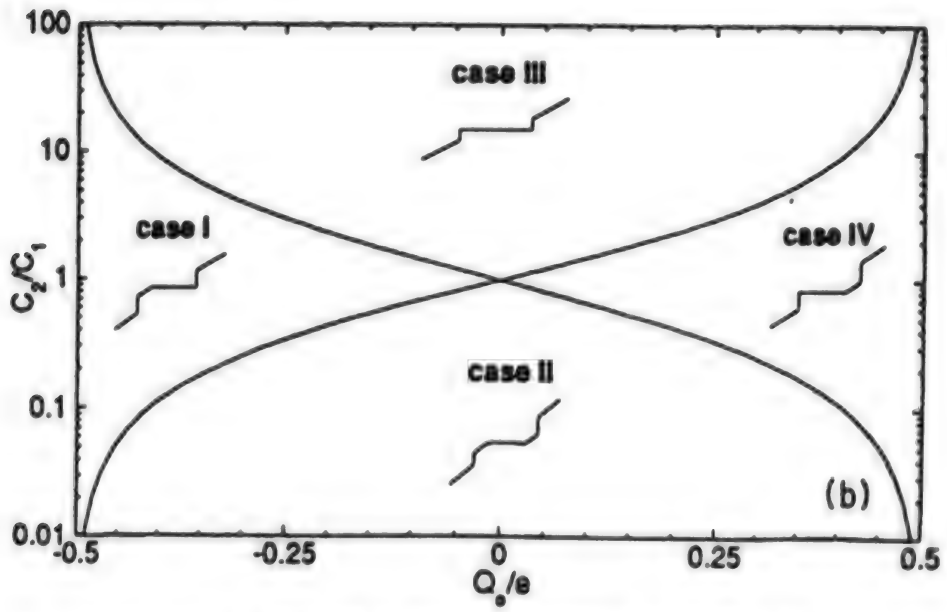

TABLE I. Width of the zero conduction region, ΔV_0, for different cases. The parenthetical restrictions show that the necessary symmetry of the $Q_0 - C_2/C_1$ phase space is preserved. Note that in cases I and IV, $\Delta V_0 \to 0$ as $|Q_0| \to e/2$, while in cases II and III, $\Delta V_0 = e/\max(C_2, C_1)$.

Case	ΔV_0
I ($Q_0 < 0$)	$(e/2 + Q_0)(C_2/C_1C_2)$
II ($C_1 > C_2$)	e/C_1
III ($C_2 > C_1$)	e/C_2
IV ($Q_0 > 0$)	$(e/2 - Q_0)(C_2/C_1C_2)$

$$Q_0 = \frac{1}{e}\left[C_1(\Delta_{\phi_1}) - C_2(\Delta_{\phi_2})\right]$$

5. Conclusion

In our STM, the sample can be cooked to about 20 K. However, the movement of the walker is unstable at low temperatures, due to the deterioration of the piezoelectric constant at low temperatures, and measurement at 20 K was not successful. An example of I-V curve measured at the temperature of liquid nitrogen is shown in Figure 14. Although I-V characteristics vary from one place to another, an intended measurement that can be made to correspond to the STM image was not successful. It is believed that a big reason for this is the difficulty involved in controlling the oxide film thickness. We believe systematic and tenacious experiments are necessary.

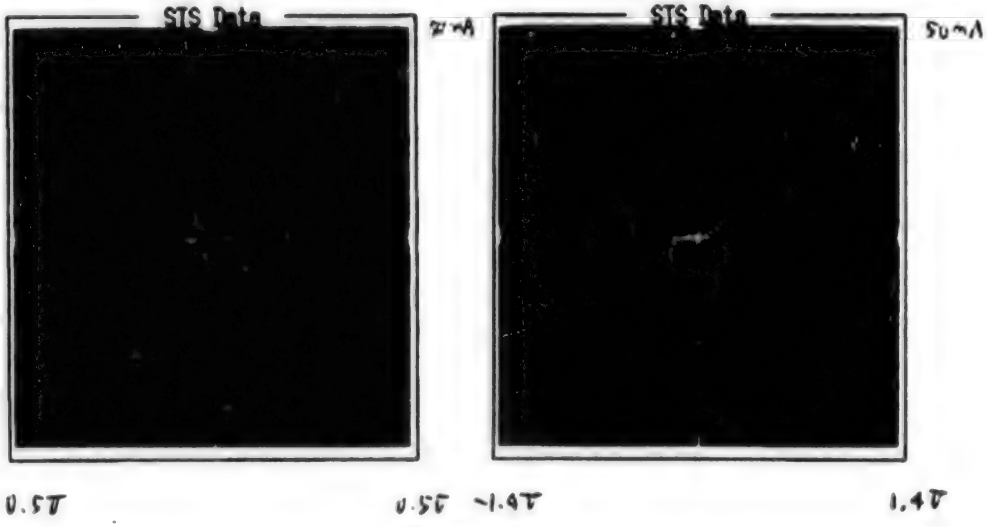

Figure 14.

References

1. Neugebauer, C.A. and Webb, M.B., J. APPL. PHYS., Vol 33, 1962, p 74.

2. Zeller, H.R. and Giaever, I., PHYS. REV., Vol 181, 1969, p 789.

3. Smith, D.P.E. and Binnig, G., REV. SCI. INSTRUM., Vol 57, 1986, p 1630.

4. Uozumi, K., Nakamoto, K., and Fujioka, K., JPN. J. APPL. PHYS., Vol 27, 1988, p L123.

5. Uozumi, K., Nishiura, M., and Kinbara, A., J. APPL. PHYS., Vol 48, 1977, p 818.

6. Wilkins, R., Ben-Jacob, E., and Jaklevic, R.C., PHYS. REV. LETT., Vol 63, 1989, p 801.

7. Hanna, A.E. and Tinkham, M., PHYS. REV., Vol B44, 1991, p 5919.

Apology: The author apologizes for an imperfect digest due to unexpectedly poor health.

Analysis of Semiconductor Surfaces by Ultrahigh-Vacuum STM

936C1098H Tokyo JAPAN SURFACE SCIENCE SOCIETY in Japanese 25 Jun 93 pp 87-107

[Article by Takafumi Yao, Faculty of Engineering, Hiroshima University]

[Text] **1. Introduction**

The clean surface of a semiconductor has a surface structure that is different from the bulk crystal structure. For example, the Si (111) clean surface is covered with a 7x7 reconstructed structure. This structure is being investigated in detail by experiments involving low-energy electron diffraction (LEED), scanning tunnel microscope (STM), transmission electron diffraction (TED), etc. It is generally explained in terms of a dimer-adatom-stacking (DAS) fault. This model consists of stacking defects existing in dimers, adsorbed atoms, and halves of unit cells. The DAS structure is a very stable surface structure since the number of the dangling bonds per unit cell is, in contrast to 49 for the unreconstructed (111) surface, a total of 19. This represents 12 in the adsorbed atom, six in the atom of the stacking defect layer, and one in the corner hole atom. Figure 1 shows the DAS model.

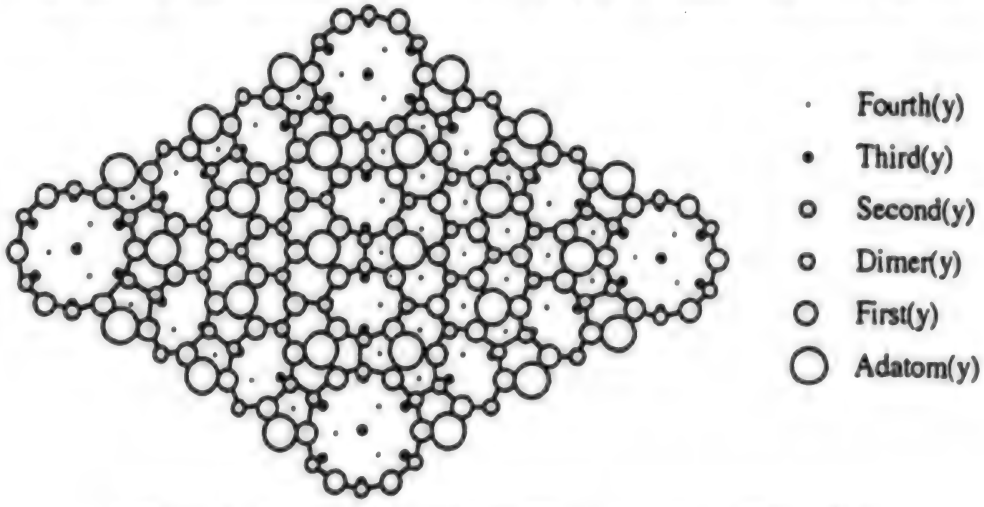

Figure 1. Dimer-Adatom-Stacking (DAS) Fault Model

An Si(100) surface cleaned by heating forms a 2x1 reconstructed structure. Since each surface atom in the unreconstructed surface has two dangling bonds, its surface energy is high, and the surface is unstable. Mutually adjacent surface atoms come close to each other and form a dimer to reduce the energy by decreasing the number of dangling bonds. In STM observations, a 2x1 structure that has a symmetric dimer as the fundamental unit is often investigated. However, according to the results of energy calculations, asymmetric dimers are energetically more stable than symmetric dimers. An atom of one of the monomers of the dimer goes to an sp^2-like state by giving an electron to an atom of the other monomer, and the atom which received the electron goes to an sp^3-like state, to form a buckling structure. The existence of c(4x2) and p(2x2) structures in the (100) surface has been confirmed by STM, LEED, He atom beam diffraction, and angle-resolved ultraviolet photoelectron spectroscopy. These structures have been explained in terms of a reconstruction model having an asymmetric dimer as the fundamental unit. The presence of the 2x1, c(4x2), and p(2x2) on the surface also was confirmed by STM observation. In the dimer strings observed in STM images, structures with a dimer deficiency are frequently recognized. The explanation for this is thought to be as follows. When a missing dimer arises, atoms in the second layer are bonded in the direction along the dimer string, thereby reducing the number of dangling bonds remaining on the deficient dimer by two. Meanwhile, there is also the possibility of an interstitial dimer with a structure in which the dimer is sunk from the surface. In these structures a large lattice deformation is generated along the dimer string, and the deformation energy is increased. However, this increment is small in comparison to the decrease in the electron energy due to the reduction in the number of dangling bonds. Therefore, the total energy goes down and the system is stabilized.

The atoms of metals adsorbed to the clean surface of a semiconductor are bonded with the atoms on the semiconductor surface. As a result, phenomena such as movement of charge, generation of local stress, termination of dangling bonds, and movement of the surface atoms take place, and a singular local structure is created. Needless to say, this local structure gives the lowest total energy of the system. Adsorption of reactive gas molecules causes further desorption of the surface atoms and adsorption of various molecules, and forms a complicated local structure. Further, when the semiconductor surface is transitioning from an amorphous layer to a crystal layer, the local distortion can be readily relaxed. Thus we would expect to find a surface structure that is different from a crystal surface that has undergone a heat treatment.

In this article, we will present several examples of a local structure analysis of semiconductor surfaces using an ultrahigh-vacuum STM. We will use the superstructure of an Al adsorbed Si(111) surface as an example of a metal adsorbed semiconductor surface. We also will describe the recrystallization process (solid phase epitaxial process) of the Si(100) surface converted to an amorphous state by argon sputtering, using this as an example of the observation of the semiconductor epitaxial process. The point to be emphasized in conjunction with the semiconductor process is that metallic adsorption can be regarded as the initial process of epitaxial conversion of silisification, and the transition of the semiconductor surface from an amorphous layer to a

crystal layer by heating is important in understanding what kind of processes are taking place in the annealing process, which is employed frequently in the manufacture of semiconductors.

2. Local Structure of Al on Si(111) 7x7

When metallic atoms are adsorbed on a clean semiconductor surface, one encounters various kinds of fine structures. For example, when a metal such as Au, Ag, or Al is adsorbed to the Si(111) 7x7 surface in the form of a monatomic layer, a stable Si-metal surface is formed, in many cases forming a $\sqrt{3} \times \sqrt{3}$ structure. The system where Al is adsorbed to the 7x7 surface has been analyzed by ARUPS or LEED. It is known that there are many phases consisting of $\sqrt{3} \times \sqrt{3}$, $\sqrt{7} \times \sqrt{7}$, 7x7 and other structures caused by the change in the reconstructed structure due to evaporation and substrate temperature (Figure 2). Of these reconstructed structures, the $\sqrt{3} \times \sqrt{3}$ structure has been investigated most vigorously. In the $\sqrt{3} \times \sqrt{3}$ structure, the sites conceivable for the adsorption of Al atoms are the T_4 site directly above the Si atom in the second layer, and the H_3 site where no atoms of the second layer are found (Figure 3). There has been much discussion, and many experiments have been conducted, but in 1984 Northrup showed that, based on energy calculations, the T_4 site is more stable than the H_3 site. Experimental results from ARUPS, LEED, STM/STS, and KRIPES also support the T_4 site. However, many uncertainties remain. One example is local structures where no periodicity exists, such as the structures in the vicinity of phase boundary and surface atomic step. But real images of these structures are now being obtained by STM. One purpose of this article is to demonstrate local structure analysis by making advantageous use of the characteristics of the STM, which is not affected by the periodicity.

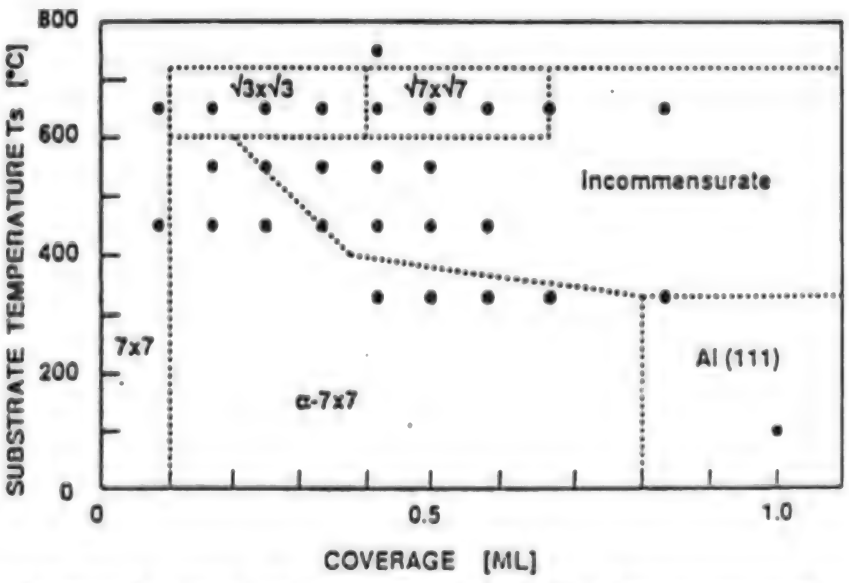

Figure 2. Phase Diagram of Al-Si(111) Superstructure

2.1 STM Observation of Al$\sqrt{3} \times \sqrt{3}$ Structure

2.1.1 Phase Boundary

Following a flash heating to about 1200°C, the Si(111) surface becomes a clean surface covered with the 7x7 structure. By evaporating Al on this surface at room temperature, the Al becomes scattered on the surface as clusters. For Cu and Ag, the existence of selective cluster sites has been reported, but the distribution of Al clusters is random without any preferential adsorption to either of the subunit cells.

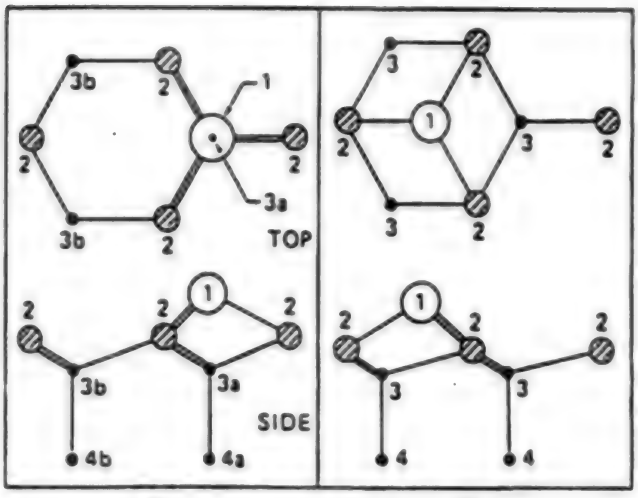

Figure 3. Al Adsorption Sites, T_4 and H_3
(1: Al atom; 2: Si atom)

Figure 3 is an STM image of the surface when it is annealed for 10 seconds at 580°C after Al evaporation, and then returned to room temperature. In the image, two steps can be observed. The Si-7x7 structure is distributed on the upper stage of the steps, while an Al-$\sqrt{3} \times \sqrt{3}$ structure is distributed on the lower stage of the steps. The region of the $\sqrt{3} \times \sqrt{3}$ structure does not form an island on the terrace. It always makes contact with the lower stage of the steps. In other words, the Al-$\sqrt{3} \times \sqrt{3}$ structure is growing to cover the Si-7x7 surface from the lower stage of the steps. When one-third ML of Al was evaporated on the Si-7x7 surface in the state of keeping the substrate temperature at 600°C, results similar to this were obtained.

Next, an STM image taken in the vicinity of the boundary between the Si-7x7 domain and the Al-$\sqrt{3} \times \sqrt{3}$ domain is shown in Figure 4(a). In the 7x7 domain the faulted sites are making contact with the boundary of the two phases. This is because more energy is required for the formation of the $\sqrt{3} \times \sqrt{3}$ structure on the faulted sites than on the unfaulted sites. Figure 4(b) is a schematic diagram showing the atomic arrangement in the vicinity of the boundary of the two different phases. In the figure, the atomic position of the T_4 site is indicated by □, the atomic position of the H_3 site by Δ, the adsorbed atomic position of the 7x7 structure by o, and the observed atomic position by •. The good agreement between the observed atomic position (•) and the T_4 site (□) indicates that Al atoms also are adsorbed at the T_4 sites in the vicinity of the boundary. The most interesting point is that the Al atoms on one line on the boundary are located at the adatom positions of the 7x7 structure. In the figure, Al atoms situated at the adatom positions are indicated by "A," and the Al atoms forming the $\sqrt{3} \times \sqrt{3}$ structure are indicated by "N."

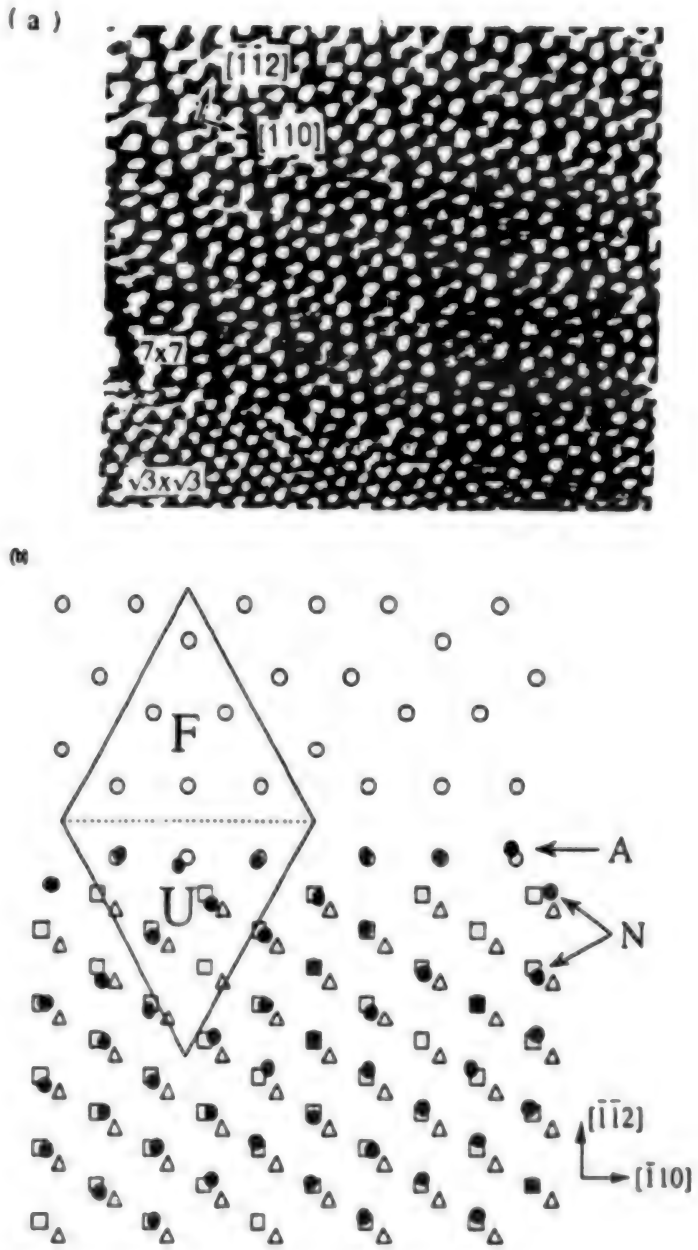

Figure 4. Phase Boundary of $\sqrt{3} \times \sqrt{3}$ Structure and 7x7 Structure at 600°C

Schematic presentation of (a) STM image and (b) atomic arrangement in the vicinity of the phase boundary. Position of the T_4 site atom is denoted by □, that of the H_3 site atom by Δ, that of the adsorbed atoms of the 7x7 structure by o, and that of measured atoms by •.

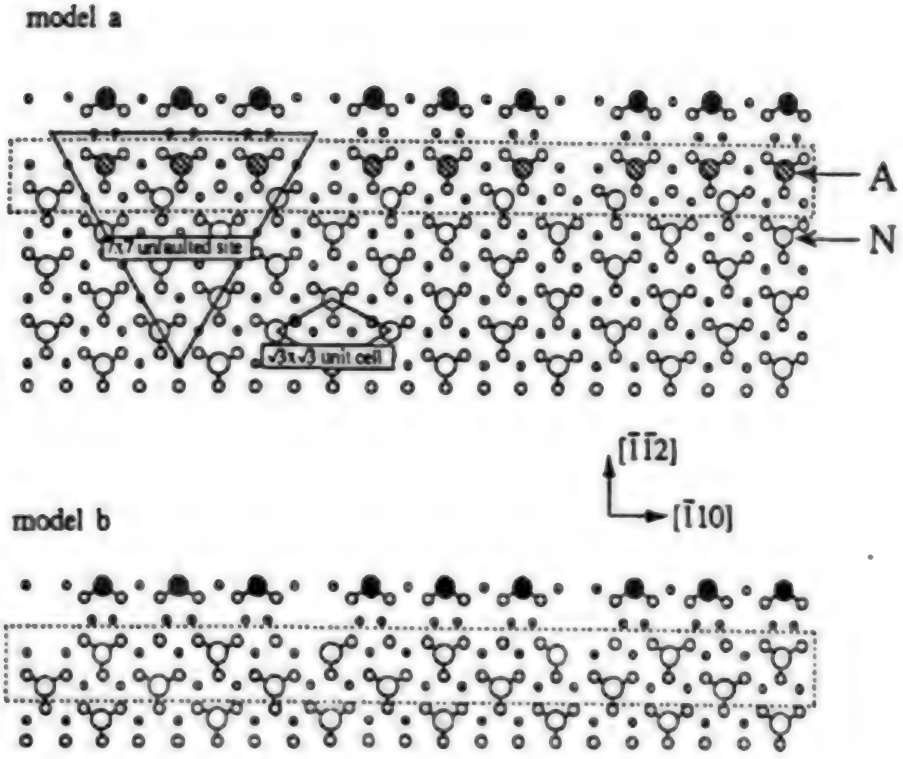

Figure 5. Structural model of Phase Boundary of Al-$\sqrt{3} \times \sqrt{3}$ and Si-7x7
(a) Al atoms fill the adatom sites at the phase boundary, and all others fill the T_4 sites. (b) All Al atoms fill the T_4 sites.

To understand why atoms are found in the boundary, the bonding model (Figure 5(a)) based on the atomic arrangement obtained experimentally and the model (Figure 5(b)) when all Al atoms form the $\sqrt{3} \times \sqrt{3}$ structure of the T_4 sites are compared. In Figure 5(a), those in one line on the boundary are adsorbed to the positions of the adatoms of the 7x7 (A) while others are adsorbed to the T_4 positions. With Si on the base, A atoms are preferentially bonded. The portion corresponding to the unfaulted sites of the 7x7 structure, and the unit cell of the $\sqrt{3} \times \sqrt{3}$ structure are indicated by solid lines. The number of dangling bonds (DBs) in the 21-fold period in the [110] direction surrounded by the broken line are 10 and six, and 12 and two for Figures 5(a) and 5(b), respectively. Judging simply from the total number of DBs, the case shown in Figure 5(a) is more unstable than that in Figure 5(b). However, in the former, the six Al atoms with DBs share the DB electrons with the nearest Si atoms, so the bonding energy is stabilized. DBs remain in the latter, so the system is unstable. Moreover, based on the fact that the boundary of the different phases is defined distinctly, it is considered that on the boundary there exist dimers characteristic of the 7x7 structure. This dimer string will be stable due to the presence of the A atoms in the case of the deformer, but it will be unstable in the latter due to the increase in the number of DBs on the boundary. As in the above, the existence of the characteristic A atoms on

the boundary is necessary in order to keep the boundary structure more stable. If the dimer string is destroyed, the Al region does not remain in the faulted sites, but extends even to the unfaulted sites, and faulted sites of the 7x7 region are arranged again in the boundary. In this way, A atoms play an important role in order to keep the Si region stable.

Summarizing these experimental findings in a schematic manner, one obtains a spatial distribution of the $\sqrt{3} \times \sqrt{3}$ as shown in Figure 6.

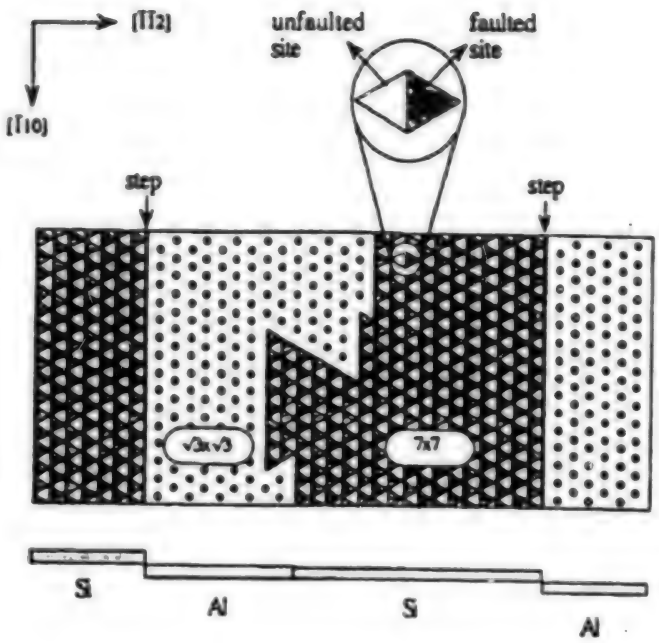

Figure 6. Overall Distribution of Al-$\sqrt{3} \times \sqrt{3}$ Structure

Even when the substrate temperature is suddenly cooled to room temperature, A atoms exist in the boundary (Figure 7). Defects are generated in the vicinity of the $\sqrt{3} \times \sqrt{3}$ domain. Double positioning the $\sqrt{3} \times \sqrt{3}$ structure also was observed. In other words, Al atoms occupy not the intrinsic positions (+), but the positions (o) with a different phase, even though they belong to the same T_4 sites. It is believed that this rearrangement is generated by the movement of the Al atoms, as indicated by the arrows. As a result of double positioning, the total number of DBs is increased. However, when seen locally, the number of DBs in the area surrounding the Al atoms in the boundary is decreased. Thus, double positioning eventually stabilizes the A atoms, and keeps the dimer strings located on the boundary stable.

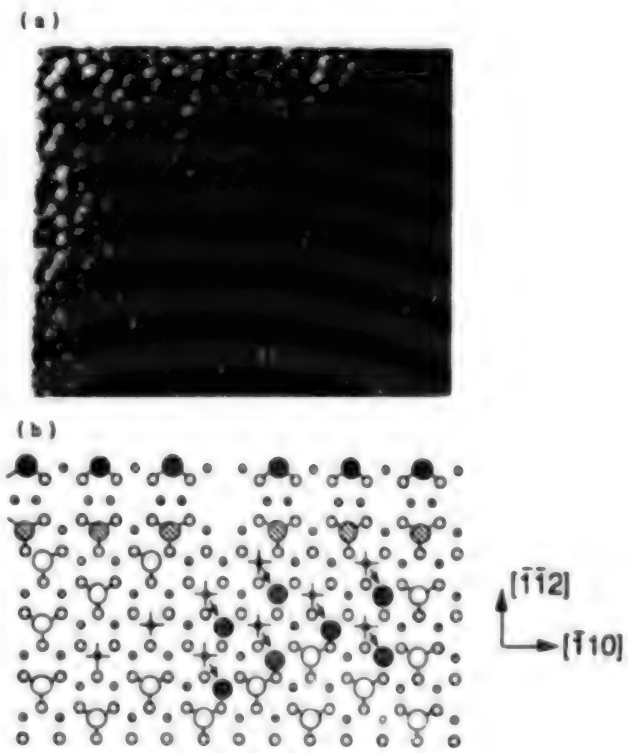

Figure 7. Phase Boundary of → Al-$\sqrt{3} \times \sqrt{3}$ and Si-7x7 Structures at Room Temperature
Schematic diagram of atomic arrangement in (a) STM image, and (b) vicinity of the phase boundary.

Hamers, et al., report that Si atoms enter the replacement positions in the Al-$\sqrt{3} \times \sqrt{3}$ domain. The Si atoms in the $\sqrt{3} \times \sqrt{3}$ domain are observed at about 1 Å lower than the Al atoms when the sample bias is +2V, but are observed at about 1 Å higher than the Al atoms when the sample bias is −2V. The results of STS at these two kinds of atomic sites are completely different. Atoms that are observed higher in the filled state of surface electrons are Si atom replacement defects. Positions that are observed lower for both biases are point holes. In this subsection, we will examine the Al replacement defects in the 7x7 domain.

A surface in which the Al-$\sqrt{3} \times \sqrt{3}$ structure and the Si-7x7 structure coexist was obtained by evaporating several ML of Al on the Si(111) surface, followed by repeated annealing at 600-900°C for several seconds. Figure 8 is an STM image (constant current mode with sample bias voltage of +1 V and tunneling current of 0.1 nA) in which the 7x7 structure (top side and the $\sqrt{3} \times \sqrt{3}$ mode coexist. A disturbance in the lattice is observed in the vicinity of the $\sqrt{3} \times \sqrt{3}$ and the 7x7 structures, and dark regions are also observed. Adatoms with a similar brightness exist in these two regions. However, the adatoms in the $\sqrt{3} \times \sqrt{3}$ structure are higher by about 1 Å than the adatoms in the 7x7 structure.

Figure 8. STM Image Near the Phase Boundary (Sample bias: +1 V)

Figure 9(a) is an STM image of the region near that of Figure 8 measured in the constant current mode. The sample bias was −1 V. For this sample, the bias of the $\sqrt{3} \times \sqrt{3}$ structure region and the 7x7 structure region are formed by two kinds of adatoms with different contrasts. The topography measurement on the line LL' in Figure 8(a) is shown in Figure 8(b). The difference of heights of the two kinds of adatoms in the $\sqrt{3} \times \sqrt{3}$ region is about 1.5 Å. An STM image similar to this was reported by Hamers, et al., and those that look higher are Si atoms replaced by Al atoms, which are called Si defects. Based on this result, the bright and dark adatoms are believed to be Si and Al atoms, respectively. In Figure 9(b), Si atoms in the 7x7 region have a brightness comparable to that of the Si defects. In contrast, the height of the Al atoms of the 7x7 region, and those of the $\sqrt{3} \times \sqrt{3}$ region have different heights. The Al atoms of the 7x7 region are higher by about 1 Å than the Al atoms of the $\sqrt{3} \times \sqrt{3}$ region. However, since the actual height difference of the actual atomic positions is small (about 0.1 Å), it is thought to be reflecting the difference in the electronic structure by the atomic arrangement of the surrounding Al atoms.

Next, let us consider the spatial distribution of the replacement atoms of both kinds. From the STM image (Figure 9(a)) it can be seen that the Si defects that exist in the $\sqrt{3} \times \sqrt{3}$ region tend to form clusters. The number of Al defects existing in the $\sqrt{3} \times \sqrt{3}$ region is 64 for the center adatom sites, in contrast to 44 for the corner adatom sites. This tendency also is observed in other regions, which seems to indicate that it is an essential difference. These experimental findings lead to the following conclusions: Al atoms replace the adatoms so as to maintain the 7x7 structure. But the Al replacement changes the electronic energy of the system, and a distortion in the dimer string is generated. It may be that the total energy of the system when the center adatoms are replaced is further reduced than in the case of the other adsorption sites, and the 7x7 structure becomes more stable due to the difference in the local structure in the surroundings of a center adatom and a corner adatom (that there are two (one) rest atoms in the vicinity of a center (corner) adatom, and that the center (corner) adatom is approaching the dimer string from one (2) direction). The ratio of the number of Al atoms to that of Si atoms is 2.4 in the $\sqrt{3} \times \sqrt{3}$ region, in contrast to 1.12 in the 7x7 region. Accordingly, the calculated Al coverage rate is 0.13 in the 7x7 region, and 0.24 in the $\sqrt{3} \times \sqrt{3}$ region. That a surface with coexisting Si and Al atoms is observed is due to the fact that the sample used is in the phase transition (desorption) process from the Al-$\sqrt{3} \times \sqrt{3}$ phase to the Si-7x7 phase. The aluminum atoms are believed to have been incorporated into the 7x7 structure. That the Al coverage rate is different in the two regions suggests that the Al atoms in the $\sqrt{3} \times \sqrt{3}$ region are partially desorbed from the surface by annealing, and the 7x7 structure is formed when the local Si concentration exceeds the threshold value.

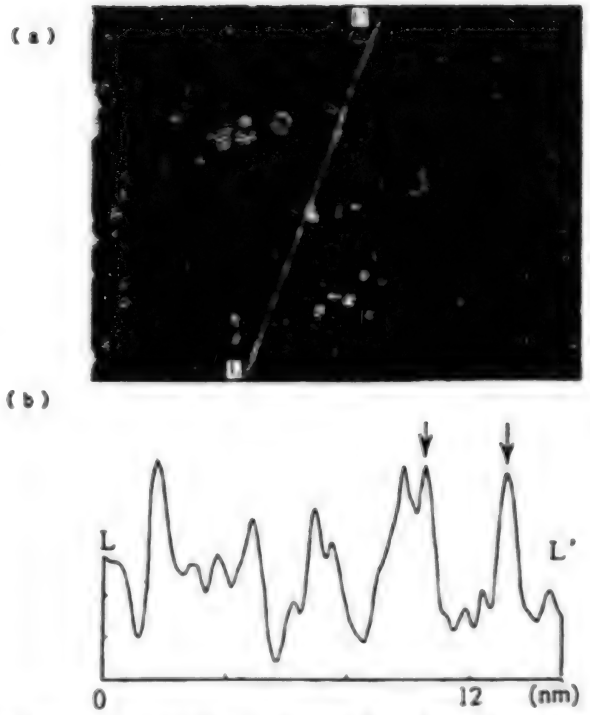

Figure 9. (a) STM Image in the Vicinity of the Phase Boundary
(b) Topography on Line LL'

2.1.3 Phase Transition From Si(111)-7x7 Structure to Al-$\sqrt{3} \times \sqrt{3}$ Structure

About one-third ML of Al is evaporated on the Si(111) surface at a substrate temperature of 600°C to form a $\sqrt{3} \times \sqrt{3}$ structure. When the substrate temperature was raised to 622°C, an "in-situ" phase transition from the Si-7x7 structure to the Al-$\sqrt{3} \times \sqrt{3}$ structure was observed. Figure 10 shows a series of STM images. Some eight to nine seconds were required to measure one picture. The time after measurement was started is indicated in the figure. The 7x7 region has roughly a triangular form whose two sides coincide with the

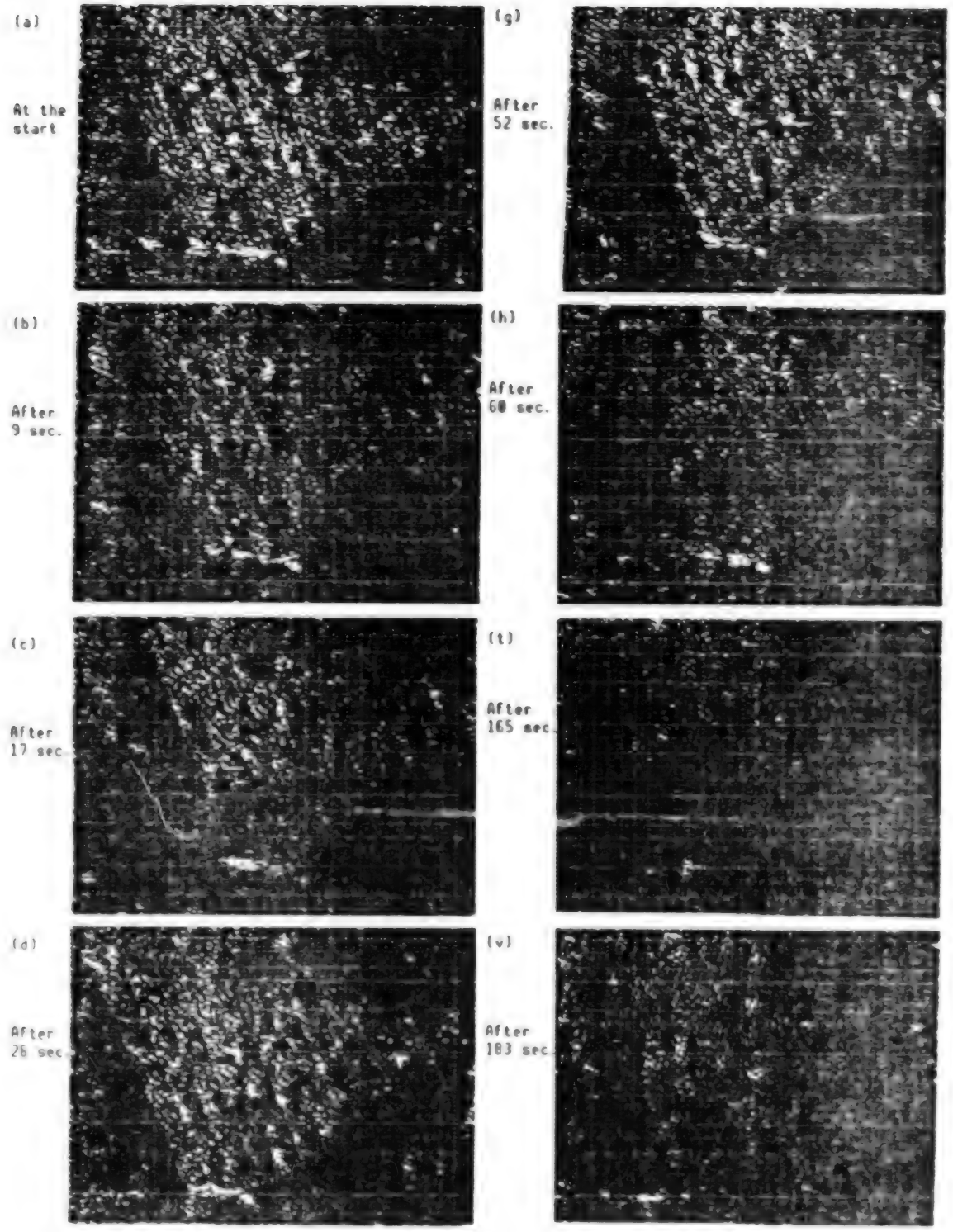

Figure 10 Real Time Observation of Phase Transition From the 7x7 Structure to the Al-$\sqrt{3} \times \sqrt{3}$ Structure

[112] and [121] steps. Since the site making contact with the [112] step is an unfaulted site, the site making contact with the Al-$\sqrt{3} \times \sqrt{3}$ structure is a faulted site. Because of the high temperature involved, and because it is in the midst of the phase transition, it is not possible to discriminate individual atoms, but its boundary is distinct.

Given the fact that the 7x7 unit can be observed in its complete form in every image in the figure, it is believed that the rate of phase transition is determined by the transformation of the stacking faults at the dimer string and the faulted site at the boundary. Accordingly, the phase transition is taking place with the 7x7 site as the unit. The characteristics of the phase transition are as follows:

(1) As seen in Figures 10(a) to 10(c), the phase transition starts from those locations most removed from the step, and proceeds toward the step.

(2) The most stable form of the 7x7 structure is the regular triangle, as seen in Figure 10(d), and, in fact, this state continues for some time.

(3) In Figure 10(e) [as published] and (f) [as published] fluctuations can be observed. This means that phase transition is occurring not only from the 7x7 to the $\sqrt{3} \times \sqrt{3}$ structure, but also from the $\sqrt{3} \times \sqrt{3}$ to the 7x7 structure. The fluctuations occur at places away from the step, and not from the step.

(4) Over time, the area of the 7x7 region decreases, but its nearly triangular shape is maintained.

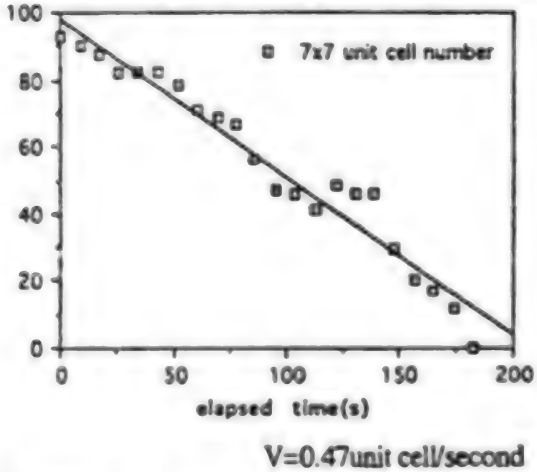

Figure 11. Variation Over time of the Area of the 7x7 Region

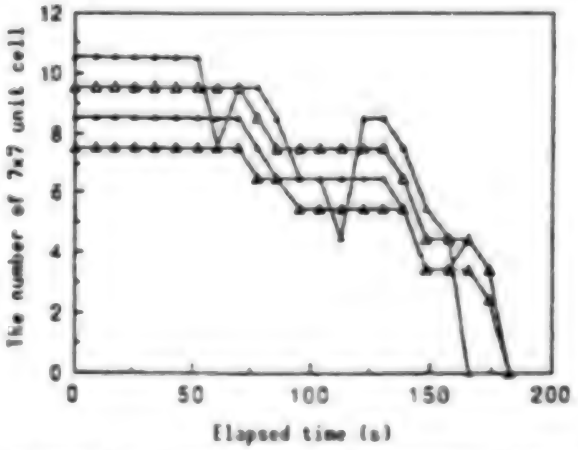

Figure 12. Changes for Different Lines

The change over time of the area of the 7x7 region in the phase transition is given in Figure 11. The vertical axis shows the number of 7x7 cells. Although a step-wise decrease can be seen, the average rate of decrease is 0.47 cells/

second. The change for individual lines of the 7x7 structure is shown in Figure 12. In the figure, the four lines from the left that make contact with the [121] step and run in the direction of the [011] step are designated four to seven. The horizontal axis is the elapsed time, and the vertical axis is the number of units of the 7x7 structure. In general, fluctuations are observed in the cell site of the fifth to the seventh lines. Beyond the fifth line, no fluctuation is observed, and the number of units decreases rapidly. Accordingly, the critical two-dimensional core of the 7x7 domain surrounded by the $\sqrt{3} \times \sqrt{3}$ domain has five cells.

In the above, an interesting phenomenon regarding the phase transition from the Si(111)-7x7 structure to the Al-$\sqrt{3} \times \sqrt{3}$ structure has been described. This is a phenomenon to which the formation theory of a two-dimensional critical core in crystal growth can genuinely be applied. Details will be delivered at the meeting, but this phase transition can be understood by phenomenological analysis.

2.1.4 α-7x7 Structure

An α-7x7 structure is formed at a low Al coverage rate, and at a relatively low temperature. However, its structure has remained unknown. The LEED pattern of this structure shows the 7x7 period, but its spot intensity is different from that of a clean 7x7 structure. According to the diffraction intensity vs. voltage curve obtained by LEED, this difference is clearly recognizable in the diffraction spots, especially in a (3/4 3/4) LEED spot pattern.

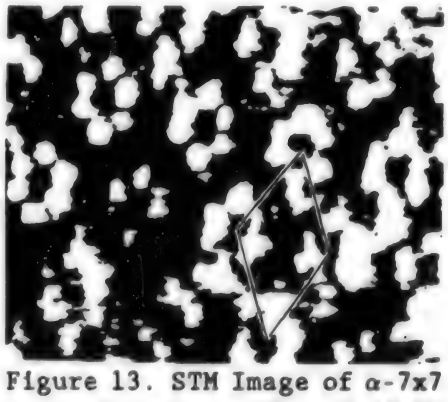

Figure 13. STM Image of α-7x7 Structure (Vs: -0.12 V)

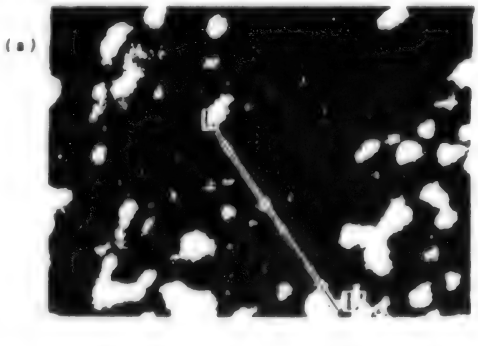

Figure 14. (a) STM Image (-2 V) (b) Topography Measurement

Figure 13 is an STM image of a film obtained by evaporating Al while keeping the Si(111) substrate at 412°C (sample bias -0.12 V and tunneling current 0.1 nA). It shows a 7x7 period, and corner adatoms are clearly observable. The central part of the 7x7 cell has a dark contrast, showing that Al atoms preferentially replaced center adatoms. The difference due to subcells of the 7x7 structure, as seen in Cu or Ag on Si(111), was not observed.

The STM images change markedly depending on the bias current between the sample and the probe. Figure 14(a) shows an STM image of a sample when the voltage is -2 V. The topography along segment LL' is shown in Figure 14(b). The corner hole of the 7x7 structure

is indicated by an arrow. For both faulted and unfaulted sites, a triangular Al cluster (A) at the central part can be seen. A similar triangular structure also appears when Cu is evaporated at room temperature on the Si(111) surface. However, in the case of Cu/Si(111), the triangular clusters are independent of the bias voltage. In contrast, in the case of Al/Si(111), they are closely related to the bias voltage.

Figure 15 is an STM image of a sample when the bias is +2 V. The triangular clusters seen in Figure 14 become more rounded with the corners removed. Clusters are linked together to form a hexagonal ring structure. A similar STM image is obtained when Pb is evaporated on the Si(111) surface. In a high-resolution STM image, six corner adatoms can be observed, though dark, inside the ring, forming a structure that is basically the same as that in the STM image shown in Figure 14(a).

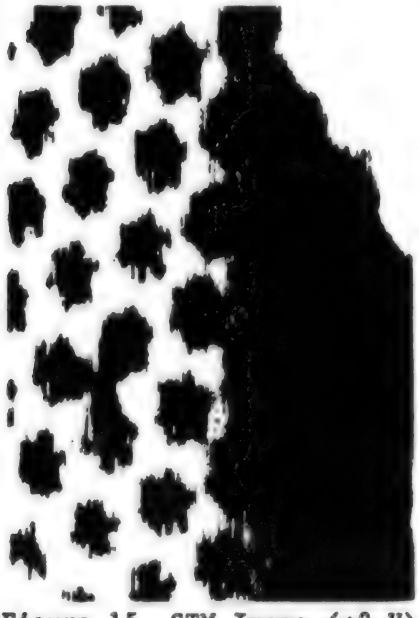

Figure 15. STM Image (+2 V)

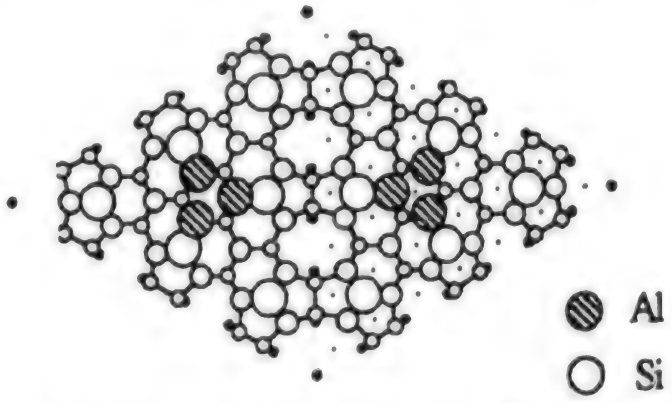

Figure 16. Model for α-7x7 Structure

Based on the above observation results, a model for the adsorption of Al atoms can be elaborated. It is shown in Figure 16. A cluster of Al atoms consists of three Al atoms each having a trimer structure. The three Al atoms are bonded to the dangling bonds of the nearest center adatom, and a trimer is formed by bonding with the adjacent Al atoms. The number of dangling bonds decreases by three per subcell according to this model, and consequently the surface energy goes down. The center atom is relaxed to a nonmetallic state through bonding with the Al atoms. Because of this, center adatoms are not observed in the occupied surface state in the vicinity of Fermi energy in Figure 8.1 [as published].

3. SPE Process in Argon Sputtered Si Film

Solid phase epitaxy (SPE) is a method in which an amorphous film formed on a single crystal substrate is made to grow epitaxially in a solid-state phase by annealing. This method has a number of advantages, such as a low growth temperature, and ease in controlling the film thickness and the growth region. It also makes it possible to form a single crystal Si (SOI) structure on an insulator by lateral solid-phase epitaxy (L-SPE) with a deposited film, to flatten the sample surface through a combination of SPE, and conversion to an

amorphous phase by ion implantation or argon sputtering. The SPE process involves subjecting an amorphous Si film formed by one of several processes—ion implantation, vacuum evaporation, chemical vapor deposition (CVD), etc., and annealed—to SPE, and then evaluating the film by electrical measurements, fast ion backward scattering, electron microscopic observations, etc. These methods involve a number of problems, such as separating the formation of an amorphous film and the annealing process, a satisfactory SPE performance is not obtained because oxygen becomes mixed in the film when it is taken out in the atmosphere, and the SPE process is affected by both of these. In our experiment, we formed an amorphous film layer on Si(100) by argon sputtering in an ultrahigh vacuum, and the sample surface was observed by STM while subjecting the film to SPE growth by annealing without exposing the sample to the air.

3.1 STM Observation of Amorphous Si Surface

Prior to conversion to an amorphous film the Si(100) cleaned surface shows a 2x1 reconstructed structure. Figure 17 is an STM image of an amorphous layer formed by argon sputtering. It shows a granular surface morphology. The surface is formed by nearly uniform particles 1~2 nm in diameter, and about 03.5~0.75 nm high.

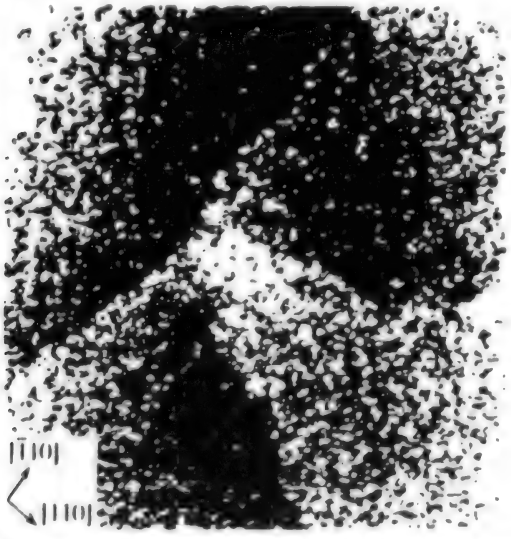

Figure 17. Ar Sputtered Amorphous Si Surface

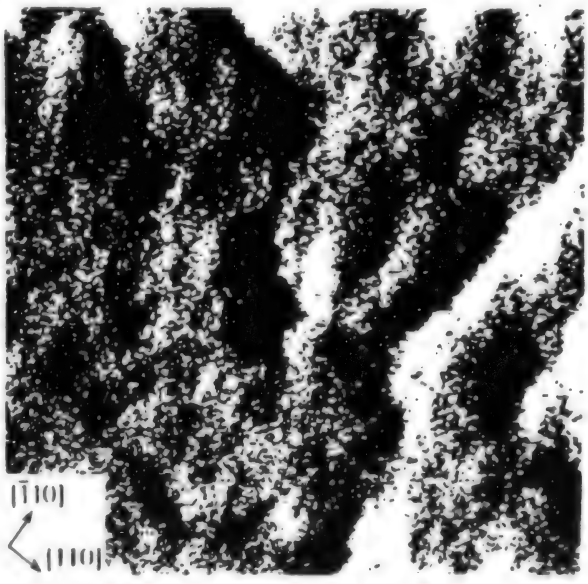

Figure 18. Amorphous Si Surface Annealed at 500°C

3.2 STM Observation of SPE Process

To achieve a satisfactory SPE, a method is normally employed in which the atomic density in the amorphous film is increased, while the influence of oxidation is reduced by annealing the deposited amorphous Si film at a low temperature, below 500°C. Figure 18 is an STM image made after annealing for 90 minutes at about 500°C. As a result of low-temperature annealing, the surface changes from a granular to a gentle surface, and the atomic density is increased by compaction due to firing of the amorphous film. Steps are formed

by the extension of grooves in the [110] and [1$\bar{1}$0] directions. Since no reconstructed structure is observed in this stage, SPE growth is not yet taking place.

When the sample was heated to 587°C, a periodic structure at the atomic level was observed locally. When the sample was further heated to 621°C, the terrace was expanded, and a reconstructed structure was observed over a wide range, as shown in Figure 19(a), and an amorphous Si film was satisfactorily grown by SPE up to the surface. The lattice spacing agreed approximately with the dimer string spacing, and the STM image showed a 2x2 structure. In the 2x2 structure, each dimer is arranged in the form of a square, but a structure in which adjacent dimer strings running parallel to the [110] direction have opposite phases and arrangement in a zigzag form was observed, as shown in Figure 19(b).

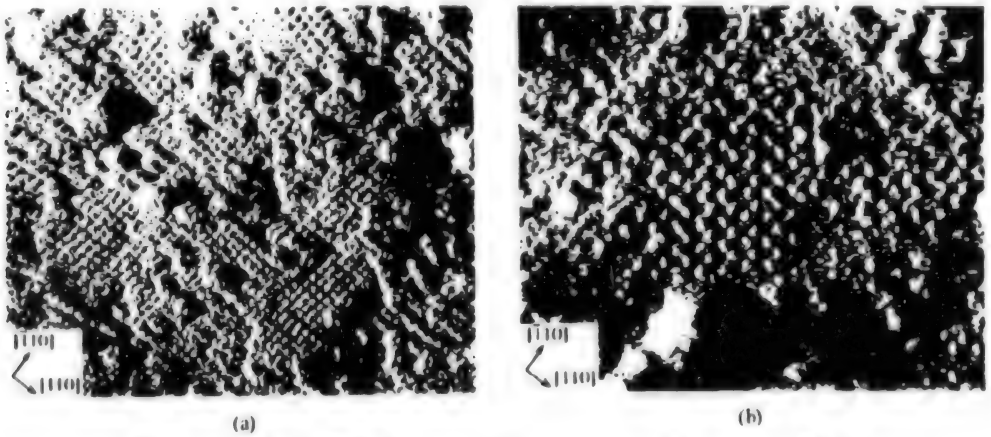

Figure 19. SDTM Images After Annealing at 621°C

These structures are reconstructed by a dimer and a missing dimer (or dimer and interstitial dimer). When the number of missing dimers increases, the number of dangling bonds decreases, and the surface energy goes down, but the lattice distortion energy in the surrounding area increases. The density of the missing dimers is regulated by balancing the decrease in the electronic energy and the increase in the distortion energy. What should be noted is that the area surrounding the reconstructed structure is amorphous, and the region of the 2x2 structure is extremely narrow, one of a side of less than 10 nm, so the number of degrees of freedom on the surface is high, and the distortion energy is believed to be reduced. Because of this, a condition characterized by a high missing dimer density, namely, the formation of a 2x2 structure in which a dimer and a missing dimer are arranged alternately, becomes possible. In the structure shown in Figure 19(b), it is believed that the tilting direction of the asymmetric dimer is inverted along the dimer string, and is reconstructed to a c(4x4) structure, as shown in Figure 20(b). H. Wang, et al., reported the appearance of a c(4x4) structure on a Si(100) clean surface after annealing at 580~630°C, and proposed a c(4x4) structure model due to missing dimers, but their model does not explain the STM image.

3.3 SPE Process

In the SPE process for an argon-sputtered amorphous Si film, we have observed by STM both 2x2 and c(4x4) structures after annealing at 587~621°C. As shown in Figure 20, it is believed that these structures are constructed of asymmetric dimers and missing dimers, and that the adjacent asymmetric dimers are arranged with the same phase in the 2x2 structure, whereas they are arranged in the opposite phase in the c(4x4) structure.

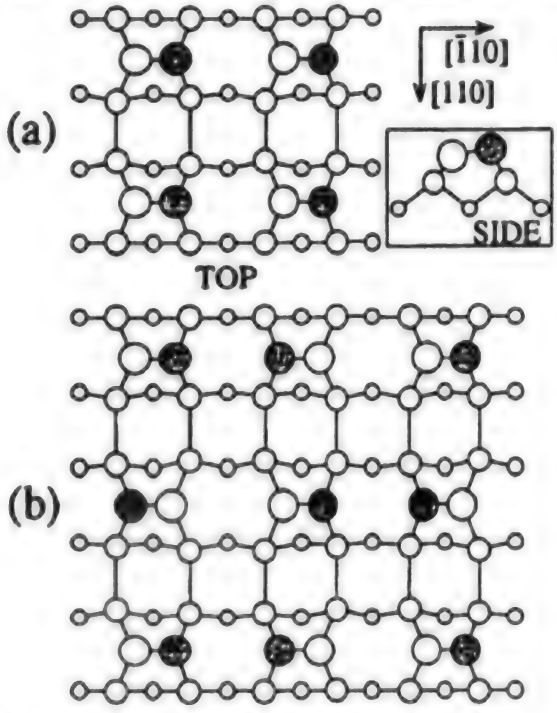

Figure 20. Models for (a) 2x2 and (b) c(4x4) Structures

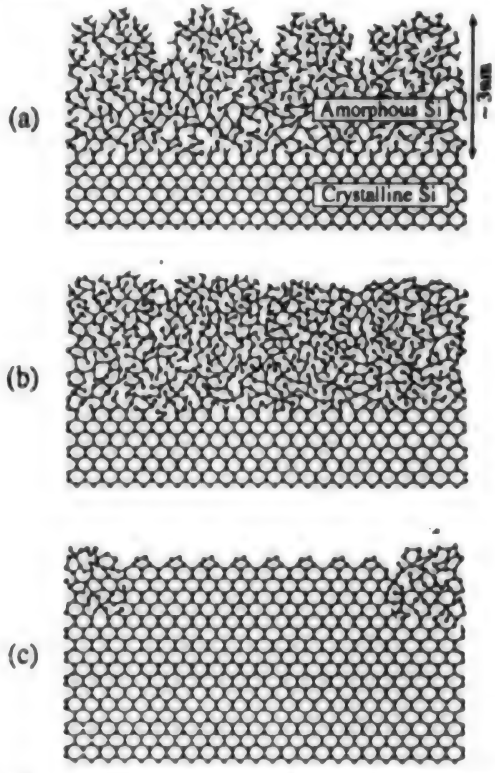

Figure 21. Models for SPE Growth Process

A model of the SPE process is shown in Figure 21. Figure 21(a) shows the vicinity of the sample surface formed by argon sputtering, and Figures 21(b) and 21(c) show the side face after low-temperature annealing at about 500°C, and after SPE growth at 587~621°C, respectively. In the figure, a solid circle represents an Si atom, and an empty circle represents an Si atom in the region converted to an amorphous state. The surface converted to an amorphous state is granular with grains having a diameter of about 1~2 nm. The amorphous film is compacted by firing at a low temperature, about 500°C, and SPE growth takes place at 587~621°C, with partial formation of the 2x2 and c(4x4) structures on the surface. Islands with a diameter of several nanometers are observed surrounding the reconstructed regions, as shown in Figure 19(a), and complete SPE is not proceeding.

4. Conclusion

In this article we have outlined our research on the superstructures on an Al Si(111) surface, and on the SPE process for an amorphous Si film using ultrahigh-vacuum STM. The advantage of using STM as a tool for surface structure analysis is that it enables one to clarify aperiodic structures at the atomic level. In combination with STS, identification of individual atoms becomes possible. It is expected that a great deal of knowledge can be obtained by STM about surface structures that previously have been unknown. Another point to be emphasized in surface research by STM is that the semiconductor processes will become understandable on the atomic level. In this article we have presented some examples of crystalline restoration by thermal annealing. STM is compatible with a process that uses gases that will make possible "in-situ" observation of the semiconductor processes. This work has been done as part of a joint research project with Masamitsu Yoshimura, Katsuhiro Uesugi, and Katsuya Takaoka, Faculty of Engineering, Hiroshima University, and Masashi Iwatsuki, Tomoshige Sato, and Takashi Sueyoshi, Japan Electron Optics Laboratory Co., Ltd.

References

1. Schlier, R.E. and Farnsworth, H.E., J. CHEM. PHYS., Vol 30, 1959, p 917.

2. Binnig, G., Rohrer, H., Gerber, Ch., Weibel, E., "7x7 Reconstruction on Si(111) Resolved in Real Space," PHYS. REV. LETT., Vol 50, 1983, p 120.

3. Takayanagi, K., Tanishiro, Y., Takahashi, S., and Takahashi, M., SURF. SCI., Vol 164, 1985. p 367.

4. Hansson, G.V., Bachrach, R.Z., Bauer, R.S., and Chiaraia, P., "New Model for Metal-Induced Reconstruction on Si(111)," PHYS. REV. LETT., Vol 46, 1981, p 1033.

5. Uhrberg, R.I.G., Hansson, G.V., Nicholls, J.M., Persson, P.E.S., and Flodstrom, S.A., "Photoemission Study of the Surface and Bulk Electronic Structures of Si(111)7x7 and Si(111)$\sqrt{3} \times \sqrt{3}$:Al," PHYS. REV., B31, 1985, p 3805.

6. Kinoshita, T., Kono, S., and Sagawa, T., "Angle-Resolved Ultraviolet-Photoelectron-Spectroscopy Study of the Si(111)$\sqrt{3} \times \sqrt{3}$-Al Surface," Ibid., Vol B32, 1985, p 2714.

7. Nishikata, K., Murakami, K., Yoshimura, M., and Kawazu, A., "Structural Studies of Al/Si(111) Surfaces by LEED," SURF. SCI., 1991.

8. Northrup, J.E., "Si(111)$\sqrt{3} \times \sqrt{3}$-Al: An Adatom-Induced Reconstruction," PHYS. REV. LETT, Vol 53, 1984, p 683.

9. Tromp, R.M., Hamers, R.J., and Demuth, J.E., "Si(001) Dimer Structure Observed With Scanning Tunneling Microscopy," PHYS. REV. LETT., Vol 55, 1985, p 1303.

10. Hamers, R.J., Tromp, R.M., and Demuth, J.E., "Scanning Tunneling Microscopy of Si(001)," PHYS. REV., Vol B34, 1986, p 5343.

11. Artacho, E. and Yudurain, F., "Proposal for Symmetric Dimers at the Si(100)-2x1 Surface," PHYS. REV. LETT., Vol 62, 1989, p 2491.

12. Chadi, D.J., "Atomic and Electronic Structures of Reconstructed Si(100) Surfaces," Ibid., Vol 43, 1979, p 43.

13. Yin, M.T. and Cohen, M.I., "Theoretical Determination of Surface Atomic Geometry: Si(001)-(2x1)," PHYS. REV., Vol B24, 1981, p 2303.

14. Zhu, Z., Shima, N., and Tsukada, M., "Electronic States of Si(100) Reconstructed Surface," Ibid., Vol B40, 1989, p 11868.

15. Tabata, T., Aruga, T., and Murata, Y., SURF. SCI., Vol 179, No 1, 1987, p 63.

16. Cardillo, J.M. and Becket, G.E., "Diffraction of He at the Reconstructed Si(100) Surface," PHYS. REV., Vol B21, 1980, p 1497.

17. Uhrberg, R.I.G., Hansson, G.V., Nicholls, J.M., and Foldström, S.A., "Experimental Studies of the Dangling- and Dimer-Bond-Related Surface Electron Bands on Si(100) (2x1)," Ibid., Vol B24, 1981, p 4684.

18. Ihm, J., Lee, D.H., Joannopoulos, J.D., and Xiong, J.M., "Structural Phase Diagrams for the Surface of a Solid: A Total-Energy, Renormalization-Group Approach," PHYS. REV. LETT., Vol 51, 1983, p 1872.

19. Pandey, K.C., in Proc. of the 17th Int. Conf. on the Physics of Semiconductors, ed. D.J. Cadi and W.A. Harrison, Springer-Verlag, New York, 1985, p 55.

20. Aruga, T. and Murata, Y., "Ordered-Defect Model for Si(001)-(2x8)," PHYS. REV., Vol B34, 1986, p 5654.

21. Ihara, S. and Ho, S.L., "Ab Initio Molecular-Dynamics Study of Defects on the Reconstructed Si(001) Surface," PHYS. REV. LETT., Vol 65, 1990, p 1909.

22. Andersen, J.N., Wigren, C., Karlsson, U.O., "Surface Related Core Level Shifts for the Si(111)$\sqrt{3} \times \sqrt{3}$:Al System," J. VAC. SCI. TECHNOL., Vol B9, 1991, p 2384.

23. Huang, H., Tong, S.Y., Yang, W.S., Shih, H.D., Jona, F., "Atomic Structure of Si(111)-($\sqrt{3} \times \sqrt{3}$)R30°-Al Studied by Dynamical Low-Energy Electron Diffraction," PHYS. REV., Vol B42, 1990, p 7483.

24. Hamers, R.J., "Effects of Coverage on the Geometry and Electronic Structure of Al Overlayers on Si(111)," Ibid., Vol B40, 1989, p 1657.

25. Nicholls, J.M., Reihl, B., and Northrup, J.E., "Unoccupied Surface States Revealing the Si(111)$\sqrt{3} \times \sqrt{3}$-Al.-Ga, and -In Adatom Geometries," Ibid., Vol B35, 1987, p 4137.

26. Tokumoto, H., Miki, K., and Kaiyama, K., J. CRYST. GROWTH, Vol 99, 1990, p 1329.

27. Crowder, B.J., J. ELECTROCHEM. SOC., Vol 118, 1971, p 943.

28. Csepregi, L., Kennedy, E.F., Gallagher, T.J., Mayer, J.W., and Sigmon, T.W., "Reordering of Amorphous of Si Implanted With ^{31}P, ^{75}As and ^{11}B Ions," J. APPL. PHYS., Vol 48, 1977, p 4234.

29. Csepregi, L., Kennedy, E.F., Mayer, J.W., and Sigmon, T.W., "Substrate-Orientation Dependence of the Epitaxial Regrowth Rate From Si-Implanted Amorphous Si," Ibid., Vol 49, 1978, p 3906.

30. Saitoh, S., Sugii, T., Ishiwara, H., and Furukawa, S., "Growth Condition of Deposited Si Films in Solid-Phase Epitaxy," JPN. J. APPL. PHYS., Vol 20, 1981, p L130.

31. Kunii, Y., Tabe, M., and Kajiyama, K., "Solid-Phase Epitaxy of CVD Amorphous Si Film on Crystalline Si," JPN. J. APPL. PHYS., Vol 21, 1982, p 1431.

32. Ishihara, H., Yamamoto, H., and Furukawa, S., "Lateral Solid-Phase Epitaxy of Amorphous Si Films on Si Substrates With SiO_2 Patterns," APPL. PHYS. LETT., Vol 43, 1983, p 1028.

33. Roth, J.A., Olson, G.L., Kokorowski, S.A., and Hess, L.D., MAT. RES. SOC. SYMP. PROC., Vol 1, 1981, p 413.

34. Wang, H., Lin, R., and Wang, X., "Structural Model of Si(100)-c(4x4)," PHYS. REV., Vol B36, 1987, p 7712.

35. Takaota, K., Yoshimura, M., Yao, T., Sato, T., Sueyoshi, T., and Iwatsuki, M., Proc. MRS Symposium, 1992.
Takaoka, K., Yoshimura, M., Yao, T., Sato,T., Sueyoshi, T., and Iwatsuki, M., PHYS. REV., 1993.

36. Tosch, St. and Neddermeyer, H., PHYS. REV. LETT., Vol 61, 1988, p 349.

37. Lander, J.J. and Morrison, J., SURF. SCI., Vol 2, 1964, p 553.

38. Hamers, R.J., PHYS. REV., Vol B40, 1989, p 1657.

39. Kinoshita, T., Kono, S., and Sagawa, T., PHYS. REV., Vol B32, 1985, p 2714.

40. Nishikata, K., Murakami, K., Yoshimura, M., and Kawazu, A., SURF. SCI., Vol 269/270, 1992, p 995.

41. Tosch, St., and Neddermeyer, H., SURF. SCI., Vol 211/212, 1989, p 133.

42. Ibid., PHYS. REV. LETT., Vol 61, 1988, p 349.

43. Palmino, F., Dumas, Ph., Mathiez, Ph., Mouttet, C., Salvan, F., and Korler, U., ULTRAMICROSCOPY, Vol 42, 1992, p 928.

44. Uesugi, K., Yao, T., Sato, T., Sueyoshi, T., and Iwatsuki, M., APPL. PHYS. LETT., 1993.

45. Yoshimura, M., Takaoka, K., Yao, T., Sato, T., Sueyoshi, T., and Iwatsuki, M., PHYS. REV., 1993.

Development of Atomic Crafting

936C1098I Tokyo JAPAN SURFACE SCIENCE SOCIETY in Japanese 25 Jun 93 pp 109-119

[Article by Masakazu Aono, Laboratory of Surface and Interface Technology, Institute of Physical and Chemical Research]

[Text] 1. Introduction

Controlling the structure of matter by manipulating individual atoms, a process that we recently have begun to call atomic crafting, which was absolutely impossible 10 years ago, is now becoming a reality. This new advance is due largely to the appearance of the scanning tunnel microscope (STM) invented by Binnig and Rohrer. This is because the STM, which was developed as a tool to "see" atoms, can also be used as a tool to "manipulate" atoms. The STM uses a probe that is brought extremely close to a sample, and it becomes possible to "manipulate" atoms within the sample through the clever use of the interaction between the atoms of the probe and the atoms of the sample.

Although it already has been demonstrated in many experiments that it is possible to manipulate individual atoms with the STM, many technical problems still remain to be solved before it can be used in practical applications. It is necessary to improve the accuracy, precision, stability, and speed of the manipulation process, and also to develop new methods for monitoring, setting the environment, and increasing the scale of the manipulation. More important than this technical research is fundamental scientific research. Studies aimed at clarifying the physical mechanisms involved in the manipulation of atoms are still very limited. Without such research it is not possible to obtain appropriate guidelines for resolving technical problems. As just noted, research on atomic crafting has only just begun.

The object of this article is to describe the current status of atomic crafting and related issues, and to present the results of our recent research. More specifically, we will present some examples of manipulation based on "removing," "imparting," and "transporting," and will discuss the various mechanisms by which they are accomplished. Moreover, we will also touch on a method we developed for "monitoring" (even without individually observing the results of STM after manipulation) these atomic manipulations.

2. Experiments

As noted above, atomic manipulation of the surface of Si(111)-7x7 and (Si(001)-2x1) will be discussed in this article. These samples were segmented from n-type wafers. The samples were set on a sample holder of an STM (VG-STM 2000 or JEOL-JSTM 4000 XV) that is operated in an ultrahigh vacuum (UHV), and were cleaned by heating them to about 1200°C in a UHV. This process produced the well-known 7x7 long-period structures for the Si(111) surface, and 2x1 structures for the Si(001) (observed by STM).

The primary element used in the STM probe was W, but Au, Ag, and Pt also were used. The manipulation of atoms was possible using any one of them, but there were important differences among them. These probes were sharpened by electropolishing, and the radius of curvature of the tip of the probe was about 100 nm, according to observations with a scanning electron microscope (SEM). The probe was covered with many contaminants. Although the probe was cleaned by heating by electron impact in a UHV, in reality many contaminants on the atomic scale still remained, so the probe was insufficient for the purpose of atomic manipulation. These atomic scale contaminants were removed by repeatedly applying a strong electric field to the tip of the probe. We would like to emphasize that such careful preparation of the probe is essential for the purpose of atomic manipulation.

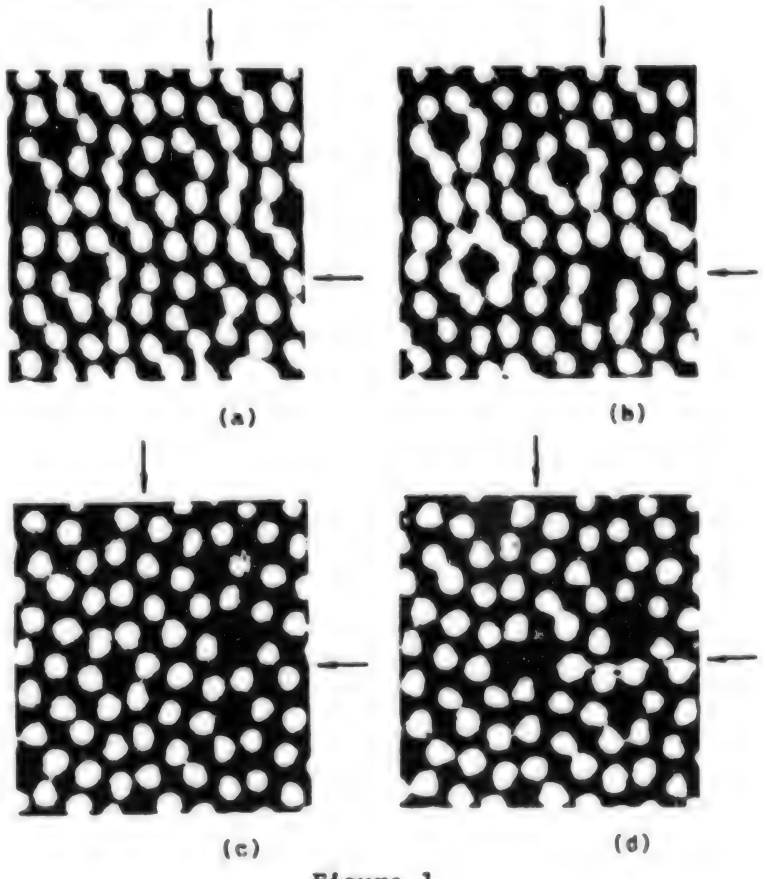

Figure 1.

3. Examples of Atomic Manipulation

A. "Removal" of a Single Atom

We are now in a position to be able to remove individual Si atoms from the Si(111) 7x7 surface one by one. An example is shown in Figure 1, Figures (a) and (c) are STM images of different regions of the surface prior to the removal of Si atoms. An STM probe (in this case W) prepared by the method described in the previous section was placed directly above the Si atom indicated by an arrow in the STM image, and it was possible to remove the Si atom by applying a voltage of +6 V to the probe for 10 ms (at this time the tunneling current was kept at 0.6 nA by means of a feedback circuit). The results are shown in Figures 1(b) and (d), respectively.

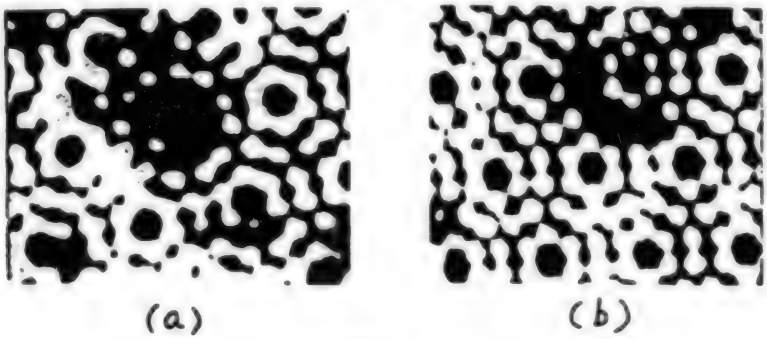

Figure 2.

The result of sequentially removing Si atoms from the six-membered ring on the periphery of a "corner hole" situated at the corners of a unit cell on the Si(111)-7x7 surface is given in Figure 2(a), and the result of sequentially removing Si atoms on the outside of the six-membered ring is given in Figure 2(b). One of the objects of this experiment was to determine, when a group of Si atoms is removed, whether nearby Si atoms are displaced substantially from their original positions. Figures 2(a) and (b) indicate that essentially the Si atoms in the vicinity are not displaced.

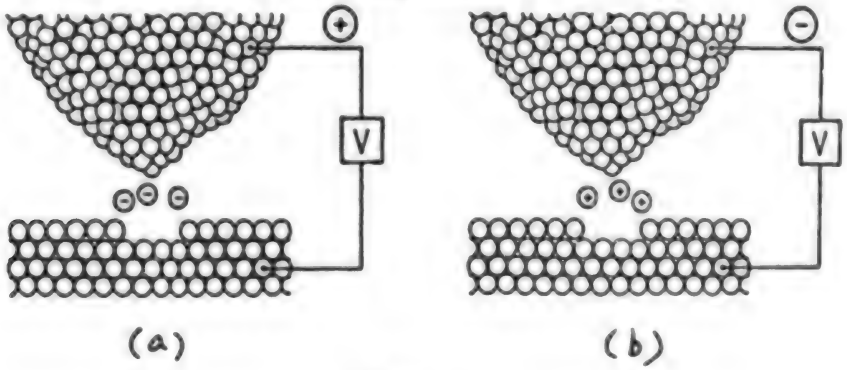

Figure 3.

Through detailed experiments we have demonstrated why Si atoms can be removed by this method. The conclusion is shown schematically in Figure 3. The reason is that the Si atoms of the sample surface "field evaporate" as negative and

positive ions when positive and negative potentials are applied to the probe, as shown by Figures 3(a) and (b), respectively.

Since field evaporation of negative ions from the sample is basically undetected by a field ion microscope (FIM), by which field evaporation has been studied most deeply, there are people who questioned the mechanism shown in Figure 3(a). However, according to recent theoretical calculations by Lang, and Miskovsky, et al., the mechanism shown in Figure 3(a), which is similar to the mechanism shown in Figure 3(b) will occur rather naturally. In field evaporation, reduction of the potential barrier of an atom due to a mirror image effect is vitally important, but the circumstances are very much different in FIM and STM. That is, in contrast to the occurrence of the mirror effect only for the needle due to the large distance (several centimeters) between the needle and the opposing electrode (screen) in the FIM, the mirror effect occurs for both the probe and the sample due to the extremely small distance (about 1 nm) between the probe and the sample for STM. In other words, the mirror effect in STM is double that of the FIM. Another important difference between FIM and STM is that while the ions field evaporated from the needle fly as free particles to the opposing electrode in the FIM, the ions field evaporated from the sample are constantly in fairly strong interaction with the probe or the sample in the STM. In this case, even though it is the same field evaporation, the conventional knowledge gained with the FIM does not necessarily apply to the STM.

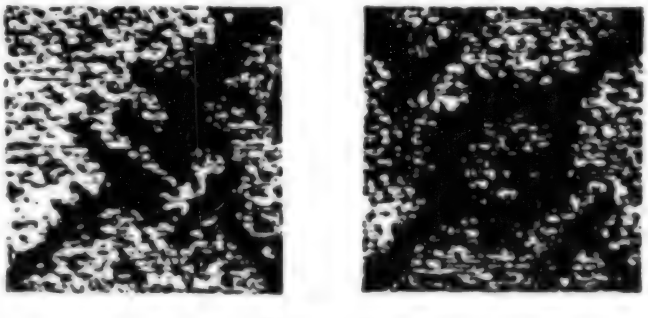

Figure 4.

In the experiments where Si atoms were removed one by one, as shown in Figures 2 and 3, the length of time the voltage was applied to the probe was short as as 10 ms. However, if the application time is increased, then Si atoms are removed one after another, and a large hole is created in the surface. Accordingly, if the probe is scanned parallel to the surface while applying a voltage, it digs a groove. Figure 4 shows a nanometer scale pattern formed by grooves dug by a probe scanning at a speed of 50 nm/s.

Let us come back to the experiments where Si atoms were removed one by one. Two crystallographical different kinds of Si atoms exist on the Si(111)-7x7 surface. One is the Si atom (corner Si atom) that exists at a corner of one unit cell, and the other is the Si atom (center Si atom) that exists at the center of the unit cell. It is known that these Si atoms are removed with a different level of probability, even under the same experimental conditions. That is, according to the results of the experiment in which a large number of Si atoms were removed at random without discriminating among them, the center Si atoms were removed more easily than the corner Si atoms with a probability 1.6 times as high. An analysis showed that this is because of the smaller bond energy of the center Si atom, which is about 0.01 eV less than that of the corner Si atom. This bond energy is consistent with the results of relevant theoretical calculations.

Another similar measurement example will be presented. In any sample surface there exists a step phenomenon on the atomic scale. In the Si(001)-2x1 surface, there exist two kinds of steps, called type A and type B. These two steps have different arrangement of Si atoms, and accordingly, there is a difference in the bond energy of the Si atoms in the different steps. Since this bond energy difference is important in conjunction with atomic layer growth on the Si(001)-2x1 surface, detailed theoretical calculations have been carried out. These calculations indicate that the difference is about 0.14 eV per dimer formed by two Si atoms. We measured the degree of difficulty involved in removing dimers of Si atoms formed from the type A and type B steps, and determined the difference of the bond energies of Si dimers of both steps by a method that is slightly different but essentially equivalent to that of the method described above. As a result, a value close to the theoretical result was obtained.

In this manner, we acquired a method that can be used to determine experimentally the difference in the bond energy of atoms that are situated at different locations of the surface. So far as this author is aware, such a measurement was impossible by any of the previously existing methods.

B. "Impartation" of Single Atom

In the removal of Si atoms as described in the previous section, it became clear that when an Si atom is removed it will stick to the probe with some degree of probability, and it is possible to impart the same Si atom to the sample surface again by field evaporation. A series of results in which Si atoms are imparted to the Si(111)-7x7 surface by the use of this phenomenon are shown in Figure 5. In the figure the Si atom imparted is indicated by the cross mark.

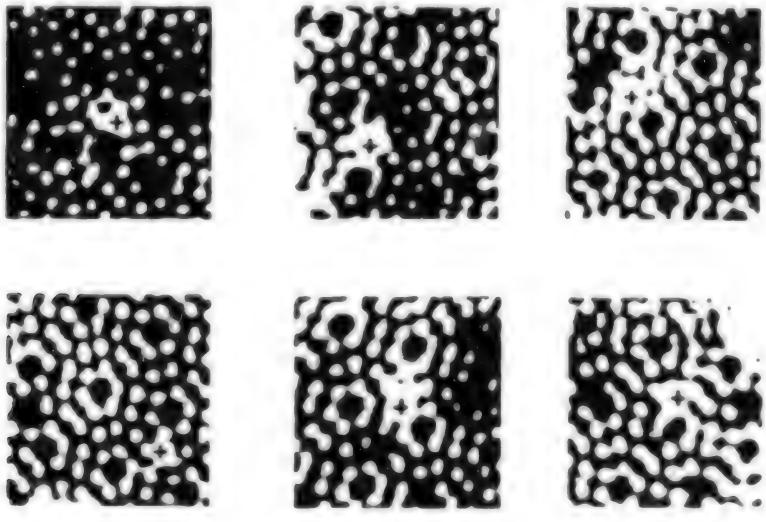

Figure 5.

The STM does not yet have the ability to analyze the individual elements that appear in the image. Accordingly, it is not possible to assert that the atoms marked by the cross are Si atoms with 100 percent certainty. However, there is

a good deal of other evidence to indicate that they are Si atoms. One indication is that the atoms marked by a cross in Figure 5 always appear in the same crystallographic positions (at the center of the triangle formed by one corner Si atom and two center Si atoms). This position is the same position where the Si atom is adsorbed when Si atoms are evaporated on the Si(111)-7x7 surface.

The reader might wonder why, if some of the Si atoms removed from the sample are adsorbed to the probe and then returned again by field evaporation to the sample, then some of the atoms that constitute the probe are not imparted by field evaporation to the sample. This is because the experiment reported in Figure 5 was done by using a W probe. It is difficult to field evaporate atoms from an element such as W, which is very hard, and has a high melting point.

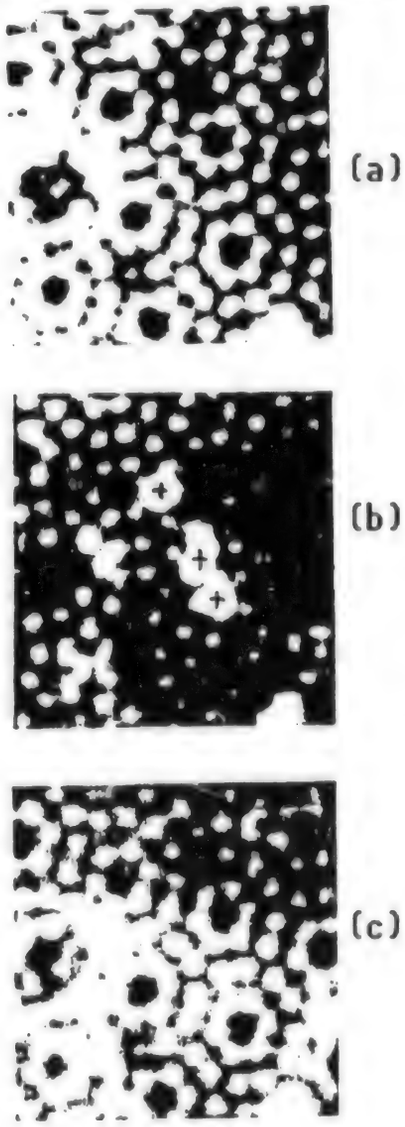

Figure 6.

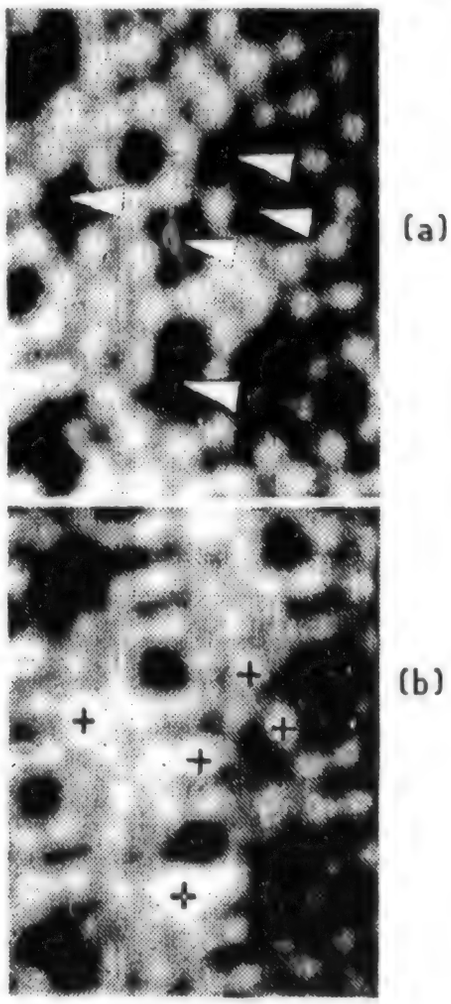

Figure 7.

Employing the technique of imparting the Si atoms adsorbed to the probe again to the sample, some interesting experiments, which are shown in Figures 6 and 7, were carried out. Figure 6

shows the results of an experiment in which, after three Si atoms were imparted (Figure 6(b)) to the Si(111)-7x7 surface (Figure 6(a)), they were removed again (Figure 6(c)). To be noted here is the fact that, after the removal of the three Si atoms, the atomic arrangement in the surface of the Si(111)-7x7, which is the base material, is not disturbed. Figure 7 shows a situation where one Si atom was imparted to each Si atom hole (indicated by arrows in Figure 7(a)), which were present from the beginning, as part of the restoration process (indicated by crosses in Figure 7(b)). It is possible to impart other kinds of atoms, which are neither atoms removed from the sample nor atoms that constitute the probe, to the sample surface. For example, an instance where atomic hydrogen (H) that had been adsorbed to the probe was imparted to the Si(111)-7x7 surface is shown in Figure 8 (Figures 8(a) and (b)) depict the surface before and after, respectively, the H atom was imparted. (The arrow shows the defect which existed from the beginning as the position marker.) The adsorption of H to a Pt probe was accomplished by introducing molecular hydrogen (H_2) at a pressure of 1×10^{-7}torr to the STM chamber. It is known that H_2 is adsorbed to the surface of Pt by dissociating as H_2—H. Since the Si(111)-7x7 surface does not adsorb H_2, the Si(111)-7x7 surface will not be affected. In fact, in Figure 8(a), which was taken in H_2 of 1×10^{-7} Torr, the 7x7 structure is clearly visible. Since H can be adsorbed by the Si(111)-7x7 surface, H supplied by the W probe can be adsorbed to the surface.

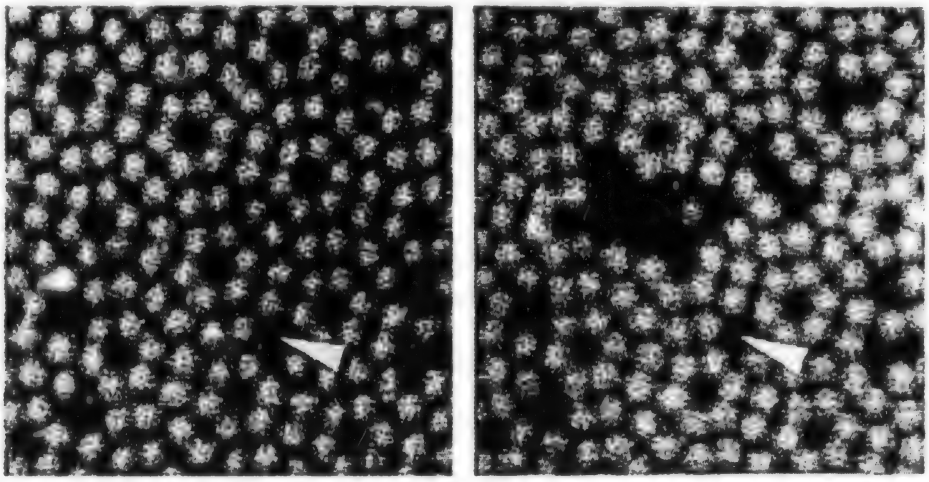

(a) (b)

Figure 8.

C. "Movement" of Single Atom

Figure 9(a) is an STM image of the Si(111)-7x7 surface to which an Si atom has been imparted (marked with a cross). An STM probe was placed at a position about 5 nm away from the atom in the upper left direction, and a voltage of +6 V was applied for 10 ms. As a result, the Si atom in question was moved to another but crystallographically equivalent position, as shown in Figure 9(b). Experiments conducted to date indicate that the movement of this Si atom does not take place in a direction directly related to the position where the probe was placed.

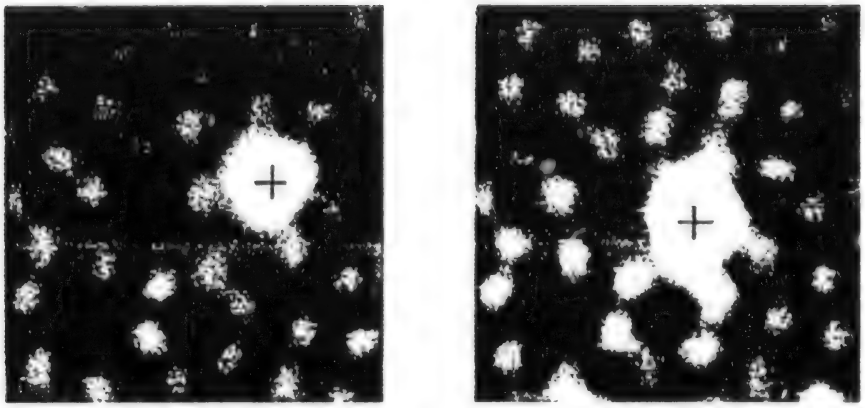

(a) (b)

Figure 9.

Currently, we are trying to clarify the physical mechanism of the movement by repeating the experiments. If the mechanism can be identified, then it may be possible to control the movement of atoms.

4. Real-Time Monitoring of Atomic Manipulation

In all of the examples of atomic manipulation described in the previous section, whether atomic manipulation was actually achieved was confirmed by studying STM images of the surfaces. However, in the high-speed atomic manipulation that will be needed for future applications, it may be too time-consuming to study individual STM images. It is desirable to be able to monitor atomic manipulation in real time. We have developed such a method.

When an electric current to be used for atomic manipulation is applied to the probe for a short time, the tunneling current is increased, so if a feedback circuit is operating to keep the tunneling current constant, the probe tries to depart from the sample in order to bring the tunneling current to the original set value. When the application of the electric current is over, the probe moves back closer to the sample and into the original position. Figure 10 shows the monitoring of such a positional movement of the probe. The duration of current application was 30 ms.

If during the actual application of a current for atomic manipulation, the removal of atoms from the sample, for example, actually takes place, the effective distance between the probe and the sample is increased, and the probe approaches the sample correspondingly. An example of this is shown in Figure 10(b). By contrast, if atoms are imparted to the probe, the effective distance between the probe and the sample is decreased, and the probe moves away from the sample correspondingly. That such positive and negative positional change of the probe are closely related to the removal and the impartation of the atom, respectively, has been confirmed by studying STM images after the event. Thus, the use of this method makes it possible to confirm in real time whether atomic manipulation was accomplished without having to study STM images. Thus, this technique makes it possible to carry out sure atomic manipulation much faster than the conventional manner.

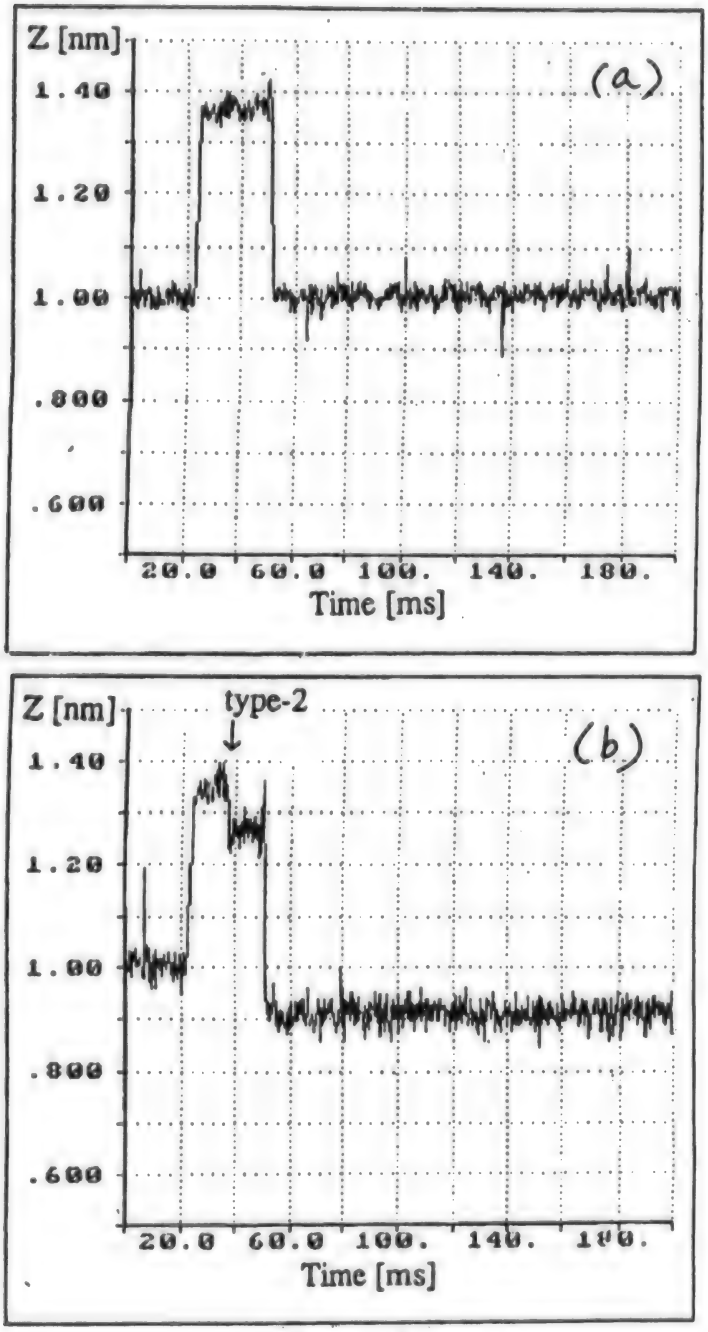

Figure 10.

5. Summary and Outlook

It has been shown that, on an Si(111)-7x7 and Si(001)-2x1) surface, the "removal," "impartation," and "movement" of Si atoms can be accomplished by the use of the effect of the electric field generated by the STM probe, and the physical mechanisms of these phenomena were discussed. In addition, a method for monitoring this atomic manipulation in real time was presented.

Based on a steady accumulation of such research, more controlled atomic manipulation will become possible in the not too distant future. When such control becomes possible, giant memories consisting of several hundreds of cerabits, or new nanometer-sized electronic elements, such as a one-electron transistor, will be realized. Moreover, new physical and chemical possibilities will be opened by constructing micromaterials or pseudomolecules with atomic arrangements that are impossible to create with any existing method, and it will be possible to measure their properties.

References

1. Binnig, G. and Rohrer, H., HELVETICA PHYS. ACTA., Vol 55, 1982, p 762; SURF. SCI., Vol 126, 1983, p 236.

2. Becker, R.S., Golovchenko, J.A., and Swartzentruber, B.S., NATURE, Vol 325, 1987, p 419.

3. Eigler, D.M. and Schweizer, E.K., Ibid., Vol 344, 1990, p 524; Eigler, D.M., Lutz, C.P., and Rudge, W.E., Ibid., Vol 352, 1991, p 600.

4. Lyo, I.W. and Avouris, P., SCIENCE, Vol 253, 1991, p 173; Lyo, I.W., Avouris, P., Schubert, B., and Hoffman, R., J. PHYS. CHEM., Vol 94, 1990, p 4400.

5. Hosoki, S., Hosaka, S., and Hasegawa, T., APPL. SURF. SCI., Vol 60/61, 1992, p 2481.

6. [Not translated]

7. Kobayashi, A., Grey, F., and Aono, M., SCIENCE, Vol 259, 1993, p 1724.

8. Iwatsuki, M., Kitamura, S., and Mogami, A., Proc. X11th Intern. Conf. Electron Microscopy, San Francisco Press Inc., San Francisco, 1990, p 322.

9. Utugi, Y., NATURE, Vol 347, 1990, p 747.

10. Huang, D.H., Uchida, H., Yoshinobu, J., and Aono, M., JPN. J. APPL. PHYS., in press.

11. Uchida, H., Huang, D.H., and Aono, M., SURF. SCI., in press.

12. Kobayashi, A., Grey, F., Uchida, H., Huang, D.H., and Aono, M., Proc. Engineering Foundation Conf., Atomic and Nanoscale Modification of Materials, Ventura, California, 1992, in press.

13. Huang, D.H., Uchida, H., and Aono, M., to be published.

14. Lang, N.D., PHYS. REV., Vol B45, 1992, p 13599.

15. Miskovsky, N.M., Wei, C.M., and Tsong, T.T., PHYS. REV. LETT., Vol 69, 1992, p 2427.

16. Uchida, H., Huang, D.H., Grey, F., and Aono, M., Ibid., Vol 70, 1993, p 2040.

17. Chadi, D.T., Ibid., Vol 59, 1987, p 1691.

18. Kobayashi, A., Grey, F., Snyder, E., and Aono, M., SURF. SCI., in press.

19. Koeler, U., Demuth, J.E., and Hamers, R.J., J. VAC. SCI. TECHNOL., Vol A7, 1989, p 2860.

20. Kuramochi, H., Uchida, H., Huang, D.H., Snyder, E.J., and Aono, M., to be published.

21. Grey, F., Huang, D.H., Kobayashi, A., Snyder, E.J., Uchida, H., and Aono, M., PROC. JPN. ACAD., Vol 69, Ser. B., 1993, p 101.

Atomic Control of Solid-Liquid Interface

936C1098J Tokyo JAPAN SURFACE SCIENCE SOCIETY in Japanese 25 Jun 93 pp 121-128

[Article by Kingo Itaya, Faculty of Engineering, Tohoku University]

[Text] **Abstract:** It is said that, "Devils live in the surface." This is because a surface has completely different properties from the interior. This is due to the unique electronic states or atomic structure of a surface. Therefore, it is extremely important in studying electrode reactions to clarify the relationship between the surface structure and its surface reactivity from a microscopic perspective. However, studies on the relationship between the surface structure of electrodes at the atomic level to reactions that take place on the surface have just been started recently by the use of surface analytical techniques (such as low-energy electron diffraction (LEED) and Auger electron spectroscopy (AES)) in an ultrahigh vacuum (UHV). These techniques, however, require movement of the electrode from a solid-liquid interface to a vacuum. In other words, in-situ observation of actual reactions taking place in the surface is not yet possible.

At the same time, it became clear from many experiments carried out in a UHV that the recently developed scanning tunnel microscope (STM) has a very high surface resolution. Moreover, measurement results proved that its measurement environment does not have to be only a UHV, but also can be in the atmosphere or in a liquid. These results showed the possibility of in-situ measurements in conditions where the electrode surface is brought into contact with a solution.

In our laboratory, beginning with the development of an in-situ electrochemical scanning tunnel microscope (ESTM) that can be operated under electron control, we have been engaged in demonstrations of this method. In this article we will take up gold and platinum electrodes in connection with a metallic electrode/solution interface, and will also touch on a semiconductor/solution interface.

1. Electrochemical STM (ESTM)

The basic configuration of the STM is shown in Figure 1. It consists of a sample that is an electrical conductor and a probe, a piezoelectric body that scans the probe in the X and Y directions, and a Z axis piezoelectric body

that controls the distance between the sample and the probe. When the probe is brought to about 10 Å from the sample, the electron clouds overlap, and the application of a bias voltage (V) between the two causes a tunneling current (J) given by the following to start to flow:

$$J = (e^2/h) \cdot (k/4\pi^2 s) \cdot V \cdot \exp(-2ks) \quad (1)$$

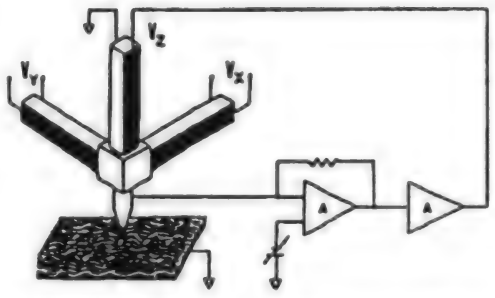

Figure 1. Basic Configuration of STM

Here, s is the distance between the sample and the probe (in Å), ϕ is the effective height of the tunnel barrier (eV), and $k = 0.5 \times (\phi)^{1/2}$.

The voltage change in the Z-axis direction obtained at this time by scanning the sample surface in the X and Y directions with the probe with a constant tunneling current corresponds to the topography of the sample surface, and its three-dimensional image is an STM image. Since the tunneling current has an exponential relationship with s, as shown in Equation (1), it changes by one order of magnitude for each increase in distance of about 1 Å. The high resolution in the vertical direction possessed by the STM is due to this relationship.

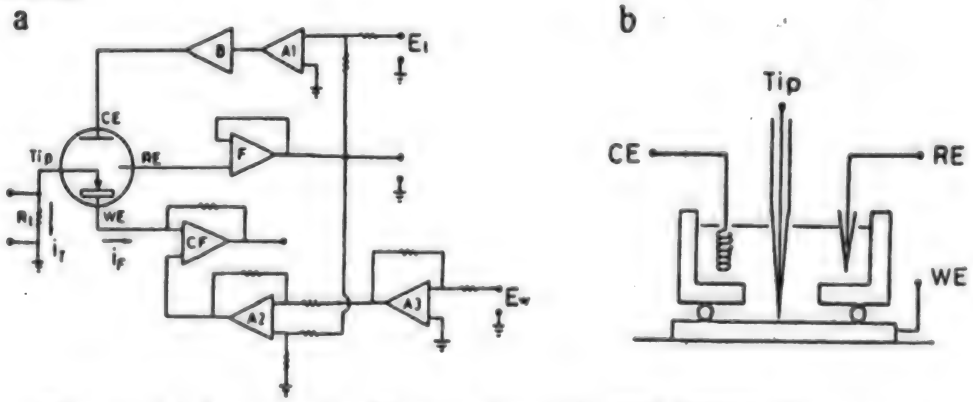

Figure 2. Quadrupole Electrochemical STM (ESTM) Apparatus
(a) Bipotentiostat; (b) Electrochemical cell

The STM can operate in a vacuum or in the atmosphere, according to the above configuration, but in an electrolytic solution electrochemical reactions take place between the sample and the probe. Thus it is not possible to control the electrochemical reactions occurring on the surface by regulating the potential of the sample electrode. The same thing also applies to the probe. Under these circumstances, the author's group developed a quadrupole-type STM system that can independently set the potentials of the sample and the probe relative to a reference electrode by applying a bipotentiostat circuit. Figure 2 shows a circuit diagram and a schematic diagram of an STM cell. In this system, the potential difference between the sample and the probe becomes the tunneling bias. With the completion of this device, in-situ observations at the atomic level of electrode surfaces where various kinds of electrochemical reactions are in progress became possible.

Although similar STM devices were announced by Wiechers and others at nearly the same time, these devices have some problems regarding the independence of the probe potential. Thus our system, which employs a more rigorous circuit, is the leading technology now.

2. Metallic Electrode/Solution Interface

As mentioned above, electrochemical reactions are nonuniform system chemical reactions, and the essence of the reactions are dominated by the atomic structure of the electrode surface. Given this perspective, investigations using single metallic crystals whose surface atoms are in a regulated arrangement are being used. In recent years, a surface treatment method for single crystal electrodes made of noble metals such as Pt, Au, Ag, and Pd was established, and it became possible to expose with relative ease an ideal electrode surface whose surface atomic arrangement is regulated in advance, to a solution. Accompanying this development, a systematic study of various kinds of electrochemical reactions that use single noble metal crystal electrodes have been advanced.

In addition, a structural analysis of electrode surfaces on the atomic and molecular levels has been accelerated by the appearance of various kinds of in-situ measurement techniques, such as infrared reflection, adsorption spectroscopy (IRRAS), and extended-range X-ray adsorption edge fine structure (EXAFS). Of these, ESTM is the most direct, and seems to be a technique with the greatest potential for the analysis of dynamic electrode reaction processes.

In what follows, we will present the results of an ESTM measurement of the surface structure of Pt and Au single crystal electrodes.

2.1 Clean Surface Structure

Figure 3 shows a cyclic voltamogram (CV) of the Pt(111) surface in a 0.05 M H_2SO_4 aqueous solution. In the 0.05–0.55 V vs. RHE region there appears a hydrogen adsorption-desorption wave characteristic of the Pt(111) surface given by

$$Pt + H^+ + e^- \rightarrow Pt\text{–}H \qquad (2)$$

Meanwhile, when the sample potential is swept toward the anode side, an oxide formation appears on the Pt surface in the vicinity of 1.4 V. This is shown in Equation (3).

$$Pt + H_2O \rightarrow Pt\text{–}O + 2H^+ + 2e^- \qquad (3)$$

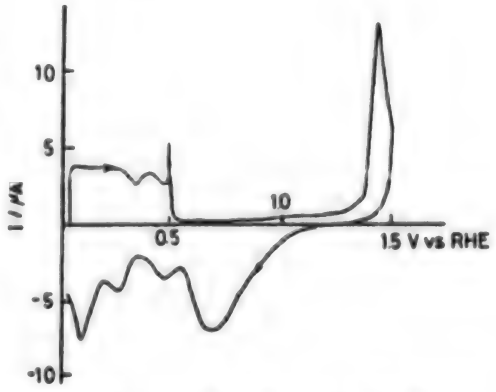

Figure 3. CV of Pt(111) Clean Surface in 0.05 M H_2SO_4 Aqueous Solution

Such an electrochemical measurement demonstrates that it is necessary to set the sample potential at the double layer region where no surface oxidation occurs in order to carry out STM measurement of a Pt(111) clean surface.

A typical STM image of the Pt(111) surface obtained by setting the sample potential at 0.9 V is shown in Figure 4. A clean surface consists of a flat terrace part with a width of several tens of nanometers, and a linear step with a height of about 2.3 Å corresponding to the size of one Pt atom. It can be seen that the step lines intersect at angles that are integral multiples of 60, reflecting the ideal surface atom arrangement of the (111) surface. A similar measurement of a Pt(100) clean surface produced the STM image shown in Figure 5. The island structure with a monatomic height of about 2 Å that appeared on the flat terrace originated from the atomic arrangement of the (100) surface.

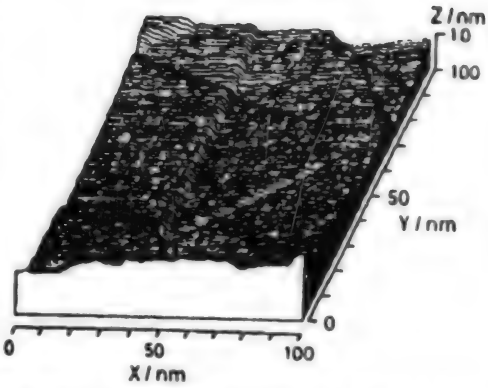

Figure 4. STM Image of Pt(111) Clean Surface Observed in 0.05 M H_2SO_4 Aqueous Solution

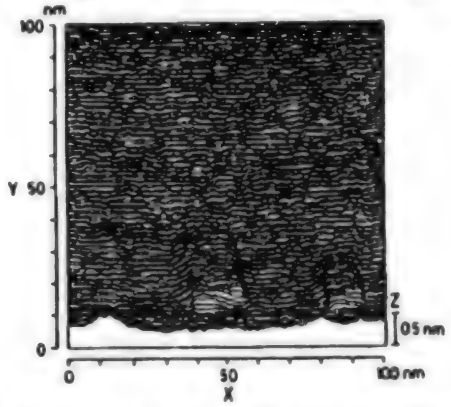

Figure 5. STM Image of Pt(100) Clean Surface Observed in 0.05 M H_2SO_4 Aqueous Solution

Figure 6 shows a CV of the Au(111) surface in an 0.1 M $HClO_4$ aqueous solution. The two oxidation waves that appear at 1.3 V and 1.6 V vs. RHE due to potential sweeps toward the anode side correspond to oxidation processes represented by Equations (4) and (5), respectively.

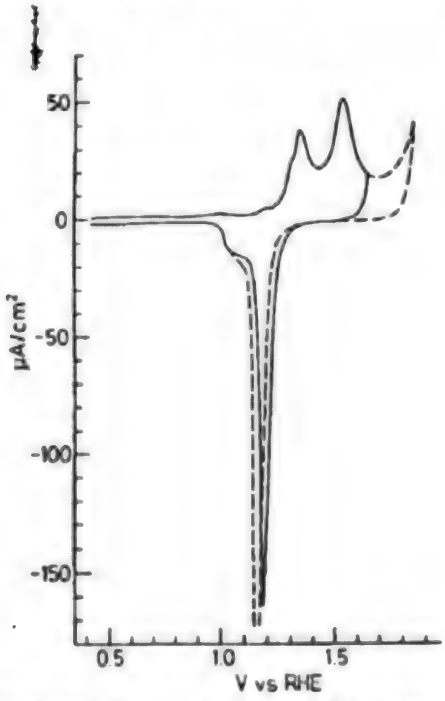

Figure 6. CV of Au(111) Clean Surface in 0.1 M $HClO_4$ Aqueous Solution

$$Au + H_2O \rightarrow AuOH + H^+ + e^-, \quad (4)$$

$$AuOH \rightarrow AuO + H^+ + e^-. \quad (5)$$

An STM image of an Au(111) clean surface when the sample potential is held at 0.8 V vs. RHE of the double layer region is shown in Figure 7. It was found that Au has a surface structure that is comparable to or better than Pt in terms of cleanliness, and it is an extremely flat surface consisting of a terrace that extends several hundreds of nanometers, and a step whose height

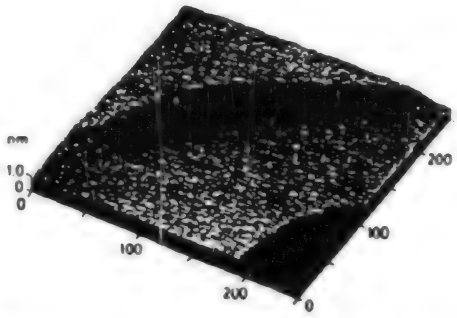

Figure 7. STM Image of Au(111) Clean Surface Observed in 0.1 M $HClO_4$ Aqueous Solution

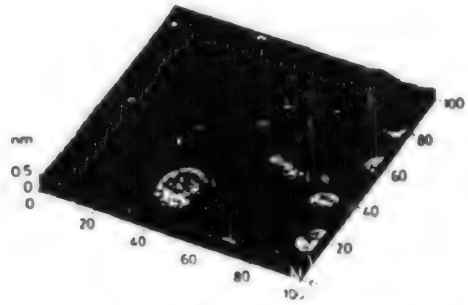

Figure 8. CV of Au(100) Clean Surface Observed in 0.1 M $HClO_4$ Aqueous Solution

corresponds to that of one to three atoms. It was confirmed that the (100) surface, shown in Figure 8, and the (110) surface have similar step-terrace structures, and it was demonstrated that the sample surfaces are ideal surfaces that are suitable for the analysis of electrochemical reactions at the atomic level.

2.2 Atomic Image on Metallic Surfaces

Being able to resolve the individual surface atoms of the electrode themselves is an extremely important task in clarifying the electrochemical reaction processes that occur on the electrode/solution surface at the atomic level. To date, atomic images of Au(100), Au(110), and Au(111) surfaces in solution have been confirmed.

Figure 9 is an STM image of an Au(111) surface observed in an 0.05 M H_2SO_4 aqueous solution. Each Au atom is arranged in three-fold symmetry with a spacing of 2.9 Å, and is resolved with a corrugation of about 0.2 Å. It can be seen that its surface structure is the (1x1) structure, which does not show any rearrangement. This is an ideal surface that is almost free from atomic defects.

A similar measurement was also carried out for the Au(100) and Au(110) surfaces, and succeeded in producing an image showing an Au atomic (1x1) structure for both surfaces.

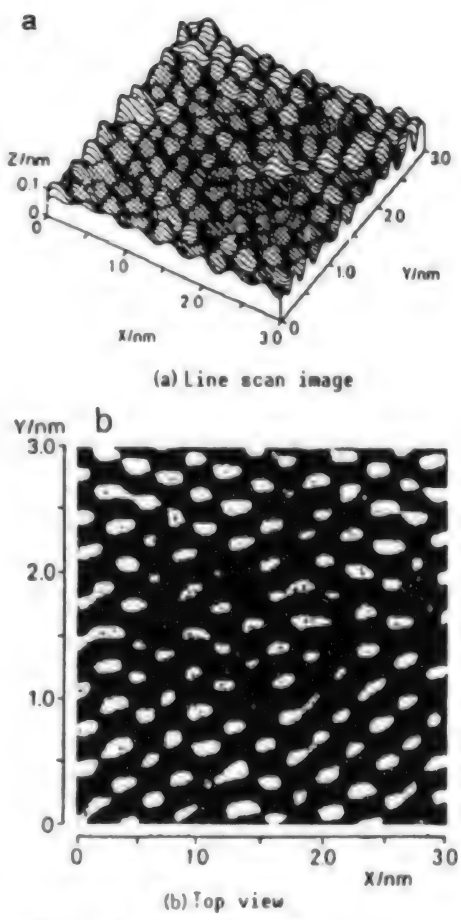

Figure 9. Au Atom Image on Au(111) Surface Observed in 0.05 M H_2SO_4 Aqueous Solution

2.3 Adsorption to Electrode Surface

Undertaking a structural analysis of atoms and molecules adsorbed to the electrode surface is an important task in the clarification of electrode reactions. There are many problems to be investigated, starting with hydrogen adsorption related to a hydrogen generation reaction.

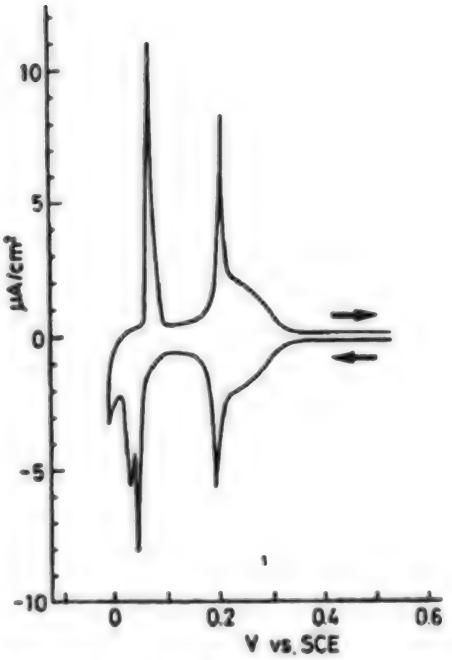

Figure 10. CV for Cu UPD Onto Au(111) Surface

The adsorption and desorption of metallic ions that occurs closer to the anode side than the equilibrium potential of the normal electrodeposition on metals of different kinds is called underpotential deposition (UPD). This phenomenon involves a number of important problems that are also related to crystal growth. Figure 10 is a CV of the Au(111) surface in an 0.05 M H_2SO_4 aqueous solution containing 1 mm of $CuSO_4$. The sample potential is swept from 0.5 V vs. SCE, in which the clean surface is exposed to the solution toward the cathode at 1 mV/s, where a current produced by bulk electrodeposition starts to rise near 0 V, and two characteristic peaks due to the UPD of Cu appear in the potential region further to the anode side. The first stage UPD starts about 0.35 V, and is completed at a sharp peak near 0.2 V.

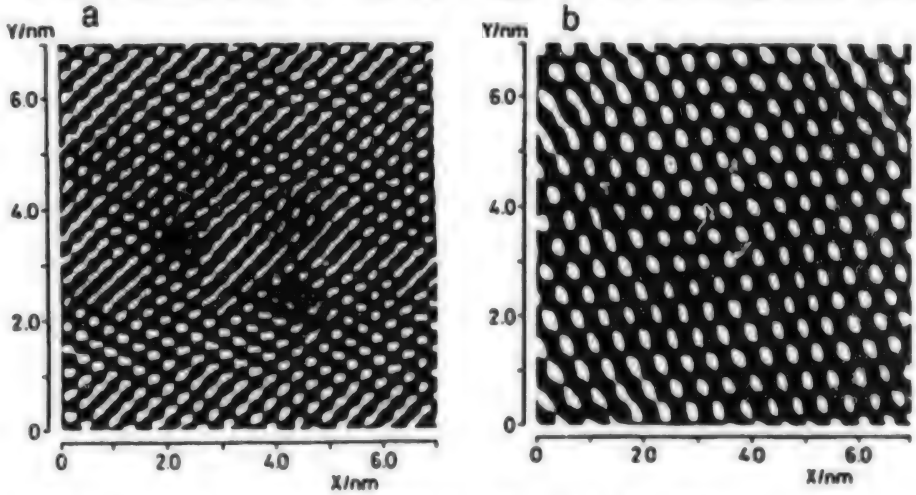

Figure 11. (a) Au Atom Image of Au(111) Surface
(b) Image of Cu Atoms Which Underwent UPD Onto Au(111) Surface

First, STM observation when the sample potential was set at 0.6 V produced an Au atomic image of the Au(111) surface, as shown in Figure 11(a). by sweeping the potential in a state where the images of the Au atoms are resolved, and at 0.15 V where the first stage UPD was completed produced the STM image shown in Figure 10(b) rather than that shown in 10(a). Based on the fact that the

undulation appearing here represents Cu atoms adsorbed by UPD, the spacing between the peaks is about 4.9 Å. This is three times that of Au, and the direction of the Cu atom string crosses that of the Au atom string on the underlying layer at about 30°. Thus, we concluded that the Cu atoms subjected to UPD form a $(\sqrt{3} \times \sqrt{3})$R30° structure. In the region of this structure one can sometimes observe boundary parts, which are indicated by a and b in Figure 12. Figure 13 is a schematic diagram of the boundary structure b. The empty circle represents an Au atom on the underlying layer, and the solid black circle shows a Cu atom that has undergone UPD. Here, it was found that the position of the Cu atom relative to the Au atom on the underlying layer is different on the right and left sides of the $(\sqrt{3} \times \sqrt{3})$R30° structure. In the face centered cubic (fcc) structure, and the hexagonal closest packed (hcp) structure, the stacking of the atomic layers is different—ABCABC, and ABABAB, respectively, If it is assumed that fcc occurs on the left side, then hcp is on the right side. it is extremely interesting that such structures appear in the initial stage of crystal growth.

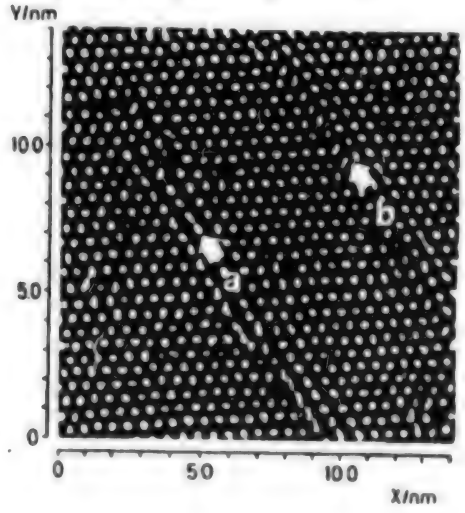

Figure 12. Boundary Structure Appearing in Cu Atom layer Which Underwent UPD in $(\sqrt{3} \times \sqrt{3})$R30 Structure Onto Au(111) Surface (arrows a and b)

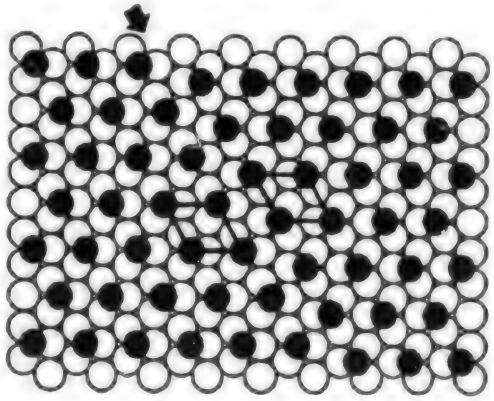

Figure 13. Model of Cu Atoms and Boundary Structure (b) of $(\sqrt{3} \times \sqrt{3})$R30 Structure

In addition, the author's group is investigating the UPD of Cu onto a Pt(111) surface, and the UPD Of Ag onto an Au(111) surface.

3. Semiconductor Surface

The author and his collaborators have been studying the application of this method to semiconductor/solution interfaces, which presents some extremely interesting problems. This is because we believe that STM is a technique that not only is useful for the analysis of the geometrical structure of semiconductor surfaces, but also is capable of directly determining the electronic levels localized in or on the surface.

What is of fundamental importance in the semiconductor/solution interface is the relationship between the potential of a semiconductor electrode in the sense of electrochemistry, and the band structure formed in the semiconductor. The author's group clarified this relationship in n-TiO_2, n-ZnO, and Si by STM measurement, and demonstrated that it is possible to determine the structure of semiconductor electrode/solution interfaces.

In recent years, it was determined that Si whose surface has been stabilized by chemical treatment has a clean surface structure at the atomic level by STM measurement in a vacuum and in the atmosphere, but similar results will be confirmed in solutions in the near future.

4. Conclusion

The possibility of making in-situ determinations with a resolution at the atomic level of the structures of electrode/solution interfaces was created with the appearance of the electrochemical STM (ESTM). This suggests that it may well be possible to construct a new electrochemical system. It is expected that surface chemical analysis at the atomic level, which has been done for experiments in an ultrahigh vacuum environment, will also be carried out in the electrochemical sector in the future. At the same time, rapid advancement in the understanding of solid/solution interfaces also will take place.

References

1. Itaya, K., SOLID STATE PHYSICS, Vol 26, 1991, p 523.

2. Itaya, K. and Tomita, E., SURF. SCI., Vol 201, 1988, p L507.

3. Weichers, J., Twomey, T., Kolb, D.M., and Behm, R.J., J. ELECTROANAL. CHEM., Vol 451, 1988, p 248.

4. Green, M.P., Hanson, K.J., Scherson, D.A., Xing, X., Ross, P.N., Carr, R., and Lindau, I., J. PHYS. CHEM., Vol 93, 1989, p 2181.

5. Trevor, D.J., Childsey, C.E.D., and Loicono, D.N., PHYS. REV. LETT., Vol 62, 1989, p 929.

6. Furuya, C., SURFACE SCIENCE, Vol 11, 1990, p 2.

7. Itaya, K., Sugawara, S., Sashikata, K., and Furuya, N., J. VAC. SCI. TECHNOL., Vol A8, 1990, p 515.

8. Honbo H. and Itaya, K., J. CHIM. PHYS., Vol 88, 1991, p 1477.

10. Magnussen, O.M., Hotlos, J., Nichols, R.J., Kolb, D.M., and Behm, R.J., PHYS. REV. LETT., Vol 64, 1990, p 2929.

11. Magnussen, O.M., Hotlos, J., Beitel, G., Kolb, D.M., and Behm, R.J., J. VAC. SCI. TECHNOL., Vol B9, 1991, p 969.

12. Hachiya, T., Honbo, H., and Itaya, K., J. ELECTROANAL. CHEM., Vol 315, 1991, p 275.

13. Sashikata, K., Furuya, N., and Itaya, K., J. ELECTROANAL. CHEM., Vol 316, 1991, p 361.

14. Hachiya, T. and Itaya, K., ULTRAMICROSCOPY, 1992, in press.

15. Itaya, K. and Tomita, E., CHEM. LETT., Vol 285, 1989.

16. Ibid., SURF. SCI., Vol 219, 1989, p L515.

17. Tomita, E., Matsuda, N., and Itaya, K., J. VAC. SCI. TECHNOL., Vol A8, 1990, p 534.

18. Becker, R.S., Higashi, G.S., Chabal, Y.J., and Becker, A.J., PHYS. REV. LETT., Vol 65, 1990, p 1917.

19. Morita, Y., Miki, K., and Tokumoto, H., APPL. PHYS. LETT., Vol 59, 1991, p 1347.

Outlook for Manipulation of Atoms, Molecules

936C1098K Tokyo JAPAN SURFACE SCIENCE SOCIETY in Japanese 25 Jun 93 pp 129-143

[Article by Kazunori Tanaka, National Institute for Advanced Interdisciplinary Research]

[Text] A large-scale project sponsored by MITI "Ultimate Manipulation Technology for Atoms and Molecules" (abbreviated Atom Technology) was launched in FY92 as a 10-year project. Its budget is ¥25 billion. In comparison to the large-scale projects conducted in the past, the nature of this project and the way it is being advanced are very different. Although formally it follows the large project policy of the past, its concept is viewed as a model project for the industrial science and technology R&D policy that began with a newly elaborated format in FY93. The object of this project is to systematically complete technologies for accurately observing and manipulating individual atoms and molecules on a surface (two dimensions) or in space (three dimensions). These will then serve common base technologies in various industrial fields, such as new materials, electronics, chemical industries, and biotechnologies. Of the total of 10 project years, R&D on basic technologies and supporting technologies will be carried out in the first period (six years). Further, the manner in which R&D is to be advanced does not follow a decentralized system, the so-called take-home research, but adopts an incentive research system in which all the workers congregate at the National Institute for Advanced Interdisciplinary Research (NAIR), which was established on 1 January 1993.

The fundamental research projects for the first period (six years starting in FY92) are as follows:

(1) Technology for the observation and manipulation of atoms and molecules on solid surfaces

—To develop a technology for observing, identifying, and manipulating individual atoms and molecules on the surface of various materials under various conditions and environments.

—To develop a technology for measuring in real time chemical reactions on solid surfaces at the level of atoms and molecules.

(2) Technology for the observation and manipulation of collections of atoms in space

—To develop a technology for observing and measuring collections of atoms on the order of $10\sim10^4$ in space, together with a technology for controlling their motion and reactions, and the movement of electrons among the collections, in order to create self-organized collected structures.

(3) Technology for the observation and manipulation of structures such as molecules and biological components

—To develop a technology for identifying individual kinds of molecules, particularly organic molecules or biological components such as DNA, and for manipulating the chemical bond or electronic state at a specified site in the molecule.

(4) Technology for the theoretical study of atomic and molecular processes

—To construct new "theoretical experimental equipment" by compounding computers and information processing software systems, and to clarify in terms of theory the adsorption, desorption, diffusion, and reaction processes of individual atoms and molecules on solid surfaces through simulation technologies.

Since this project is oriented toward basic long-term research, it is important to carry out such research through the incentive joint research system, seeking the participation of leading researchers from industry, government, and universities, in a wide range of domestic and overseas fields. This article summarizes the activities of the National Institute for Advanced Interdisciplinary Research (NAIR), and the Angstrom Technology Partnership, both of which were established in February 1993. A third organization, the Research Body for Atom Technology, is seeking to integrate the work of the other two. These organizations, buttressed by appointments from universities, are working toward the goal of creating a technology for the manipulation of atoms and molecules.

Background

Electronic devices

- Post giga-chip technology
- Miniaturization down to nanometers
- Quantum-mechanical devices
- Molecular devices

Materials

- Ultrathin films, superlattices
- Synthesis (assemblies) of nanostructures
- Clusters
- Porous Si

Processes — dynamic atomic-scale observation and control
— new chemical phenomena

Structures— atomic-scale observation and identification
— new nanostructures

Properties— nonbulk properties
— new physical phenomena

Common Needs

To develop atomic-scale technology (observation and manipulation)
— Nanotechnology

↓

To explore atomic-scale phenomena (physics and chemistry)
— Nanoscience

Electronics, materials science, surface chemistry and physics, biotechnology, genetic engineering

SPM-STM, AFM, ——— (Rohrer & Binnig)
Breakthrough technology

But, still far from maturity from an application point of view

Atom Technology: Ultimate manipulation of atoms and molecules

Initiated in FY1992

National R&D program sponsored by MITI

¥25 billion (~$210 million) for 10 years

~¥1.1 billion for FY1992
~¥1.2 billion + α for FY1993

Long-term fundamental research

Generic technology

Electronics
Chemical industry
Biotechnology

Implemented through the concentrated joint research system

NAIR--National Institute for Advanced Interdisciplinary Research

AIST, MITI

Founded on 1 January 1993

Research Groups of NAIR

Atom Technology: National R&D Program

Cluster Science: In-house research

Bionic Design: In-house research

ATP--Angstrom Technology Partnership

Founded on 16 February 1993

Technology Research Consortium commissioned the task of carrying out the project "Atom Technology"

30 private companies including overseas companies

Organization (in process)

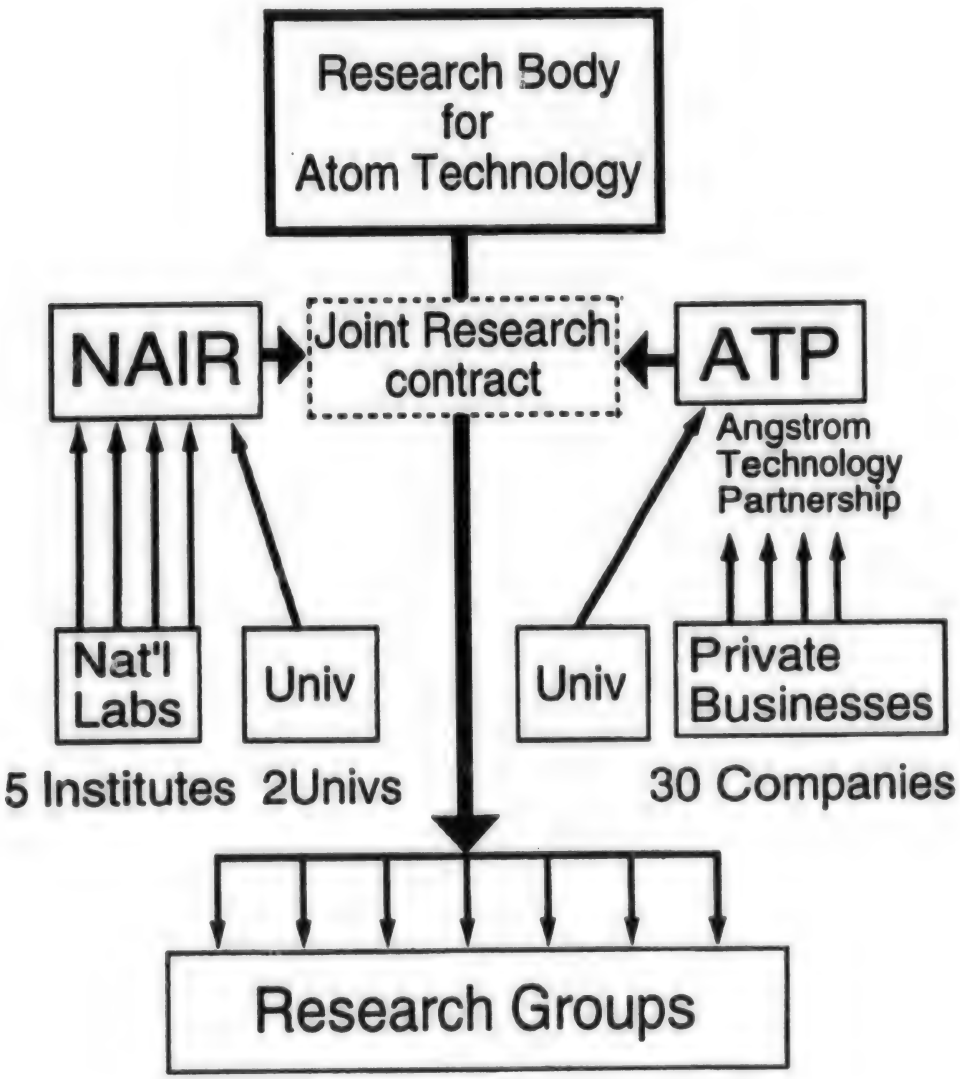

Personnel

Research body for Atom Technology

Project leader	E. Maruyama (ATP)
Subleaders	K. Terakura (University of Tokyo, NAIR)
	K. Tanaka (NAIR)
Group leaders	H. Tokumoto (NAIR)
	M. Ichikawa (ATP)
	M. Ozeki (ATP)
	T. Okada (ATP)
	T. Kanayama (NAIR)
	T. Tanaka (Concurrently)
	K. Terakura (Concurrently)

—45 people total (May 1993)

Tokumoto Group (H. Tokumoto)

Research area

Observation and manipulation of atoms and molecules on solid surfaces using scanning mechanical-probe techniques.

Objective

Establishment of high-grade scanning mechanical-probe techniques which enable us to identify individual atoms and molecules, and to determine their electronic states. Finding new atomic- and molecular-scale phenomena by using these techniques.

Themes

Ultrahigh precision scanning mechanical-probe techniques
Multifunctional tip techniques
Low-temperature scanning mechanical-probe techniques
Electrochemical scanning mechanical-probe techniques

Ichikawa Group (M. Ichikawa)

Research area

In-situ observation and formation of atom-scale structures using focused-beam technology.

Objective

Establishment of fundamental technology for formation of atomic-scale structures using beam-induced surface reaction.

Themes

Atomic-manipulation microscopy
Characterization techniques using AMM
Beam-induced surface reaction phenomena

Okada Group (H. Okada)

Research area

Studies of organic molecules and biological macromolecules by multi-sensing/functional-scanning probe microscopy and optical technology

Objective

Establishment of multi-sensing/functional-scanning probe microscopy combined with laser-induced fluorescence spectroscopy for high-speed sequence analysis of DNA using these techniques.

Themes

Multi-sensing/functional scanning probe microscopy
Sequential movement of bases from one end of DNA
High-speed sequence analysis of DNA

Kanayama Group (T. Kanayama)

Research area

Formation of nanostructures with atomic accuracy by growing and manipulating nanocrystals in a three-dimensional space.

Objective

Achievement of self-organization of nanostructures using composite nanocrystals as building blocks.
Molecular biology with inorganic materials.

Themes

Growth of nanocrystals which are trapped in three-dimensional space.
manipulation and in-situ characterization of their structures and electronic properties.
Self-organization of nanostructures through surface modification and selective excitation.

Ozeki Group (M. Ozeki)

In-situ dynamic observation and control of atom-molecule processes on the top surface of growing thin films.
Self-limiting mechanisms by chemical reaction, III-V compounds.

Tanaka Group (K. Tanaka)

Process diagnostics and structure control of thin films growing on heterosurfaces.
Amorphous-microcrystal-single crystal magnetic thin film.

Terakura Group (K. Terakura)

Theoretical studies of atom-molecule processes through first-principle calculations.
Strong interaction with experiment groups.

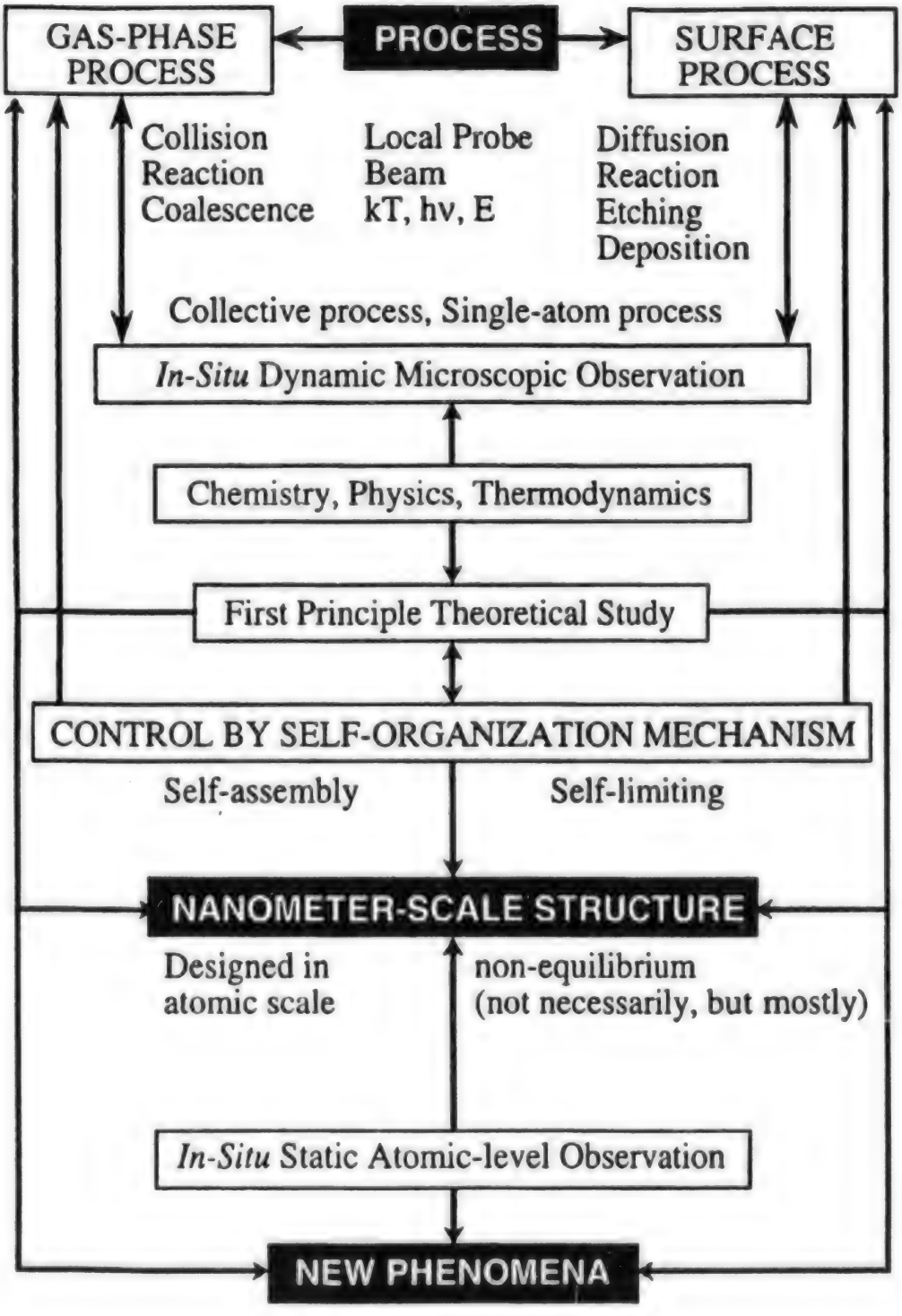
GAS-PHASE PROCESS
PROCESS
SURFACE PROCESS
Collision
Reaction
Coalescence
Local Probe
Beam
kT, hv, E
Diffusion
Reaction
Etching
Deposition
Collective process, Single-atom process
In-Situ Dynamic Microscopic Observation
Chemistry, Physics, Thermodynamics
First Principle Theoretical Study
CONTROL BY SELF-ORGANIZATION MECHANISM
Self-assembly
Self-limiting
NANOMETER-SCALE STRUCTURE
Designed in atomic scale
non-equilibrium (not necessarily, but mostly)
In-Situ Static Atomic-level Observation
NEW PHENOMENA

SPM (STM, AFM, ···)

In-situ, dynamic characterization

Self-organization (micro → macro)

First principle studies

New Generation of Tunneling Microscopes

936C1098L Tokyo JAPAN SURFACE SCIENCE SOCIETY in Japanese 25 Jun 93 pp 145-160

[Article by Osamu Nishikawa, Department of Electronic Engineering, Faculty of Engineering, Kanazawa University]

[Text] **1. Introduction**

Many people associate tunneling microscopes with the scanning tunnel microscope (STM), which was invented by Drs. G. Binnig and H. Rohrer in 1982, but the history of microscopes utilizing the tunneling phenomenon of the electron goes back to 1937. In that year, Professor E.W. Miller, who was then a graduate student at Berlin University, invented a field emission microscope in which electrons are emitted from a metallic needle having an extremely sharp tip by the tunneling phenomenon when a high negative current is applied to the tip. With a field electron microscope (FEM), it is not possible to see individual atoms because of the low resolution of about 10 Å. This is due to the uncertain spread of the position of the emitted electrons, according to the Heisenberg uncertainty principle. In 1951, Professor Miller invented the field ion microscope (FIM). The FIM utilizes the tunneling phenomenon of an electron from a hydrogen atom to an atom at the tip of the needle. The FIM made it possible to directly see an atom for the first time in history. Later, Miller, et al., invented the atom-probe (A-P) by combining the FIM with a mass spectrometer equipped with a detector that can sense a single atom, thereby making it possible to analyze and identify atoms observed by FIM one after another.

The STM, meanwhile, draws the arrangement of surface atoms by controlling the tunneling current flowing between a single atom at the tip of a sharp needle and an atom on the sample surface. Also, scanning tunnel spectroscopy (STS), which explores the electronic state of individual atoms based on the change in voltage of the tunneling current, was developed, and it was learned that the tunneling characteristic changes markedly depending on the atomic arrangement of electronic state of the needle point (tip). In other words, in order to correctly interpret the plotted STM image and to evaluate the STS characteristic with certainty, it is necessary to know the atomic arrangement, composition, and electronic state of the needle tip. The sharpness of the scanning probe is comparable to that of the needle tip of the FEM or FIM. Thus, to satisfy these requirements, it was thought that the most appropriate technique

was to probe the electronic state of an extremely small region of the needle tip by field emission electron spectroscopy (FEES), in which the atomic arrangement of the needle tip is observed by FIM, to clarify the composition by A-P, and to measure the voltage characteristic of the current.

This article presents the principle and the structure, and some examples of the characteristics of various pieces of equipment from the FEM to the FEES. In addition, the features and the expected characteristics of a new type of FIM and A-P that are being developed by the present author will be discussed.

2. Principle and Structure

The structures of various pieces of equipment from the FEM to A-P are very simple. Both the FEM and FIM consist of only a sharp needle (tip) and an opposing screen placed in a vacuum device (mirror body) (Figure 1). For FEM observation, a low-pressure imaging gas such as He or Ne is introduced after evacuating the inside of the mirror body, and a positive high-voltage current is applied to the needle. At this time, if the radius of curvature of the needle point r is 500 Å, and if the applied voltage V is 10 kV, the electric field intensity at the needle point F can be represented by $F = V/\beta r$. Thus, if the factor determined by the shape of the needle point β is assumed to be 5, F is given approximately by 4 V/Å. If one assumes that an He atom is brought close to the needle point, the level of the electron of the He atom at a position 5 Å from the surface will be raised by the electric field by 20 V. Then, since the ionization potential of an He ion is 24.5 V, the ground level of the electron in the He will be at the same height as the Fermi level of the surface of the needle point with a work function of 4.5 V. Thus, since the width and the height of the potential barrier between the surface and the He atom are small, the electron on the He tunnels to the atom at the needle point to become an He^+. This ionization phenomenon, which is due

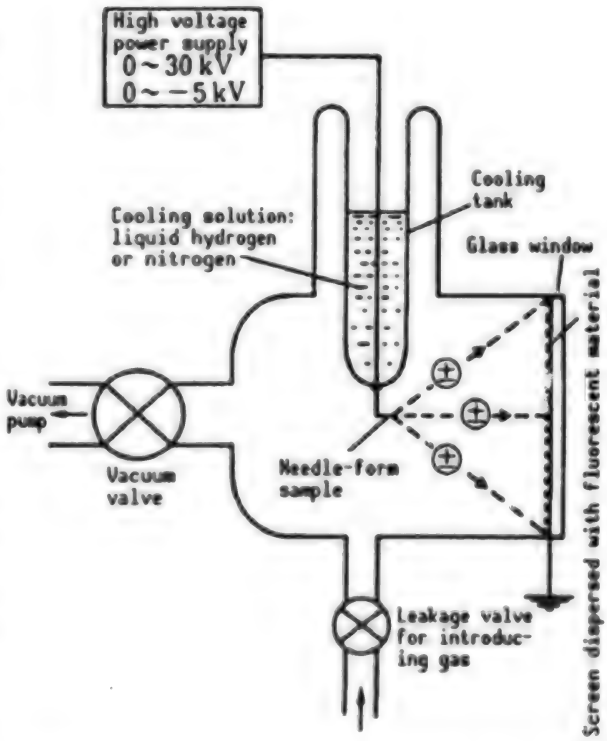

Figure 1. Basic Configuration of FIM
When an inert imaging gas is introduced into the mirror body, and a positive current is applied to the needle, this apparatus operates as an FIM, which emits gas ions from the tip of the needle. When a negative current is applied, it operates as an FEM. The needle is cooled to suppress the thermal motion of gaseous atoms to enhance the resolution of FIM.

to an electrostatic field, is called field ionization. For gases other than He the ionization potentials are lower than He, so the ionization electric fields are also lower.

The ion flies to the screen after receiving a repulsive force from the needle, which has a positive potential. Since the trajectory of the ion runs roughly along the radially expanding electric life of force that joins the atom on the needle point to a point on the screen, the magnification of the image of the ion is approximately equal to the ratio of distance R between the needle and the screen to the radius of curvature r of the needle point. Hence, for R=10 cm and r=1000 Å, the magnification is 10^6. Thus, two atoms on the needle separated by 3 Å will be imaged as two bright spots 0.3 mm apart, so atoms can be seen. However, because a gaseous atom is under thermal motion, the resolution will deteriorate somewhat if the flight trajectory deviates from the electric line of force due to the thermal motion. If the needle is cooled by liquid nitrogen or hydrogen, or by a freezer (Figure 1), the gaseous ion makes contact with the needle point several times before ionization to lose thermal energy, so the thermal motion is reduced. Then the ion flies along the electric line of force, and the resolution of the FIM image projected on the screen is improved.

In the FEM, the imaging gas is evacuated, then a needle current is applied to the needle. If the intensity of the electric field is assumed to be about one-tenth of the electric field intensity of the field ionization, 0.4 V/Å, then at a position 10 Å from the needle, the potential barrier on the surface is lowered to the Fermi level by the electric field. Electrons are field emitted by the tunneling phenomenon from the hemispherical surface of the needle point, and a bright-dark image is projected on the screen by incident electrons (Figure 2). The magnification of the image is the same as that of the FIM image. However, the resolution of the emission position of the electron has an indeterminate spread due to the indeterminacy principle. Thus, the resolution has a low value of about 10 Å, and individual atoms cannot be seen. However, a unique feature of the scanning electron microscope (SEM) is that, by opening a small detection hole at the center of the screen and placing a Faraday cup behind the screen, it is possible to detect an emitted electron that passed through the hole. By spectrally analyzing the energies of these electrons, the electronic state of the fine region of the needle point corresponding to the hole, and the work function ϕ of each crystal surface of the needle point, can be determined from the voltage, V_T, characteristic of the emission current, I_C. The method for finding such an energy distribution of emitted electrons is FEES. What needs to be

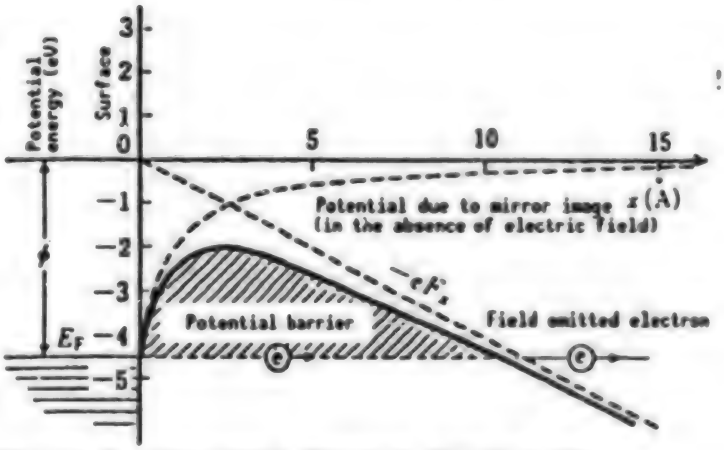

Figure 2. Potential Diagram Showing the Principle of Field Emission

noted here is the fact that the tunneling characteristics of FEM and STM are essentially the same. The change in the emission current I_C due to the electric field intensity F of the needle point is given by:

$$I_C \propto \exp\ (-6.8 \times 10^7\ \phi^{3/2}/F) \qquad (1)$$

and the tunneling current I_T of STM is represented in general by:

$$I_T \propto \exp\ (\phi^{1/2}/s) \qquad (2)$$

Since s is the distance between the needle point and an atom on the sample surface, by substituting the relationship $F = \phi/s$ seen in Figure 2 into Equation (2), it can be seen that Equation (2) goes over to Equation (1). This shows that data obtained by FEES and data obtained by STS can be directly compared.

The high electric field of the needle point also causes a phenomenon called field evaporation, which desorbs the surface atoms themselves as positive ions. Figure 3 is a potential diagram showing the principle of field evaporation. The potential curve $M^- + A^+$ showing the ionic bonding of a surface atom A and the base M is lowered by neFx by the electric field. Here, n is the valence number of the ion, e is the charge of the electron, F is the intensity of the electric field, and x is the distance between M and A. The neutral bonding curve M + A is deepest at the radius r_0 of A, and its depth is equal to the binding force between M and A. If $M^- + A^+$, and M + A intersects at r_0, A will move to $M^- + A^+$ which has a lower energy state. In other words, A is ionized and becomes A^+. Since the energy level of the ionization bonding is equal to the energy for ionizing A to the n valence, I_n, minus n times the work function ϕ, $I_n - n\phi$, at the coordinates (r_0, A) the following relationship obtains:

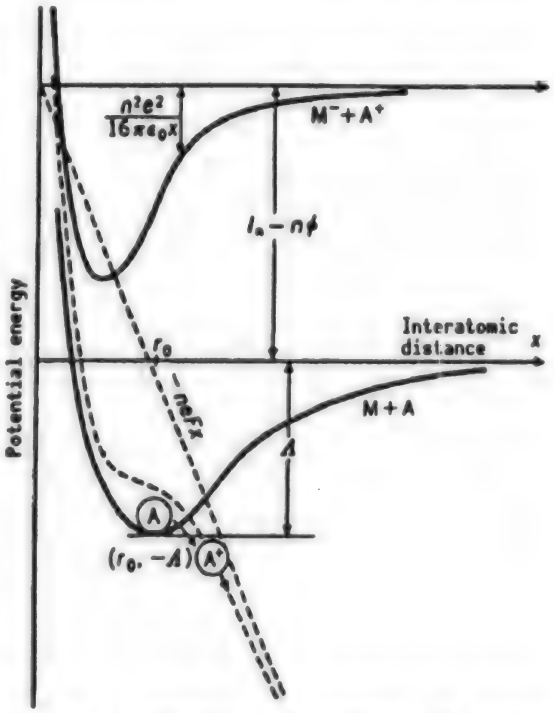

Figure 3. Potential Diagram for Field Evaporation

$$ner_0F + n^2\ e^2/16\pi\ \epsilon_0 r_0 = A + I_n - n\phi \qquad (3)$$

The second term on the left-hand side is the mirror image potential between A^+ and its mirror image A^-. Substituting the dielectric constant ϵ_0=8.85 x 10^{-12} C/Vm, π=3.14, and e=1.6 x 10^{-19}C, the electric field F_n at which A evaporates as an n valent ion is given by:

$$F_n = \frac{\Lambda + I_n - n\phi}{ner_0} - \frac{3.6n^2}{r_0^2} \quad V/\text{Å} \tag{4}$$

and it can be seen that the binding force Λ is determined by measuring F_n. The electric field F_2 for which the W atom, which has a high interatomic binding force, is evaporated as a divalent ion is obtained by substituting Λ=8.67 eV, r=1.304 Å, n=2, I_2=25.68 eV, and ϕ=4.52 eV in Equation (4), and has a large value of F_2=5.5 x V/Å, which agrees approximately with the measured value. In addition, the corresponding value for Al, whose binding force is weak, is small at 3.3 eV, and substituting r_0 1.248 Å, n=1, I_1=5.984 eV, and ϕ=4.2 eV yields a low value of 1.61 V/Å. This suggests that measurement of the evaporation electric field makes it possible to investigate the binding state between atoms or in polymers.

Field evaporation proceeds regularly by monatomic layer beginning with the topmost layer of the surface. Thus, it constitutes an ideal surface cleaning method. Also, by observing the FIM image of each layer, it is possible to carry out a three-dimensional assessment of the structure of the sample. Another feature of field evaporation is that it does not disturb the surface structure. Thus, when used in an STM, this phenomenon makes it possible to remove, attach, or move specific atoms to enhance the level of circuit integration by atomic scale processing. Also, efforts to develop techniques for inserting elements with unique functions, such as a monatomic switch, are in progress. In addition, field evaporation is an extremely efficient process for high-energy ionization. Even at cryogenic temperatures it is possible to achieve an evaporation rate of more than 10 atomic layers by increasing the electric field. To take advantage of this property, active efforts are under way to develop a point ion source with a high degree of beam convergence and a high current density. Further, by analyzing evaporated atoms thoroughly, it is possible to carry out compositional analysis, and the A-P was developed to take advantage of this property.

3. Time-of-Flight Type Atom Probe

The A-P combines both FIM and a mass spectrometer. There are two types of mass spectrometer—the magnetic field deflection type or the quadrupole type—which are suitable for the study of the gas-surface reactions that continuously generate large numbers of ions. But another device that is used widely is the time-of-flight (ToF) analyzer. In the A-P analysis shown in Figure 4, when an interesting region is recognized in FEM-FIM images projected on the screen, the needle is rotated with the point of the sample corresponding to the needle point as the center to shift the image on the screen so as to align the desired region with the small probe hole, which is at the center of the screen.

When a pulse voltage is applied to the needle in that state, surface atoms are field evaporated instantaneously, but only those ions that are evaporated from the region of the needle point corresponding to the probe hole enter the flight space by passing through the hole. These are made incident on and are detected by a high sensitivity detector, and the mass of each of the incident ions is identified according to Equation (5).

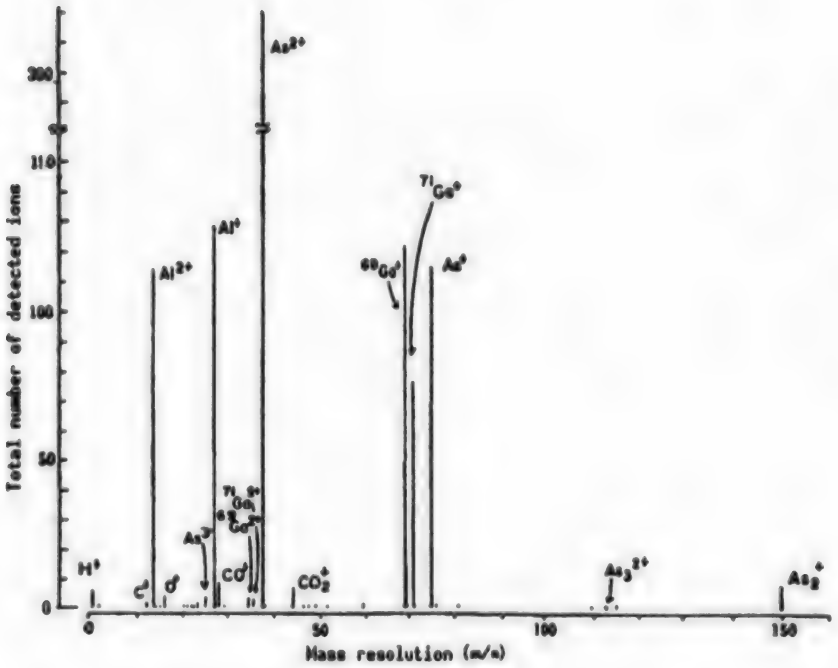

Figure 4. Mass Spectrum Obtained by A-P Analyzing Al-GaAs Interface
Ga and Al are detected as monovalent and divalent ions, and As is detected as monovalent to trivalent ions, and as cluster ions such as As_3^{2+}, As_2^+, etc. C^+, O^+, CO^+, and CO_2^+ were detected from contaminated surface layers.

The region of analysis is an extremely limited region that can be varied from the size of a single atom to a region with a diameter of several hundreds of angstroms by changing the diameter of the probe hole. Accordingly, one feature of this type of A-P is that it is possible to analyze and identify in detail all ions having mass, from a single atom to more than several thousands, that are generated simultaneously. Also, since there are no restrictions within a certain range for the mass of ions that can pass the magnetic field, as in the case of the magnetic deflection type, there is no ion that fails to be detected. Since, however, in ToF the number of channel timers for measuring the time of flight corresponds to the number of incident ions, it is not suited for the analysis of gas-surface reaction products where a large number of ions are generated continuously. Moreover, if several ions with the same mass are incident at the same time, they are recorded as a single ion. Thus, in this respect, too, the magnetic field deflection type is advantageous. The reason why ToF is popular nonetheless is that it fulfills the basic objective of A-P, which is to detect incident ions without missing any.

The mass resolution $\Delta m/m$ of ToF is determined by the accuracy with which the time of flight is measured. When an atom at the needle point is instantaneously field evaporated by a pulsed electric current with a narrow time width or a pulsed laser beam, an ion of mass m and valency n is accelerated, and will be incident on the detector by flying a flight space of l in a fraction of a second t. Since the flight velocity v is l/5, m can be determined from:

$$m/n = 2e\ Vt^2/\ell^2 \quad (5)$$

where V is the voltage applied at the time of evaporation, which is the sum of the stationary voltage and the pulse voltage. Although a pulse width of less than 1 ns is desirable, such a high frequency pulse is not easily transmitted with high efficiency to the needle point of a semiconductor material. Thus, for field evaporation in conducting semiconductor analysis, the needle point is irradiated with a pulsed laser instantaneously. In this case, V consists exclusively of the stationary voltage. For V=10 kV and l=2 m, t=20.12 μs for a Pt atom where m=194, and 20.176 ns for an isotope where m=195. This means that to achieve a high degree of resolution that can separate isotopes, it is necessary to increase the distance of flight and to measure t with an accuracy of one nanosecond. In other words, the accuracy of the time of field evaporation and the pulse width also have to be set with an accuracy of one nanosecond. As it stands, it is not easy to narrow down the time duration of evaporation by a voltage pulse to below 1 ns, and suppression of the energy spread of ions is also difficult. Accordingly, the mass resolution power of ToF is generally lower than that of magnetic field deflection, although there is a report that the mass resolution can be enhanced to $\Delta m/m$ 10,000.

There are various types of ToF devices. These include a linear type, an energy compensation type, and an imaging type, depending on the shape of the flight space. Also, their respective functions and mass resolutions are different. The linear type has a simple structure, but there are fluctuations in the velocity of flight due to slight differences in the voltage at the time of ion evaporation, and its mass resolution is low. In the compensation type, fluctuations of the flight velocity are compensated for by deflecting the trajectory of evaporated ions by 163° using a deflection electrode, or by reflecting the ions with an electrostatic field. As shown in Figure 4, in the example of an analysis of a compound GaAs semiconductor the mass resolution is so high that one can clearly separate isotopes of each element. As a result, possible applications of trace analysis by A-P are being expanded from metals and semiconductors to conductive polymers and superconducting ceramics.

In contrast to the linear type and the compensation type, in the image type a spherical ion detector centered at the needle point is installed at the position of the FIM screen. A large number of the same kind of ions evaporated from the hemisphere at the needle point are incident on the detector at the same time, and the distribution of a specified kind of atom at the needle point is imaged since the incident positions correspond to the evaporation positions at the needle point. However, the flight distance is only 10 cm, and $\Delta m/m$ is about 1/50, which is smaller than the corresponding value for the linear type. In recent years, work on a new type of image, called position-sensitive A-P (POSAP), is in progress. In this system, the incident positions in the detector for all ions, regardless of whether they are different or the same, are recorded in detail. Thus, by making a three-dimensional plot, of the detected ions in the order of detection, it is possible to make a three-dimensional drawing of the compositional distribution of atoms at the needle point. It is expected that this advance will add a new dimension—the ultra-microscopic perspective—to the problem of materials development.

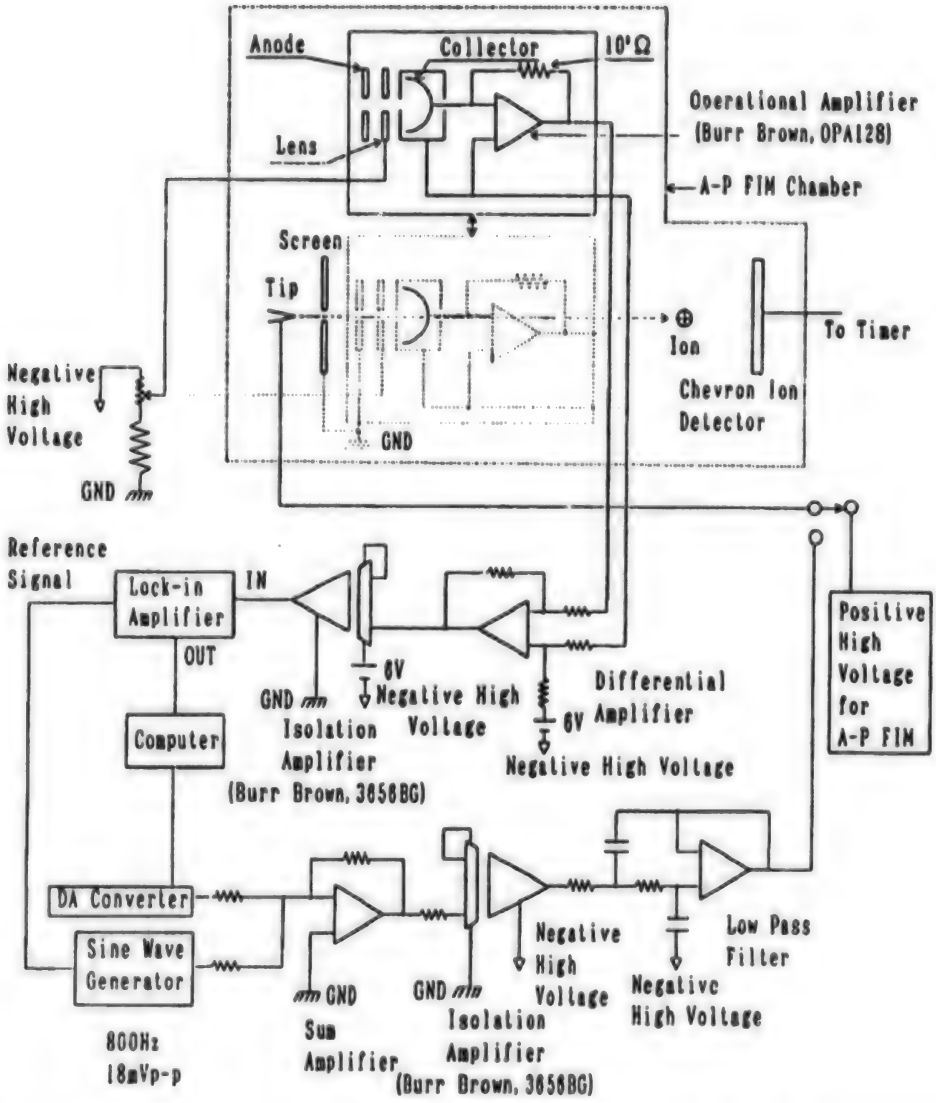

Figure 5. Configuration and Electronic Circuit of A-P Incorporated Field Emission Electron Spectrometer

A tip and a screen in front of the device constitute an FIM. As the voltage applied to the tip is changed from positive to negative, electrons are emitted from the tip, and FIM operates as FEM. The probe hole at the center of the screen is a hole for passing ions field evaporated, or field emitted electrons from the region on the tip that corresponds to the hole, and it is so arranged that a collector which collects electrons emitted into the A-P flight space can be inserted behind the hole. The potentials of the collector and the tip are nearly equal, the energy distribution of the field emitted electrons can be determined by measuring the change in the incident current due to the change in the collector potential, and the electronic state of the region of A-P analysis can be found. The tip voltage in A-P analysis is the sum of a stationary voltage and a pulse voltage for instantaneous field evaporation. For the analysis of highly-resistant materials, the tip is irradiated with a laser pulse to cause field evaporation within 1 ns.

4. Surface Analysis Using A-P/FEES

As an experiment, a Faraday cup used in a FEES was incorporated in an A-P device (Figure 5). This device makes it possible to clarify the composition and electronic state of a minute region of the needle point corresponding to the probe hole of the screen by analyzing the emitted electrons by FEES. Some interesting results have been obtained by the use of this device. New information about the disappearance of Si surface levels by hydrogen adsorption, Si clusters evaporated on an Mo surface, and the electronic states of a Ge film grown on an Ir surface will be reported.

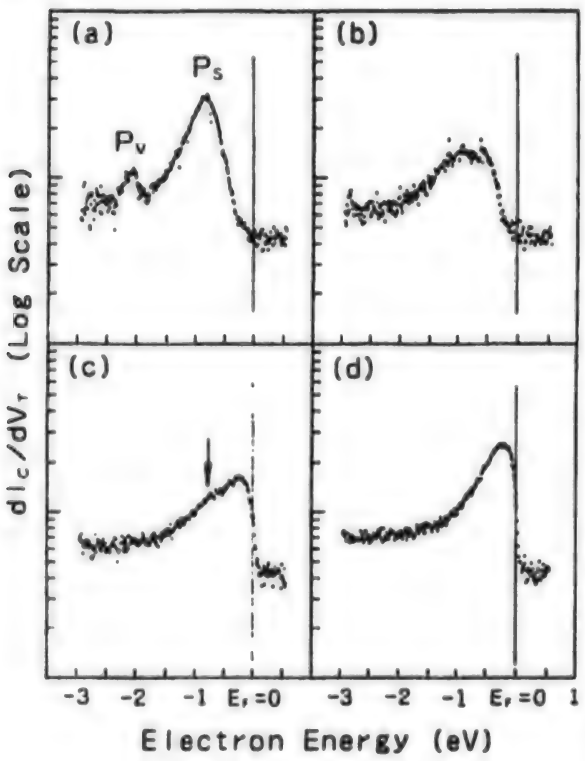

Figure 6. FEES Spectra
(a) Spectrum of emitted electrons from the evaporated Si clusters. The thickness of the Si film has a small value of about two atomic layers, but the emission current rises from a level about 0.5 eV below the Fermi level, indicating that Si is in a semiconductor state. Ps and Pv are peaks produced by emitted electrons from the surface state and the valence electrons, respectively. The ordinate is the change in the emission current I_C due to applied voltage V_T: dI/dV_T.
(b) Spectrum when the Si film thickness is reduced to about 1.5 atomic layer due to field evaporation. Pv disappeared, but the spectrum is still semiconductor-like.
(c) Spectrum when the film thickness is less than a monatomic layer. The spectrum rises from E_F, and is metallic. A shoulder is seen in the Ps level.
(d) Spectrum from the Mo surface. The shoulder has disappeared, and is metallic.

That Si atoms evaporated on a clean Mo surface form clusters has been confirmed by SEM observation. An electric current from the Si cluster starts to rise from a level about 0.5 V lower than the Fermi level, reflecting the energy gap of the semiconductor. It reveals a structure that reflects the density of states as the depth increases. However, as the energy level goes deeper, the width and the height of the tunnel barrier to the electrons become large, and the emission current decreases (Figure 6(a)). When the clusters are evaporated gradually, the thickness of the Si film is reduced, the clusters shrink, and the FEES spectrum is shifted to a metallic spectrum influenced by the Mo on the base (Figures 6(b) and (c)). When the Mo surface of the base appears, the spectrum rises from the Fermi level, and shows a characteristic

metallic spectrum (Figure 6(d)). This demonstrates that even a small cluster consisting of several tens of atoms creates an electronic state similar to that of a semiconductor. The work function of the Si cluster determined by the I_C–V_T relationship shows that it is about 10 percent greater than that of the base. When Mo is heated, a silicide with a metallic electronic state is formed, and its work function is smaller by about 10 percent than that of the base.

In contrast to the formation of clusters by Si atoms on Mo, it was recognized by A-P/FEES that Ge applied to an Ir base grows in layers. It has been shown that the Ge layer exhibits a metallic electronic state when the thickness of the Ge layer is smaller than 10 atomic layers, and the differences in the growth process and the electronic state of Si and Ge for different bases are being investigated.

5. A-P Analysis of Compound Semiconductors and Conductive Polymers

To investigate the compositional change that occurs at the interface of a compound GaAs semiconductor and an Al film, a sample where an Al film was evaporated on a GaAs needle point was analyzed. In Figure 4—which shows the detection of ions from H^+ to As_3^{2+}—Al^+ and CO^+, and $^{69}Ga^{2+}$, $^{71}Ga^{2+}$, and $^{75}As^{2+}$ are clearly separated. If the ions are plotted in the order of detection, one can obtain the compositional distribution in the depth direction. For example, when an Al film was evaporated on a GaAs needle at a temperature of 50 K and then subjected to A-P analysis at that low temperature, it was found that Al and GaAs do not mix, and that the interface was atomically steep. However, when the temperature of the needle was raised and kept at the higher temperature one hour, then analyzed at 50 K, the formation of a mixed layer of Al and As was recognized. An AlAs film was formed when the needle was heated to 900 K for 70 seconds. However, the interface of the AlAs film and the base GaAs layer was steep (Figure 7).

In the analysis of a conductive polymer polypyrrole (PP), a PP film sample was formed by polymerizing the pyrrole electrochemically at the tip of a platinum needle. When the PP has an ideal structure, as shown in Figure 8(a), H^+ with mass number 1, the fragment surrounded by curves in the figure, NH^+, C_2H^+, $C_4H_2^+$, etc. should be detected. When PP is completely oxidized and O is replaced by H, it will go to the structure as shown in Figure 8(b). An analysis of the fresh PP showed the presence of more ions such as COH^+, $CNOH^+$, etc., that contain oxygen. These were detected more abundantly than NH^+, CNH^+, etc., revealing that during the initial period of oxidation even fresh PP is in the state shown in Figure 8(c) (Figure 9). An analysis of a sample that was kept in the air for three months found almost no ions such as H^+ and NH^+ that do not contain O, and only fragments such as CO^+, $C_2O_2^+$, $C_2O_2^{2+}$, CNO^+, $C_2N_2O_2^+$, $C_2N_2O_2^{2+}$, and $C_3N_2O_3^{2+}$ as shown in Figure 8(b) were detected (Figure 10). This result shows that complete oxidation of PP produces the structure shown in Figure 9(b), and that the double bond, which has a strong bonding force, cannot be cut by field evaporation. A further analysis of the completely oxidized film showed a gradual increase in the number of H^+ ions detected, and the appearance of a PP layer that gives the mass spectrum shown in Figure 9.

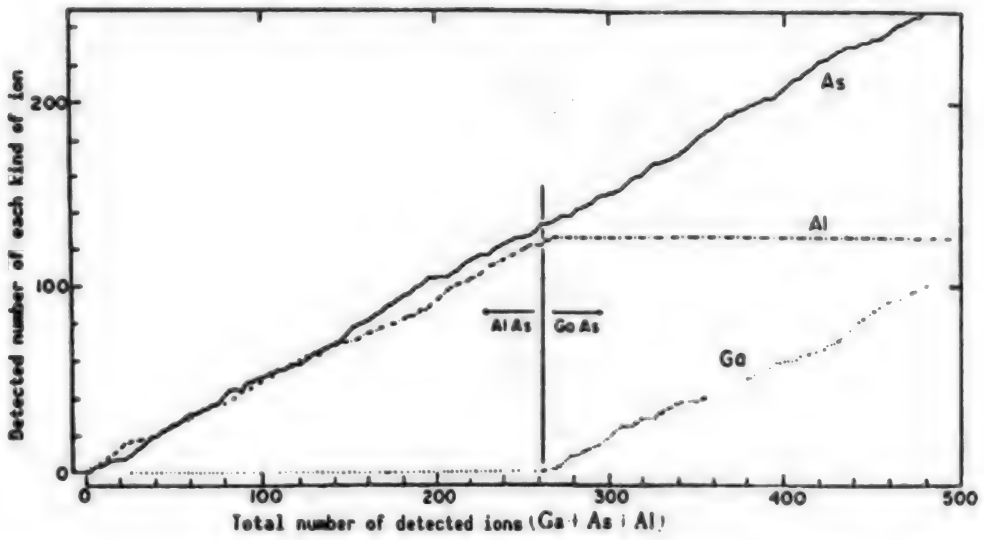

Figure 7. Order of Ion Detection Obtained by A-P Analyzing GaAs With Axis Direction [001] on Which an Al Film Is Evaporated, Followed by Heating for 70 Seconds at 900 K

The ordinate represents the detected number of specified ions. The abscissa is the total number of detected ions. AlAs later was formed by Al–Ga replacement due to heating, and the interface of AlAs and GaAs was atomically steep.

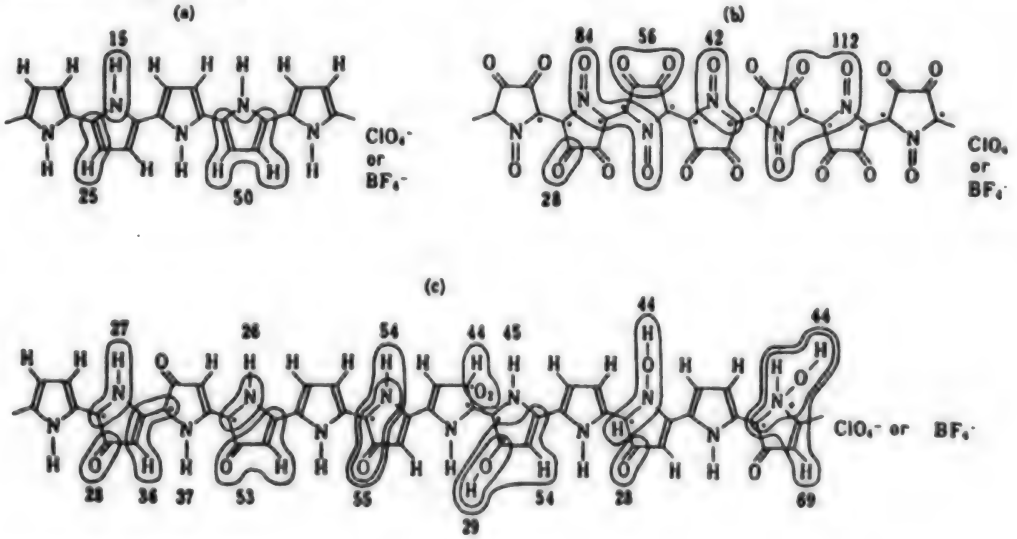

Figure 8. Structure of PP

(a) Ideal structure. (b) Structure of completely oxidized PP. (c) Structure of PP at the initial stage of oxidation. ClO_4^- and BF_4^- are dopants. A closed curve indicates a fragmentary ion detected by A–P, and the attached number is its mass. The curve does not intersect a double bond. A point indicates an unpaired electron generated by oxidation.

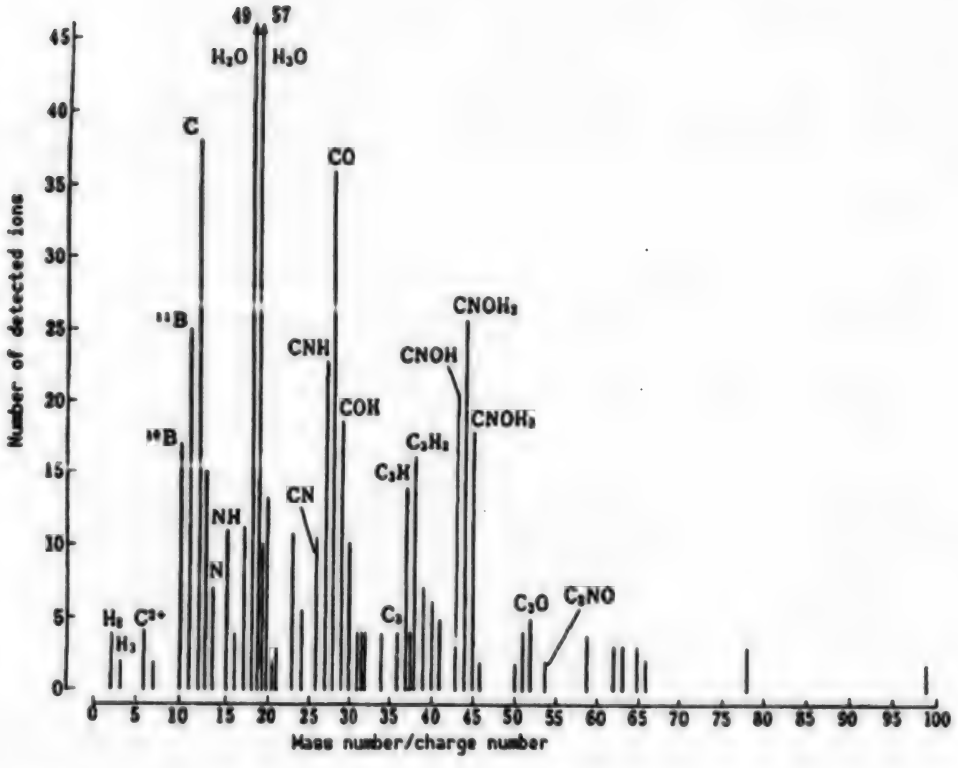

Figure 9. Mass Spectrum of PP by A-P Analysis

That oxygen is contained in the fragment ions shows that this sample is in part in the stage of initial oxidation. Since the mass resolution of A-P $\Delta m/m$ is at a high value of 1/100, isotopes of B are distinctly separated.

The thickness of the oxide layer estimated from the number of detected ions was about 660Å. In other words, a fresh PP tends to be oxidized, and enters the initial stage of oxidation, as shown in Figure 9, in a short time in the air or in a synthesis process. However, the process of transition from this initial stage to the state of complete oxidation shown in Figure 10 is slow. A completely oxidized layer about 660Å thick is formed in the air in about three months.

In order to give conductivity to the PP, ClO_4 or BF_4 is doped, and B^+ can be seen in Figure 9. The dopant B is not detected in the completely oxidized layer (Figure 10). However, as fragments such as C or CH that are not combined with oxygen start to appear, B also begins to be detected. A detailed examination of the order of detection of B and O revealed that a repulsive force acts between B and O, and B is ejected from the oxidized region. Further, oxygen seems to be contributing to the bonding at the metal-PP interface. When In is evaporated on the PP surface, and A-P analysis proceeds from the In layer to the underlying PP, the interface In atoms are detected along with PP fragments containing oxygen. However, a systematic study of this phenomenon has not yet started.

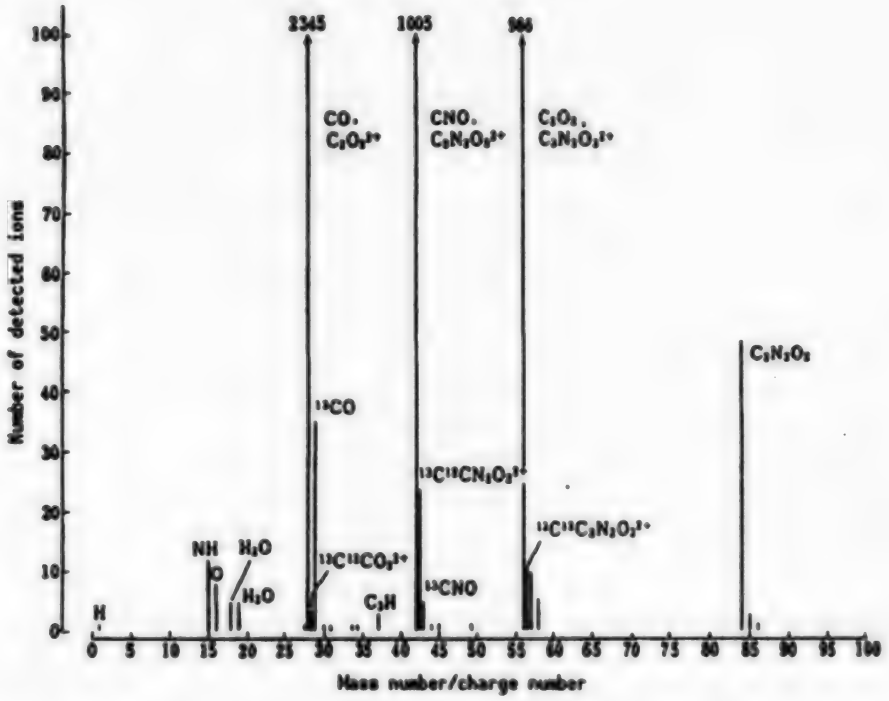

Figure 10. Mass Spectrum of Completely Oxidized PP

Detected ion species agree very well with the fragments shown in Figure 8(b). Since mass resolution is so high as to decompose the peaks due to isotopes, it can be determined that C_2O_2 is mixed with the CO peak, and that $C_2N_2O_2$ is mixed with CNO.

6. New Type FIM and Scanning Type A-P

Images obtained by FEM and FIM reflect the tunneling probability of the electron from a minute region of the needle point, and the tunneling probability from a gas atom to a single atom. Accordingly, a measurement of the brightness of the image will give the tunneling probability directly above each atom at the needle point. Therefore, studies designed to measure emission current using a counter were tried. However, it was not easy to shrink the incidence port of a counter down to a size corresponding to one atom at the needle point, or to achieve an exact alignment. Also, the quantity of information is restricted by the number of counters that can be installed. Thus, this technique did not become popular. Another method is to photograph the image and to determine the tunneling probability from its brightness. However, this has a number of disadvantages, such as the fact that the width of exposure allowance of existing photosensitive materials is a small value of only two orders of magnitude, the brightness of the image is not proportional to the quantity of incident light, etc.

While we were looking for a sensitive material that could correct these disadvantages, there was developed a photosensitive material with accumulative phosphorescence, an exposure allowance of four orders of magnitude, and whose brightness is proportional to the incident quantity of X-rays of electron

beams. An exposure allowance of four orders of magnitude means that it can create an image of a region with a high electric field intensity, and a large work function. It is precisely such a region whose image has been extremely dark due to its low tunneling probability and small field emission current, and whose surface atoms can hardly be seen because of the low ionization probability of gaseous atoms. in view of this fact, we decided to record FIM images by employing photosensitive materials with accumulative phosphorescence in place of conventional sensitive materials. However, since data on the sensitivity of the new materials to low-energy electrons and ions, on differences due to ion species, and on the linearity of the sensitivity are not available, we are now engaged in a preliminary experiment to collect such data. Accordingly, we are not yet in a position to provide detailed results of our work, but by summarizing past data we believe that we can directly measure the directivity of tunneling, and changes in tunneling probability, due to the neighboring atoms. We expect that determination of the tunneling probability from an atom at the needle point will contribute significantly to the analysis of STM images and STS spectra.

Although the various devices ranging from FEM to A-P have excellent characteristics, the preparation of samples is not easy, and the application range is severely limited due to the fact that samples to be used for observation and analysis are restricted to an extremely narrow region because they must be hemispheres with a radius of less than 1,000 Å that of a needle point obtained by sharpening one end of a fine wire by polishing. Therefore, we decided to develop a new type of device, the scanning atom-probe (SAP), which is capable of analyzing planar samples.

The SAP offers some advantages in terms of sample preparation and the shape of the electrode. In contrast to the conventional method, samples will be prepared by segmenting a plate-like sample to create a shape like that shown in Figure 11 using a cutter or lithography to obtain a large number of needles. The spacing between the needles can be reduced by machining techniques, but the present object is to obtain a spacing of 10 μm to 0.1 mm. The advantages of this technique are that it is possible to determine differences in structure and composition due to the position on the sample surface by the observation and analysis in sequence of adjacent points on the same sample, and that it is easy to prepare sample needles having a layered structure. Another advantage is that the structure and compositional change at the interface from one layer to another is significant.

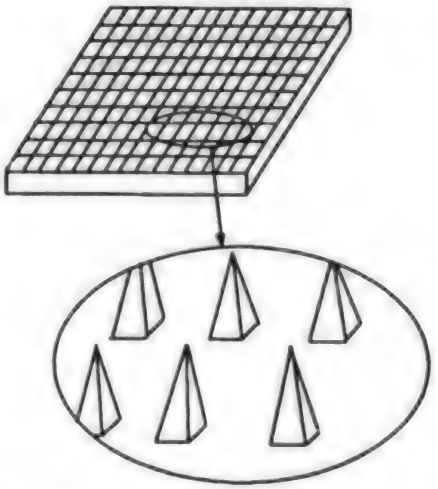

Figure 11. Shape of Planar Sample for SAP After Processing

The electrode is an acceleration electrode that can generate a high electric field only at specified needle points on the sample surface. In the conventional FEM and A-P, the electrode opposite the needle to which a high voltage

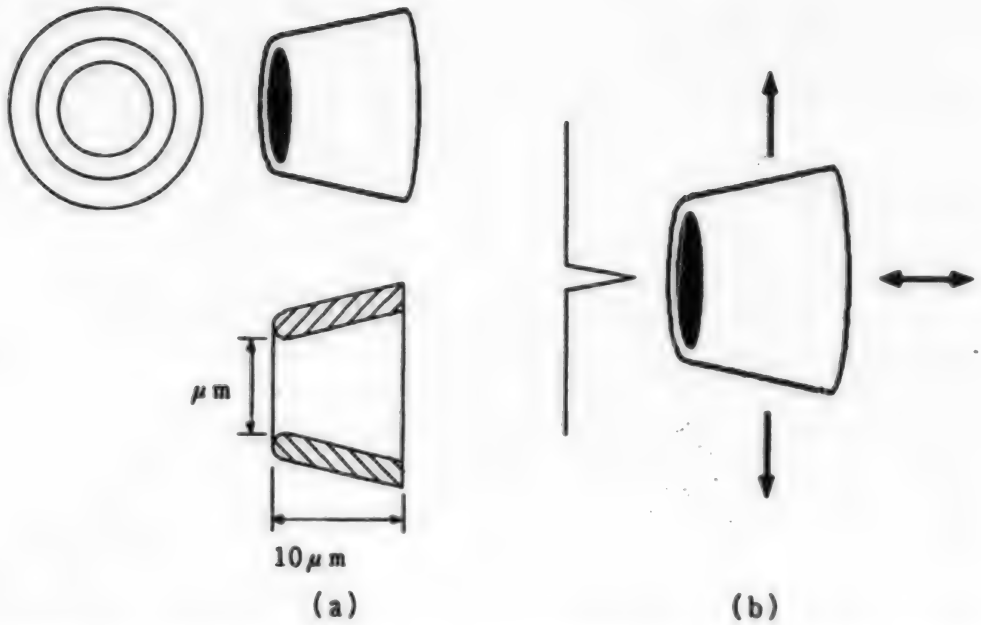

Figure 12. Diagram Showing the Arrangement of the Tip and Acceleration Electrode for SAP
(a) Anticipated shape and size of the acceleration electrode.
(b) Arrangement of a specified needle and the acceleration electrode.

The electrode or the sample surface moves two-dimensionally so that it will be possible to observe and analyze the tip on the sample surface sequentially.

is applied is a grounded screen, or sometimes a grounded metallic plate, for cooling that surrounds the needle. In either case, the distance from the needle point to the opposing electrode is from several millimeters to more than 10 cm. If a high voltage current is applied to a plate-like sample for such an electrode, high electric fields are generated for all needles, causing field emission and field evaporation, and therefore it is not possible to observe individual needles. Therefore, in SAP a small funnel-like acceleration electrode is manufactured and placed at a position 0.01-1 μm away from the needle point (Figure 12). Then, the high electric field will be generated only at a specified needle point facing the acceleration electrode. At present, we are calculating electric field distribution at the needle point and in the vicinity of the acceleration electrode to optimize the electrode shape.

7. Future Problems and Outlook

We have noted that FEM, FIM, and A-P possess excellent characteristics that are not found in other devices. At the same time, however, they operate under a severe restriction in that the samples are sharp needles made of conductive materials, and that the region of observation and analysis is limited to a narrow hemisphere at the needle point. Presented below are some of these restrictions together with possible countermeasures.

1. **Evaporation Electric Field:** Field evaporation caused by a high electric field generated at the needle point creates the characteristics unique to A-P, but in materials with a low evaporation field, compound semiconductors, and ceramics, where the bonding force between the constituent atoms is weak, and conductive polymers, atoms with weak bonding forces undergo selective field evaporation in a low electric field, which makes FIM observation and A-P analysis difficult to carry out. In other words, even if we try to carry out an A-P analysis by applying a pulsed current on top of a constant current, or if we irradiate the target with a pulsed laser beam, atoms or molecules that can evaporate in a low field will evaporate by the action of the low field created by the constant current, and those that are detected as the result of the application of the pulsed current are only those atoms or molecules that are bound strongly to the base material. Thus the true composition cannot be determined. However, because field evaporation makes A-P possible, there is currently appropriate technique that can relax this restriction.

2. **Sample Preparation:** Several conductive ceramics, such as TiN, $BaTiO_3$, and Y-Ba-Cu-O, which are high critical temperature superconducting materials, have been analyzed, and some interesting results regarding compositional distribution and bonding states have been obtained. However, it is not easy to cut out these materials, or to sharpen the needle point such that they can be used for A-P analysis. The SAP device described above is a new system designed to resolve this problem.

3. **Compounding A-P and STM To Enhance the Reliability of STM and STS:** It is known that STM images and STS spectra change markedly depending on the atomic arrangement, shape, and compositional distribution of the needle point. In order to enhance the reliability of observational and analytical results obtained by STM and STS, it is necessary to investigate not only the atomic arrangement, shape, and compositional distribution of the needle point, but also the tunneling probability. The only way to satisfy these requirements is to use a technique for investigating the arrangement, composition, electronic states, and tunneling probability of atoms at the tip of the STM scanning probe by an A-P/FEES, for which a wide exposure allowance FIM device is feasible. The next task is to push a research program that will further enhance the reliability and reproducibility of STM images and STS spectra.

4. **Manipulation of Surface Atoms:** At present, efforts to develop technology capable of ultimate fine surface processing by moving, evaporating, and attaching specific atoms observed by STM are actively under way. Although it is believed that the mechanisms of evaporation and attachment are due to field evaporation of the atoms that have been moved it is also believed that the evaporation mechanism may be different from those of FIM and A-P, since the spacing of the needle point and the sample surface is very small, about 10 Å. Because of this, the author's group is planning to carry out research aimed at obtaining the basic knowledge required to clarify the mechanism of moving atoms by the use of the composite equipment described above.

Although there are many problems and restrictions, the development of research apparatus that will take advantage of the unparalleled excellent characteristics of these devices is steadily progressing, and the number of potential applications is expanding. For example, development of POSAP and SAP, and combining these devices with STM, will supply the basic knowledge needed for the development of highly functional materials through ultimate fine surface processing technology. The number of workers engaged in this problem is growing, and our knowledge concerning the behavior of surface atoms and the field evaporation phenomenon—which are the basic phenomena of movement, evaporation, and attachment of atoms—is increasing.

It is believed that, in the future, tasks assigned to A-P and STM will be increasingly diversified corresponding to advancements in nano technology. However, the development of technologies to deal with these new demands has been continually advancing. Accordingly, the number of applications for the unique characteristics of A-P and STM as tools for the analysis of minute regions will continue to grow in the future, and it is expected that progress will be marked by the appearance of a new generation of problems, and by the introduction of new techniques.

References

1. Binnig, G., Rohrer, H., Gerber, Ch., and Weibel, E., PHYS. REV. LETT., Vol 50, 1982, p 120.

2. Müller, E.W., Z. PHYZIK, Vol 106, 1937, p 541.

3. Ibid., Vol 131, 1951, p 136.

4. Müller, E.W., Panitz, J.A., and McLane, S.B., REV. SCI. ISNTR., Vol 39, 1968, p 83.

5. Berghaus, Th., Brodde, A., Neddermeyer, H., and Tosch, St., SURF. SCI., Vol 193, 1988, p 235.

6. Hamers, R.J., Tromp, R.M., and Demuth, J.E., PHYS. REV. LETT., Vol 56, 1986, p 1972.

7. Nishikawa, O., Koyama, H., Kodama, N., and Tomitori, M., COLLOQUE DE PHYSIQUE, Vol 50, 1989, p C8-507.

8. Nishikawa, O., SCIENCE, Vol 49, 1978, p 19.

9. Swanson, L.W. and Bell, A.E., "The Physics and Technology of Ion Sources," Ed., I.G. Brown (Wiley, New York, 1989) p 313.

10. Eigler, D.M. and Schweizer, E.K., NATURE, Vol 344, 1990, p 524.

11. Zeppenfeld, P., Lutz, C.P., and Eigler, D.M., ULTRAMICROSCOPY, Vol 42-44, 1992, p 128.

12. Sakurai, T., APPL. PHYS., Vol 48, 1979, p 55.

13. Utsumi, T. and Nishikawa, O., APPL. PHYS. LETT., Vol 21, 1972, p 110.

14. Tsong, T.T. and Liou, Y., PHYS. REV. LETT., Vol 55, 1985, p 2180.

15. Waugh, A.R., Richardson, C.H., and Jenkins, R., SURFACE SCI., Vol 266, 1992, p 501.

16. Nishikawa, O., Kaneda, O., Shibata, M., and Nomura, E., PHYS. REV. LETT., Vol 53, 1984, p 1252.

17. Nishikawa, O. and Kato, H., J. CHEM. PHYS., Vol 85, 1986, p 6758.

18. Nishikawa, O. and Naga, M., PHYS. REV., Vol B37, 1988, p 3685.

19. Panitz, J.A., PROGRESS IN SURF. SCI., Vol 8-6, 1978, p 219.

20. Cerezo, A., Hyde, J.M., Miller, M.K., Beverini, G., Setna, R.P., Warren, P.J., and Smith, G.D.W., SURFACE SCIENCE, Vol 266, 1992, p 481.

21. Bostel, A., Blavette, D., Menand, A., and Sarrau, J.M., COLLOQUE DE PHYSIQUE, Vol 50, 1989, p C8-501.

22. Nishikawa, O., Tomitori, M., and Iwawaki, F., MATERIALS SCIENCE AND ENGINEERING, Vol B8, 1991, p 81.

23. Nishikawa, O., Koyama, H., and Tomitori, M., SURFACE SCIENCE, Vol 246, 1991, p 246.

24. Ashino, M., Tomitori, M., and Nishikawa, O., APPL. SURF. SCI., Vol 66, 1993, p 430.

25. Nishikawa, O., ANALYSIS, Vol 2, 1988, p 95.

26. Nishihara, J., Amenija, Y., Matsushita, T., J. PHYS. SOC. OF JAPAN, Vol 45, 1990, p 398.

27. Nishikawa, O., patent pending.

- END -

Foreign Broadcast Information Service (FBIS) and Joint Publications Research Service (JPRS) publications contain political, military, economic, environmental, and sociological news, commentary, and other information, as well as scientific and technical data and reports. All information has been obtained from foreign radio and television broadcasts, news agency transmissions, newspapers, books, and periodicals. Items generally are processed from the first or best available sources. It should not be inferred that they have been disseminated only in the medium, in the language, or to the area indicated. Items from foreign language sources are translated; those from English-language sources are transcribed. Except for excluding certain diacritics, FBIS renders personal names and place-names in accordance with the romanization systems approved for U.S. Government publications by the U.S. Board of Geographic Names.

Headlines, editorial reports, and material enclosed in brackets [ ] are supplied by FBIS/JPRS. Processing indicators such as [Text] or [Excerpts] in the first line of each item indicate how the information was processed from the original. Unfamiliar names rendered phonetically are enclosed in parentheses. Words or names preceded by a question mark and enclosed in parentheses were not clear from the original source but have been supplied as appropriate to the context. Other unattributed parenthetical notes within the body of an item originate with the source. Times within items are as given by the source. Passages in boldface or italics are as published.

SUBSCRIPTION/PROCUREMENT INFORMATION

The FBIS DAILY REPORT contains current news and information and is published Monday through Friday in eight volumes: China, East Europe, Central Eurasia, East Asia, Near East & South Asia, Sub-Saharan Africa, Latin America, and West Europe. Supplements to the DAILY REPORTs may also be available periodically and will be distributed to regular DAILY REPORT subscribers. JPRS publications, which include approximately 50 regional, worldwide, and topical reports, generally contain less time-sensitive information and are published periodically.

Current DAILY REPORTs and JPRS publications are listed in *Government Reports Announcements* issued semimonthly by the National Technical Information Service (NTIS), 5285 Port Royal Road, Springfield, Virginia 22161 and the *Monthly Catalog of U.S. Government Publications* issued by the Superintendent of Documents, U.S. Government Printing Office, Washington, D.C. 20402.

The public may subscribe to either hardcover or microfiche versions of the DAILY REPORTs and JPRS publications through NTIS at the above address or by calling (703) 487-4630. Subscription rates will be provided by NTIS upon request. Subscriptions are available outside the United States from NTIS or appointed foreign dealers. New subscribers should expect a 30-day delay in receipt of the first issue.

U.S. Government offices may obtain subscriptions to the DAILY REPORTs or JPRS publications (hardcover or microfiche) at no charge through their sponsoring organizations. For additional information or assistance, call FBIS, (202) 338-6735,or write to P.O. Box 2604, Washington, D.C. 20013. Department of Defense consumers are required to submit requests through appropriate command validation channels to DIA, RTS-2C, Washington, D.C. 20301. (Telephone: (202) 373-3771, Autovon: 243-3771.)

Back issues or single copies of the DAILY REPORTs and JPRS publications are not available. Both the DAILY REPORTs and the JPRS publications are on file for public reference at the Library of Congress and at many Federal Depository Libraries. Reference copies may also be seen at many public and university libraries throughout the United States.

END OF FICHE DATE FILMED

3 MAY 1994